ADAPTATION OF DIFFERENT PATCH GEOMETRIES TO ACHIEVE BROADBAND OPERATION OF MICROSTRIP ANTENNA ON CUSTOMIZED COMPOSITE SUBSTRATE IN X-BAND

A thesis submitted in partial fulfillment of the

requirements for the degree of

Doctor of Philosophy

by

Debashis Sarmah
Registration No. 004 of 2008

Department of Physics
School of Science
Tezpur University
Napaam, Tezpur - 784028
Assam, India

June, 2013

This thesis is dedicated to, my beloved parents

Mr Sushil Sarmah and Mrs Anupoma Devi

Abstract

Over¯ the past few years, microstrip antenna has become an indispensible component of wireless communication systems due to its low profile, compactness and simplicity in fabrication. The widespread proliferation of wireless communication technology, where high data transfer rates is involved, a demand on broadband antenna systems operating in the microwave range has also increased. The basic microstrip antenna structure with its narrow bandwidth, generally falls short in fulfilling the requirements of robustness and wide operational band. Against this backdrop, material and structural modification of microstrip antenna structure become necessary to adequately improve performance to meet these needs. Due to numerous applications of microstrip antennas in satellite communications, military communications, RADAR, amature radio and surface communications which operate in the X-band (8 GHz to 12 GHz) region, development of antenna with requisite performance characteristics in this frequency band has assumed renewed importance.

The modification in performance of microstrip antenna can be accomplished by modifying the substrate parameters, the patch geometries or the ground plane. Conventional antenna substrate like glass epoxy/FR4, PTFE and PTFE based materials such as RT-Duroid, provides limited scope of tailoring the properties and geometry of the substrate. Particulate polymer composites provide a new alternative as substrate materials, where the properties can be controlled by varying the quantity and properties of the inclusions in the matrix material. Titania (TiO_2) and alumina (Al_2O_3) as fillers in LDPE matrix shows sufficient flexibility in varying the permittivity by varying the volume fraction and low permittivity loss $\sim 10^{-3}$ over the X-band qualifies as good candidates to be used as substrate for microstrip antenna. Different thermal and physical properties of the developed composite materials relevant for antenna substrate materials have been characterized.

Rectangular patch antennas fabricated on the particulate composite materials developed in the present work show performance comparable and in some case, better than commercially available substrates. The graded permittivity of substrate by changing the percentage volume fraction of titania in LDPE matrix enhances the bandwidth.

Most of the patch geometry modifications for bandwidth enhancement are carried out on the same plane for the need for ease in fabrication and implementation with minimum increase in patch dimensions and profile modifications include introduction of slots, stubs and superstrates among others. An E-shaped patch with arms terminating in transverse section and coupling two V-slotted semicircular patches capacitively coupled to a simple rectangular patch are employed to achieve enhancement of bandwidth. Bandwidths of more than 10% are observed in the two designs.

Ground plane modification in which the substrate and patch is sunk in the mounted object to obtain a flush mounted surface profile has been designed and studied. Bandwidth enhancement has been obtained in this design. Cross slots at the center and three equal rectangular slots at the radiating edges are introduced leading to further increase in the operational bandwidth. An identical patch-substrate combination as in the flush mounted design is stacked over it without the ground plane. This design with the Superstrate patch significantly enhances the -10dB bandwidth up to as much as 25.11% and hence can be used as a broadband antenna in the X-band.

To study the electric field orientation in the rectangular antenna designed on the modified substrate, a full wave FDTD modeling algorithm is developed. The algorithm provides an insight into the electric field distribution within the structure.

DECLARATION BY THE CANDIDATE

I hereby declare that the thesis "**Adaptation of Different Patch Geometries to Achieve Broadband Operation of Microstrip Antenna On Customized Composite Substrate in X-band**", being submitted to the **Tezpur University** in the **Department of Physics** under the **School of Science** in partial fulfillment for the award of the degree of Doctor of Philosophy in Physics, has previously not formed the basis for the award of any degree, diploma, associateship, fellowship or any other similar title or recognition.

Date: 23/12/2013

Place: Tezpur

(Debashis Sarmah)

Department of Physics

School of Science

Tezpur University

TEZPUR UNIVERSITY

Napaam, Tezpur-784028
DISTRICT: SONITPUR::ASSAM::INDIA

CERTIFICATE

This is to certify that the thesis entitled **"Adaptation of Different Patch Geometries to Achieve Broadband Operation of Microstrip Antenna on Customized Composite Substrate in X-band"**, submitted to the Tezpur University in partial fulfillment for the award of the degree of Doctor of Philosophy in Physics is a record of research work carried out by Mr. Debashis Sarmah under our supervision and guidance.

All helps received from various sources have been duly acknowledged.

No part of this thesis has been submitted elsewhere for award of any degree.

Supervisor

(Nidhi S. Bhattacharyya)
Professor
Department of Physics
Tezpur University

Co- Supervisor

(Satyajib Bhattacharyya)
Professor
Department of ECE
Tezpur University

Date: December 23, 2013
Place: Tezpur

TEZPUR UNIVERSITY

Napaam, Tezpur-784028
DISTRICT: SONITPUR::ASSAM::INDIA

Certificate of the External Examiner and ODEC

This is to certify that the thesis entitled "**Adaptation of Different Patch Geometries to Achieve Broadband Operation of Microstrip Antenna On Customized Composite Substrate in X-band**" submitted by Mr. Debashis Sarmah to Tezpur University in the **Department of Physics** under the **School of Science** in partial fulfillment for the award of the degree of Doctor of Philosophy in **Physics** has been examined by us on_____ and found to be satisfactory.

The committee recommends for the award of the degree of Doctor of Philosophy.

Supervisor   Co Supervisor   External Examiner

(N. S. Bhattacharyya)   (S. Bhattacharyya)   (   )

Date: _____   Date: _____   Date: _____

Acknowledgements

Nabanita ba, Swati ba, Bidyut, Angshuman da, Upamanyu da, Momi ba, Prakash da, Manasi ba, Somik, Madhurjya, Sahoo da, Bhaskar da, Durga da, Manjit, Pritam, Palash, thank you all for your support and encouragement.

Also I am grateful to all the research scholars of Tezpur University for sharing a wonderful time during my research work. Ranjan and Pranab needs special mention.

No one walks alone on the journey of life. And I do not know where to start to thank all those people who walked with me and helped me along the way continuously urging me in my work and shared my insights. My lab-mates Subasit da, Jyoti, Kunal, Sikha, Pragyan, Tanuj, Arunav and Pulin, a big thank you for all the wonderful times, academic and otherwise, that we shared together.

I would like to thank Kangkon, Bimal, Mridushmita Phukan ba, Papori ba, Priyanka ba, Mridusmita Dutta ba, Vaswati ba, Jahnabi, Anil Deka, Sidhartha, Manash, Rupam Nath, Ripunjoy Deka and Nalini Sarmah for your encouragement.

Thank you Subrat, Diganta and Niranjan da for your support and encouragement.

My dear Maa and Baba, without your love, blessings and untiring help and support it would not have been possible to reach here. Words are not enough to express my gratitude towards my beloved parents. I am thankful to my brothers Fasu and Janu for their help and support.

Last but not the least, thank you Sumki, for your help and support and for always being there. Thank you Pravash Khura, Nili Khuri, Tuku and Rupam for your encouragement.

Debashis Sarmah

CONTENTS

List of tables

List of figures

List of symbols and abbreviations

EMI	Electromagnetic Interference
PIFA	Printed Inverted F Antenna
PIL	Printed Inverted L Antenna
FDTD	Finite Difference Time Domain
LDPE	Low Density Polyethylene
HDPE	High Density Polyethylene
VF	Volume Fraction
M	Molar
XRD	X-ray Difraction
SEM	Scanning Electron Microscopy
TLM	Trransmission line model
CTE	Coefficient of Thermal Expansion
TRL	Through-Reflect-Line
VNA	Vector Network Analyzer
MPA	Microstrip Patch Antenna
CAD	Computer Aided Design
CER	Cyanoacrylate Epoxy Resin
CP MSA	Circularly Polarized Microstrip Antenna
AR	Axial Ratio
TM	Transverse Magnetic
RF	Radio Frequency

RL	Return Loss
EDM	Electrical Discharge Machine
ε_{eff}	Effective permittivity
ε_r	Relative permittivity
ε''	Imaginary part of the complex permittivity
ε'	Real part of complex permittivity
μ_r	Relative permeability
A	Ampere
dB	decibel
E	Electric field vector
H	Magnetic field vector
EM	Electromagnetic
f_r	Resonant frequency
GHz	Giga Hertz
K	Co- efficient of thermal conductivity
Q	Quality Factor
Z_0	Characteristic impedance
λ_0	Free space wavelength
λ_g	Guide wavelength

CHAPTER I

INTRODUCTION TO THE RESEARCH PROBLEM

1.1 Introduction

1.2 The Research Direction

1.3 Thesis Structure and Outline

.

1.1 INTRODUCTION

We are linked to an ever increasing number of radio services such as personal communications, navigation, broadcasting and RADAR communication. The lunge in number of wireless services in different frequency bands has increased the number of antennas in a system drastically. The increasing number of antennas causes design complexity, increase in size and issues relating to electromagnetic interference. Antennas with small size and broad operational bandwidth can efficiently address these issues. Microstrip antennas have low profile, light weight and simplicity of design so that, it can be effectively assembled in planar structures [1-8]. But the main drawback of microstrip antennas is its low bandwidth. It is very important for the microstrip antenna designers to develop techniques to enhance its operational bandwidth. Schematic of microstrip antenna in figure 1.1 shows basically two regions for incorporating modifications to enhance the performance, one at the radiator patch level and the other is below the patch.
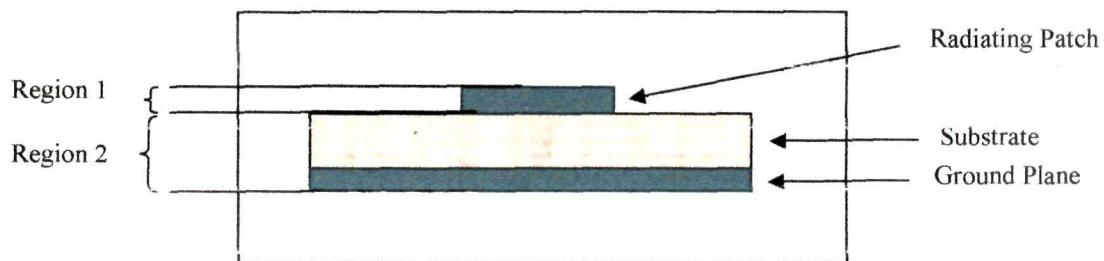
Figure 1.1   Schematic of a microstrip antenna showing different regions

The patch geometry modification is one of the most common ways to be considered for enhancement of microstrip antenna performance. Embedding suitable slots in a radiating patch enhances impedance bandwidth. Different slotted patch structures like cross-slot, L-slot, U-slot, T-slot etc. are some of the designs [12, 13, 46-55] reported to achieve broadband operation of microstrip antennas. Greater impedance bandwidth with a reduction in antenna size can be achieved by shorted pin loaded structures [3, 56-57]. The shorting makes the microstrip antenna as quarter wave structure reducing the antenna size

Adaptation of different patch geometries to achieve broadband operation of microstrip antenna on customized composite substrate in X-band

1

[3]. Planar inverted structures like inverted F (PIFA), inverted L (PIL), inverted U, with single and multiple folded edges are other efficient designs to achieve broadband operation [3]. L-shaped folded slits, different embedded rectangular slots and meandered slits are incorporated by antenna researchers to achieve dual broadband operations where the current path is enlarged, so that the electrical length of the patch increases in comparison to the ordinary patch [3]. Other designs like multipatch designs, three dimensional V-shaped designs are few relatively complex designs in the process of increasing the bandwidth of operation [3, 36-38]. Multiple patches directly coupled to radiating and nonradiating edges of a microstrip antenna can be employed to enhance the bandwidth of operation [3, 39, 40]. Incorporating these kinds of multiple techniques can enhance the operational bandwidth of microstrip antennas by either changing the current distribution or increasing the current path. Compactness of antenna structures and wide polarization bandwidths can be achieved by using circularly polarized antennas with stubs and slots [4].

Performance enhancement can be achieved by modifications in region 2 (figure 1.1) below the patch. Some reported modifications in ground plane are, application of meandering slots to reduce the Q value of antenna [27], shortened ground plane with truncated corners [26,27] etc. For most practical applications, patch antennas are used with a finite ground plane, which usually causes degradation such as increased cross polarization and backward radiations, thereby leading to decreased antenna gain. The problem is tackled by using cavity ground structures, where the microstrip antenna resides in a metallic cavity so that radiation losses due to surface waves are eliminated [1-5, 28]. However, such patch antennas have a narrow band width, which limits their practical applications. Wang and Zhang [28] used capacitive probe-

Adaptation of different patch geometries to achieve broadband operation of microstrip antenna on customized composite substrate in X-band

2

feeding with shorted pin to enhance the bandwidth of cavity-backed antenna. Further increase in operating bandwidth can be obtained by placing superstrate material over the antenna structure with reduction in patch dimension [58-62].

In region 2 below the patch, the substrate materials also play an important role in design and performance of the microstrip antenna. The substrate provides mechanical strength and also reduces the size of antenna [1]. Substrate height and complex permittivity influence the antenna properties and performance. The dielectric used also degrades electrical properties of antenna as the surface waves produced on the dielectric extract a part of the total power available for direct radiation (space waves) [3]. The properties that are taken into consideration while selecting it as substrate for microstrip antenna include: complex permittivity, processing homogeneity, dimensional stability with temperature, humidity and aging [29-34]. Other physical properties such as resistance to chemicals, machinability, mechanical strength, bonding ability, etc, are important in choosing a substrate material. glass epoxy/FR4, PTFE and PTFE based materials such as RT-Duroid are commonly used as substrates for microstrip antennas [5]. These conventional substrates do not provide much room for modification of substrate properties. Thermoset polymer systems, including epoxy, bismaleimide-triazine-epoxy, polycyanate resin, polyimide resin, triazine resin and cross-linked polystyrene resin, have been reported as alternate substrate materials. Particulate composites are reinforced polymers [29-34] offer various design flexibilities and performance enhancement by modifying the quantity and properties of constituent materials.

The foregoing survey is used as a broad guideline while formation of the present research work and has been planned and structured into five phases as described below.

Adaptation of different patch geometries to achieve broadband operation of microstrip antenna on customized composite substrate in X-band

3

1.2 THE RESEARCH DIRECTION

There are numerous applications of microstrip antennas in satellite communications, military communications, RADAR, amature radio and surface communications which operate in the X-band (8 GHz to 12 GHz) region. Precision approach RADAR (PAR) (9-9.2 GHz), traffic light crossing detectors (10.4 GHz), motion detectors (10.57 GHz) etc. are some specific applications in this frequency range. Broadband antennas are of immense demand for these systems. In this research work, modifications of patch, ground plane and substrate are integrated to obtain broadband operation of microstrip antenna in X - band. The work is directed towards:

- Development of suitable dielectric composite materials having the desirable microwave properties for the application in microstrip antennas.

- Investigation of other requisite properties for microwave device applications like density and homogeneity, thermal and inertness to environmental condition.

- Alteration in substrate construction for improved performance

- Modification in patch geometries and ground plane structure to achieve broadband operation of microstrip antennas

- Finally, the field distributions within the substrate material of rectangular patch antenna on graded substrate are modelled using three-dimensional Finite-Difference Time-Domain (3D FDTD) method. The results are compared with that of rectangular patch antenna designed at the same frequency and fabricated on single layer substrate.

1.3 THESIS STRUCTURE AND OUTLINE

The thesis structurally consists of eight parts and two appendices. Small sized titania and alumina as reinforcers in low density polyethylene

Adaptation of different patch geometries to achieve broadband operation of microstrip antenna on customized composite substrate in X-band

4

matrix are developed as possible dielectric composite substrate material. The preparation technique of the composites is illustrated in **chapter II**. The chapter also includes the micro structural studies like XRD, SEM micrographs to estimate shape, size, distribution and ascertaining of structure. Measurements of important properties like density, water absorbance, thermal conductivity, coefficient of thermal expansion are included in this chapter. Finally the composites are examined for their microwave properties.

Applicability of the developed composite materials as substrate for microstrip antennas is investigated by fabricating simple rectangular patch antenna on the materials as substrates. Different performance parameters of the antennas are studied in X-band of frequencies. To enhance the performance of microstrip antennas, substrate grading is investigated and is discussed in **chapter III**.

Chapter IV and V includes studies on modification of patch geometries. In **chapter IV**, a modified E-shaped patch antenna is developed for wideband applications. Different steps of designing and fabricating the antenna is thoroughly discussed in detail.

Circularly polarized broadband antennas for compact communication applications are currently of great importance. Studies are conducted to improve the performance by applying a new design concept of two V-slotted semicircular patches capacitively coupled with centre rectangular patch, are discussed in the **chapter V.**

For improved aerodynamics of antenna elements used in airborne systems, a special grooved structure is employed. The space to accommodate the antenna structure is created by a metal cavity located on the metallic ground. It enables the antenna to be placed suitably inside the cavity, which serves as a shielding room for the antenna subsystem. The design is discussed in **Chapter VI**. To further enhance the bandwidth of operation, special slotted

Adaptation of different patch geometries to achieve broadband operation of microstrip antenna on customized composite substrate in X-band

5

patch geometry is studied. A superstrate patch over the geometry is placed to achieve consistent broadband performance.

Theoretical background of the 3D FDTD technique is discussed in **chapter VII.** The technique has been adopted for graded substrate microstrip antennas. The H-field and E-field are updated in the leap frog manner. MATLAB code has been developed using the FDTD formulation to determine the field distribution throughout the substrate and computation of S_{11} parameter.

Chapter VIII summarizes the suitability of the developed dielectric material as substrates for microstrip antennas. The achievements of the entire work and future direction of work that can be incorporated are also highlighted.

Appendix A, gives the detail equations for PML boundary conditions as applied in the modelling. Code for the 3D FDTD formulation is developed in the MATLAB platform. The E and H field updating code modules employed are given in **Appendix B.**

Adaptation of different patch geometries to achieve broadband operation of microstrip antenna on customized composite substrate in X-band

6

References

1. Carver, K.R. and Mink, J.W., Microstrip Antenna Technology, *IEEE Trans. Antennas Propagat.*, **29**, 2-24, (1981).

2. Deschamps, G.A., Microstrip Microwave Antennas, *3rd USAF Symp. On Antennas*, (1953).

3. Wong, K.L., *Compact and broadband microstrip antennas* (New York, John Wiley and Sons, Inc., 2002)

4. Guha, D., Microstrip and Printed Antennas: Recent Trends and Developments, *TELSIKS 2003*, **39-44**, (2003).

5. Hall, P.S. and James, J.R., *Handbook of Microstrip Antennas*, (London, Peter Peregrinus Ltd. 1989).

6. Gutton and Baissinot, G., Flat Aerial for Ultra High Frequencies, *French Patent No. 703113*, (1955).

7. Lewin, L., Radiation from Discontinuities in Stripline, *Proc. Inst. Elec. Eng.*, **107**, 163-170, (1960).

8. Sabath, F., Mokole, E.L., and Samaddar, S.N., Definition and Classification of Ultra-Wideband Signals and Devices, *Radio Science Bulletin*, **313**, 12-26 (2005).

9. Ghosh, D., De, A., Taylor, M.C., Sarkar, T.K., Wicks, M.C. and Mokole, E.L., Transmission and Reception by Ultra-Wideband (UWB) Antennas, *IEEE antennas and propagate.* **48**, 67-99, (2006).

10. Wong, K.L. and Chiou, T.W., Broadband Single Patch Circularly Polarized Microstrip Antenna with Dual Capacitively Coupled Feeds, *IEEE trans. Antennas and propagat.* **49**, 41-44, (2001).

11. Taragonski, S.D. and Pozar, D.M., Design of Wideband Circularly Polarized Aperture Coupled Microstrip Antenna, *IEEE trans. Antennas and propagat.* **41**, 214-220, (1993).

12. Gardiol, F.E. and Zuercher, J.F., Broadband Patch Antennas – A SSFIP Update, *IEEE AP-S int. symp. Dig.* 2-5, (1996).

Adaptation of different patch geometries to achieve broadband operation of microstrip antenna on customized composite substrate in X-band

7

13. Lee, K.F., Luk, K.M., Tong, K.F., Shum, S.M., Huynh, T. and Lee, R.Q., Experimental and simulation studies of the coaxially fed U-slot rectangular patch antenna, *IEE Proc. Microw. Antennas Propag.*, **144**, 354-358, (1997).

14. Herscovici, N., New Considerations in the Design of Microstrip Antennas, *IEEE trans. Antennas and propagat.* **46**, 807-812, (1998).

15. Hong, W., Chen, T.L., Chang, C.Y., Sheen, J.W. and Lin, Y.D., Broadband Tapered Microstrip Patch Antenna with Aperture Coupling, *IEEE trans. Antennas and propagat.* **51**, 1922-1928, (2003).

16. Gao, S., Li, L.W., Leong, M.S. and Yeo, T.S., A Broad Band Dual Polarized Microstrip Patch Antenna with Aperture Coupling, *IEEE trans. Antennas and propagat.* **51**, 898-900, (2003).

17. Luxey, C. and Laheurte, J.M., Simple Design of Dual Beam Leaky-Wave Antennas in Microstrips, *IEEE Proc. Microwave Antennas and Propagat.* **144**, (1997).

18. Chen, T.L. and Lin, Y.D., Microstrip Leaky-Wave Antenna Fed by Short End CPW-to-Slot Transition, *Eletron. Lett.* **35**, (1999).

19. Chen, T.L., Lin, Y.D. and Sheen, J.W., Microstrip Fed Microstrip Second Higher Order Leaky-Mode Antenna, *IEEE trans. Antennas and propagat.* **49**, 855-857, (2001).

20. Huynh, T. and Lee, K.F., Single Layer Single Patch Wideband Microstrip Antenna, *Electron. Lett.* **31**, 1310-1312, (1995).

21. Wong, K.L. and Hsu, W.H., Broadband Triangular Microstrip Antenna with U-shaped Slot, *Electron. Lett.* **33**, 2085-2087, (1997).

22. Hsu, W.H. and Wong, K.L., A Wideband Circular Patch Antenna, *Microwave opt. tech. lett.* **25**, 327-328, (2000).

23. Wong, K.L., Tang, C.L. and Chiou, J.Y., Broadband Probe Fed Patch Antenna with a W-shaped Ground Plane, *IEEE trans. Antennas and propagat.* **50**, 827-831, (2002).

Adaptation of different patch geometries to achieve broadband operation of microstrip antenna on customized composite substrate in X-band

8

24. Lo, Y.T., Harrison, D.D., Solomon, D., Deschamps, G.A., and Ore, F.R., Study of Microstrip Antennas, Microstrip Phased Arrays, and Microstrip Feed Networks, *Rome Air Development Center, Tech. Rep.* TR-77-406, (1977).

25. Derneryd, A.G., A Theoretical Investigation of the Rectangular Microstrip Antenna Element, *Rome Air Development Center, Tech. Rep.* TR-77-206, (1977).

26. Prombutr, N., Kirawanich, P. and Akkaraekthalin, P., Bandwidth Increasing Technique Using Modified Ground Plane with Diagonal Edges, *IETE Journal of Research*, **55**, 196-200, (2009).

27. Kuo, J.S. and Wong, K. L., A compact microstrip antenna with meandering slots in the ground plane, *Microwave Opt. Technol. Lett.* **29**, 95-97, (2001).

28. Wang, F.J. and Zhang, J.S., Wide Band Cavity-backed Patch Antenna For PCS/IMI2000/2.4 GHz WLAN, *Progress in Electromagnetics Research*, **74**, 39-46, (2007).

29. Nowicki, T.E., Microwave Substrates, Present and Future, *Proc. Workshop Printed Circuit Antenna Tech., New Mexico State Univ., Las Cruces*, **26**, 1-22, (1979).

30. Traut, G.R., Clad Laminates of PTFE Composites for Microwave Antennas, *Proc. Workshop Printed Circuit Antenna Tech. New Mexico State University, Las Cruces*, **27**, 1-17, (1979).

31. Murthy, V. R. K., Sunderam, S. and Viswanathan, B., *Microwave Materials*, (Delhi, Narosa Publishing House, 1990).

32. Bahl, I. and Ely, K., Modern Microwave Substrate Materials, *Microwave Journal*, **33**, 131 (1990).

33. Traut, G. R., Clad Laminates of PTFE Composites for Microwave Antennas, *Microwave Journal*, **23**, 47 (1980).

Adaptation of different patch geometries to achieve broadband operation of microstrip antenna on customized composite substrate in X-band

9

34. Donnet, J. B., Bansal, R. C., and Wang, M. J., *Carbon Black, Science and Technology,* (Florida, CRC press, 1983).

35. Pozar, D.M., Microstrip Antennas, *Proc. IEEE,* **80,** 79-91, (1992).

36. Croq, F. and Pozar, D. M., Millimeter-wave design of wide-band aperture-coupled stacked microstrip antennas, *IEEE Trans. Antennas Propag.,* **39,** 1170-1176, (1991).

37. Liu, Z.-F., Kooi, P.-S., Li, L.-W., Leong, M.-S.and Yeo, T.-S., A Method for Designing Broadband Microstrip Antennas in Multilayered Planer Structures, *IEEE Trans. Antennas Propag.,* **47,** 1416-1420, (1999).

38. Kim, J.H., Kim, H.C. and Chun, K., Performance Enhancements of a Microstrip Antenna with Multiple Layer Substrates, *Int'l. Sympos. Signal, Systems and Electronics,* 319-322, (2007).

39. Kumar, G. and Gupta, K.C., Broadband Microstrip Antennas Using Additional Resonators Gap Coupled to the Radiating Edges, *IEEE Trans. Antennas and Propagat.* **AP-32,** 1375-1379, (1984).

40. Kumar, G. and Gupta, K.C., Nonradiating Edges and Four Edges Gap Coupled Multiple Resonator Broadband Microstrip Antennas, *IEEE Trans. Antennas and Propagat.,* **AP-33,** 173-178, (1985).

41. Ali, W.K.W. and AI-Charchafchi, S.H., Using Equivalent Dielectric Constant to Simplify the Analysis of Patch Microstrip Antenna with Multi Layer Substrates, *IEEE AP-S Int'l. Sympos.,* **2,** 676-679, (1998).

42. Jha, K.R. and Singh, G., Analysis and design of rectangular microstrip antenna on two-layer substrate materials at terahertz frequency, *J. Comput. Electron.* **9,** 68-78, (2010).

43. Ang, B.-K. and Chung, B.-K., A Wideband E-shaped Microstrip Patch Antenna for 5-6 GHz Wireless Communications, *Progress in Electromagnetid Research,* **75,** 397-407, (2007).

Adaptation of different patch geometries to achieve broadband operation of microstrip antenna on customized composite substrate in X-band

10

44. Yang, F., Zhang, X. X., Ye, X., and Rahmat-Samii, Y., Wide-band E-shaped patch antennas for wireless communications, *IEEE Trans. Antennas Propagat.*, **49**, 1094-1100, (2001).

45. Yang, C.-F., Hseih, C.-Y. and Cheng, C.-M., Design Small-Size and Wide-Band T-shaped patch Antenna on Ceramic Substrate, *WCNC 2007 Proceedings*, (2007).

46. Kim, M. K., Kim, K.., Suh, Y. H., and Park, I., A T-shaped microstrip-line-fed wide slot antenna, *Proc. IEEE Antennas Propagat. Soc. Int. Symp.*, **3**, 1500-1503, (2000).

47. Guo, Y. X., Bian, L. and Shi, X. Q., Broadband circularly polarized annular-ring microstrip antenna, *IEEE Trans. Antennas Propag.*, **57**, 2474-2477, (2009).

48. Nasimuddin, Esselle, K. P. and Verma, A. K. Wideband circularly polarized stacked microstrip antenna, *IEEE Antennas Wireless Propa. Lett.*, **6**, 21-24, (2007).

49. Targonski, S. D. and Pozar, D. M., Design of wideband circularly polarized aperture-coupled microstrip antenna, *IEEE Trans. Antennas Propag.*, **41**, 214-220, (1993).

50. Zavosh, F. and Aberle, J.T., Improving the Performance of Microstrip-Patch Antennas, IEEE Antennas and Propagation Magazine, **38**, 7-12, (1996).

51. Wong, K.-L. and Yang, K.-P., Small dual Frequency Microstrip Antenna with Cross Slot, *Electronics Letters*, **33**, 1916-1917, (1997).

52. Yang, K.-P., and Wong, K.-L., Inclined-Slot-Coupled Compact Dual-Frequency Microstrip Antenna with Cross Slot, *Electronics Letters*, **34**, 321-322, (1998).

53. Tong, K.-F., Luk, K.-M., Lee, K.-F. and Lee, R.Q., A Broad Band U-Slot Rectangular Patch Antenna on a Microwave Substrate, *IEEE Trans. On Antennas and Propagat.*, **48**, 954-960, (2000).

Adaptation of different patch geometries to achieve broadband operation of microstrip antenna on customized composite substrate in X-band

11

54. Misran, N., Shakib, M.N., Islam, M.T. and Yatim, B., Design Analysis of a Slotted Microstrip Antenna for Wireless Communication, *World Academy of Science, Engineering and technology,* **49**, 448-450, (2009).

55. Weigand, S., Huff, G.H., Pan, K.H. and Bernhard, J.T., Analysis and Design of Broad Band Single Layer Rectangular U-slot Microstrip Patch Antennas, *IEEE Trans. Antennas and Propagat.,* **51**, 457-468, (2003).

56. Wong, K. L. and Lin, Y. F., Small broadband rectangular microstrip antenna with chip resistor loading, *Electron. Lett.* **33**, 1593-1594, (1997).

57. Wong, K. L. and Lin, Y. F., Microstrip-line-fed compact broadband circular microstrip antenna with chip-resistor loading, *Microwave Opt. Technol. Lett.* **17**, 53-55, (1998).

58. Choi, W., Pyo, C., Cho, Y. H., Choi, J. and Chae, J., High gain and broadband microstrip patch antenna using a superstrate layer, *Proc. IEEE Antennas Propagat. Soc. Int. Symp.,* **2**, 292-295, (2003).

59. Alexopoulos, N. G. and Jackson, D. R., Fundamental superstrate (cover) effects on printed circuit antennas, *IEEE Trans. Antennas Propagat.,* **32**, 807-816, (1984).

60. Luk, K. M., Tam, W. Y. and Yip, C. L., Analysis of circular microstrip antennas with superstrate, *IEE Proc.,* **136**, 261-262, (1989).

61. Bernard, L., Loison, R., Gillard, R. and Lucidarme, T., High directivity multiple superstrate antennas with improved bandwidth, *IEEE Antennas Propagat. Soc. Int. Symp.,* **2**, 522-525, (2002).

62. Gürel, Ç.S. and Yazgan, E., Bandwidth widening in an annular ring microstrip antenna with superstrate, *Proc. IEEE Antennas Propagat. Soc. Int. Symp.,* 692-695, (1995).

Adaptation of different patch geometries to achieve broadband operation of microstrip antenna on customized composite substrate in X-band

12

CHAPTER II

SUBSTRATE PREPARATION AND CHARACTERIZATION

2.1 Introduction

2.2 Material Selection and Synthesis

2.2.1 Material selection

2.2.1.1 Selection of host matrix

2.2.1.2 Selection of inclusions

2.2.2 Synthesis of small sized alumina and titania particles

2.2.3 Fabrication of dielectric composite material

2.3 Microstructural Studies

2.3.1 X-ray diffraction

2.3.2 SEM results

2.4 Other Relevant Property Studies

2.4.1 Density and water absorbance studies

2.4.2 Thermal Property Studies

2.4.2.1 Design of modified Lee's method to measure thermal conductivity

2.4.2.2 Coefficient of thermal expansion measurement set up

2.4.2.3 Thermal conductivity and coefficient of thermal expansion measurement results

2.5 Microwave Characterization of the Composites

2.5.1 Measurement of complex permittivity using cavity perturbation technique

2.5.2 Measurement of complex permittivity using Nicolson-Ross technique

2.5.3 Comparison of measured complex permittivity using cavity perturbation technique and Nicolson-Ross technique

2.6 Discussion and Conclusions

References

2.1 INTRODUCTION

Development of microstrip antenna design most importantly needs the selection of a suitable substrate material which should be compatible with the performance objectives like high radiation power, wide operational frequency band etc., along with ease and cost effectiveness of processing technique. Polymers are finding wide applicability as substrates in microstrip antenna designs for handheld devices as they are of low cost, light weight, stronger, more durable and have good surface adhesion for metallization. Improvements in properties of polymers can be done by reinforcing it with different materials [1-3]. Such a reinforced physical mixture, forming a composite, offers the advantage of optimizing relevant antenna substrate properties like dielectric properties, dimensional stability and heat dissipation etc. by varying the filler components [4-6]. Fine adjustments of material properties can further lead to performance enhancement of microstrip antennas [4]. In addition, the materials should be resilient to stressful environmental conditions maintaining their properties without degradation over time. Particle filled composite shows greater fabrication flexibility in getting the desired properties by simply altering shape, size and distribution of reinforcing particle in the composite.

This chapter initially discusses the choice of reinforcers and matrix phases for microwave applications, preparation techniques and other structural characterizations. Other correlated facets like thermal stability, heat dissipations and inertness to environment, which play a significant part in microwave operation of antennas, are investigated. The later part of the chapter accounts for measurement results of complex permittivity, which is a crucial design parameter of the developed composite materials with reference to their suitability for antenna substrate applications.

Adaptation of different patch geometries to achieve broadband operation of microstrip antenna on customized composite material in X-band

13

2.2 MATERIAL SELECTION AND SYNTHESIS

The materials to be used as substrate for microstrip antennas should be compatible with the design requirements. Processing technique employed to obtain composite materials should be able to control particle size, size distribution, reduction of agglomeration and filler concentration uniformity issues. In addition, the synthesis process of substrate material should be easy and cost effective.

2.2.1 Material selection

2.2.1.1 Selection of host matrix

Low density polyethylene (LDPE) is a solid polymer having melting point 383 K (110 ⁰C). LDPE constitute of chemical elements carbon and hydrogen (figure 2.1). LDPE has more branching (about 2% of the carbon atoms) than high density polyethylene (HDPE), so its intermolecular forces (instantaneous – dipole induced – dipole attraction) are weaker, its tensile strength is lower, and its resilience is higher. It helps in reinforcing metal oxide inclusions with homogeneous distribution. Also, since its molecules are less tightly·packed and less crystalline because of the side branches, its density is lower [7].

Data sheet [8] shows that it is not reactive at room temperatures, except by a strong oxidizing agent. Practically no solvents dissolve it at room temperature. However, several solvents like carbon tetrachloride, toluene, xylene, cychlohexane etc. can dissolve it at higher temperatures.

The dissolved polymer precipitates out, as the solution cools down to room temperature. It can withstand temperatures of 80 ⁰C continuously and 95 ⁰C for a short time without dimensional alterations. The mechanical properties of LDPE are between those of rigid materials like polyester and linked polymers like vinyls. In addition, it has low dielectric loss at

Adaptation of different patch geometries to achieve broadband operation of microstrip antenna on customized composite material in X-band

14

microwave frequencies and thus may be appropriate as host matrix for microwave antenna substrate applications. The details of relevant properties are given in table 2.1.
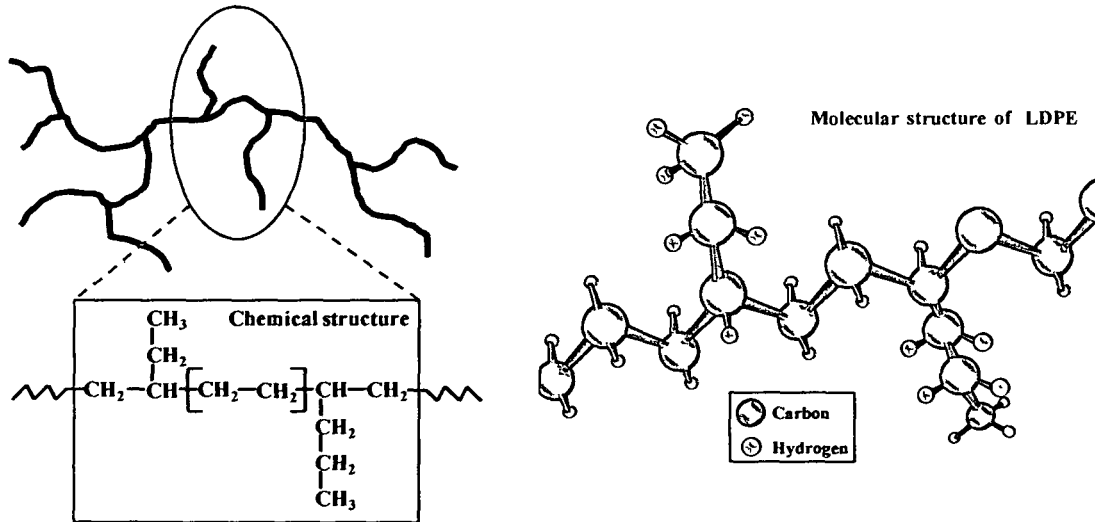
Figure 2.1   Structural formula and molecular structure of LDPE

2.2.1.2 Selection of inclusions

Alumina and titania are selected to be used as inclusions in the host polymer matrix. Both alumina and titania has higher value of dielectric constant and thermal conductivity in comparison to LDPE. Coefficient of thermal expansion (CTE) is less than LDPE for both the materials.

Table 2.1   Microwave, physical and thermal properties of LDPE

Materials	Microwave property		Physical property	Thermal property	
	Dielectric constant 10 GHz	Dielectric loss	Density (gm/cc)	Thermal conductivity (W/cm K)	CTE ($10^{-6} \times K^{-1}$)
*LDPE	2.2-2.35	0.0003	0.91-0.92	0.008	100-200
**Titania	85	0.004	1.70	0.05	7.5
**Alumina	9.6-10.4	0.0001	3.75	0.37	6.3

Goodfellow- Material information
** Microwave Material, "V R K Murthy, S Sundaram, B Viswanathan", Narosa Publishing House

Adaptation of different patch geometries to achieve broadband operation of microstrip antenna on customized
composite material in X-band

15

These materials are included in different volume fraction (VF) in the polymer matrix to form composite material. Relevant properties of these materials [1] are provided in table 2.1.

2.2.2 Synthesis of small sized titania and alumina particles

Small size of the filler particles is used to ensure large surface to volume ratio and to avoid scattering of the probing wave. Reduced size titania is prepared using acid hydrolysis process [9], in which 1M titanium isopropoxide is added to 2M HCl solution in 50 cc double distilled water. The whole solution is stirred for 6 hours at 200 °C using a magnetic stirrer. The solution is dried at 800 °C to obtain crystals of titania, and grounded to obtain fine titania powder.

For alumina, reduce particle size is achieved using a special heat treatment method. The bulk alumina particles are mixed with double distilled water and the mixture autoclaved for 1 hour. The mixture is then treated in a heat chamber at 800 °C and subsequently grounded to obtain a fine powder.

XRD studies of the materials are carried out to determine their size, shape and crystalline properties.

2.2.3 Fabrication of dielectric composite material

Most studies to date have employed the conventional approach of blending dielectric particles into polymers [10-12]. Such methods lack control on particle size and distribution within the polymer matrix due to the intrinsic incompatibility between inorganic particles and organic matrices. Chemical synthesis techniques show great promise for producing high quality dielectric composites, which are discussed in the present chapter. In most of the RF applications, there is a practical need to disperse the particulate inclusions homogeneously in polymer media, to achieve isotropic properties with respect to EM waves. However, in case of particulate composite, the

Adaptation of different patch geometries to achieve broadband operation of microstrip antenna on customized composite material in X-band

16

distribution of inclusions and its effective volume fraction in the polymer composites significantly influence the dielectric and thermal properties [13-16] of the composite system. One of the most attractive features of the particulate composite is that their properties can be varied over a wide range by the choice of shape, size and quantity of the constituents in the polymer matrix. Particle reinforced dielectric composites are fabricated by mixing the synthesized inclusions in the dissolved matrix and stirring for sufficient time to get uniform blending. The composite production is inexpensive.

LDPE is dissolved in cyclohexane and stirred continuously at 70 °C to make a homogeneous mixture. Alumina and titania particles are added to the polymer matrix in the desired percentage volume fraction (VF), given by the following expression,

$$VF = \frac{V_f}{V_f + V_p} \times 100\%$$ (2.1)

where, V_f is the volume of the fillers and V_p is the volume of the polymer.

Tetraethyl orthotitanate (2-3 drops) or titanium ethoxide [Ti(OC$_2$H$_5$)$_4$] is mixed as coupling agent to reduce the viscosity of the solution so as the quantity of fillers can be increased [18-21]. The coupling agent also reduce the molecular polarizability in the filler-polymer "interphase" region by enhancing "physical wetting" between the inorganic and organic phase and uniform dispersion of the filler within the bulk polymer. The homogeneous liquid is then poured in the appropriately shaped mold and allowed to cool gradually at room temperature. The preparation and environment conditions are maintained identical for each batch of samples. The processing chart is given in figure 2.2. Alumina and titania are added up to 6 %VF in the matrix, beyond which sinkage of the inclusions take place in the solution.

Adaptation of different patch geometries to achieve broadband operation of microstrip antenna on customized composite material in X-band

17
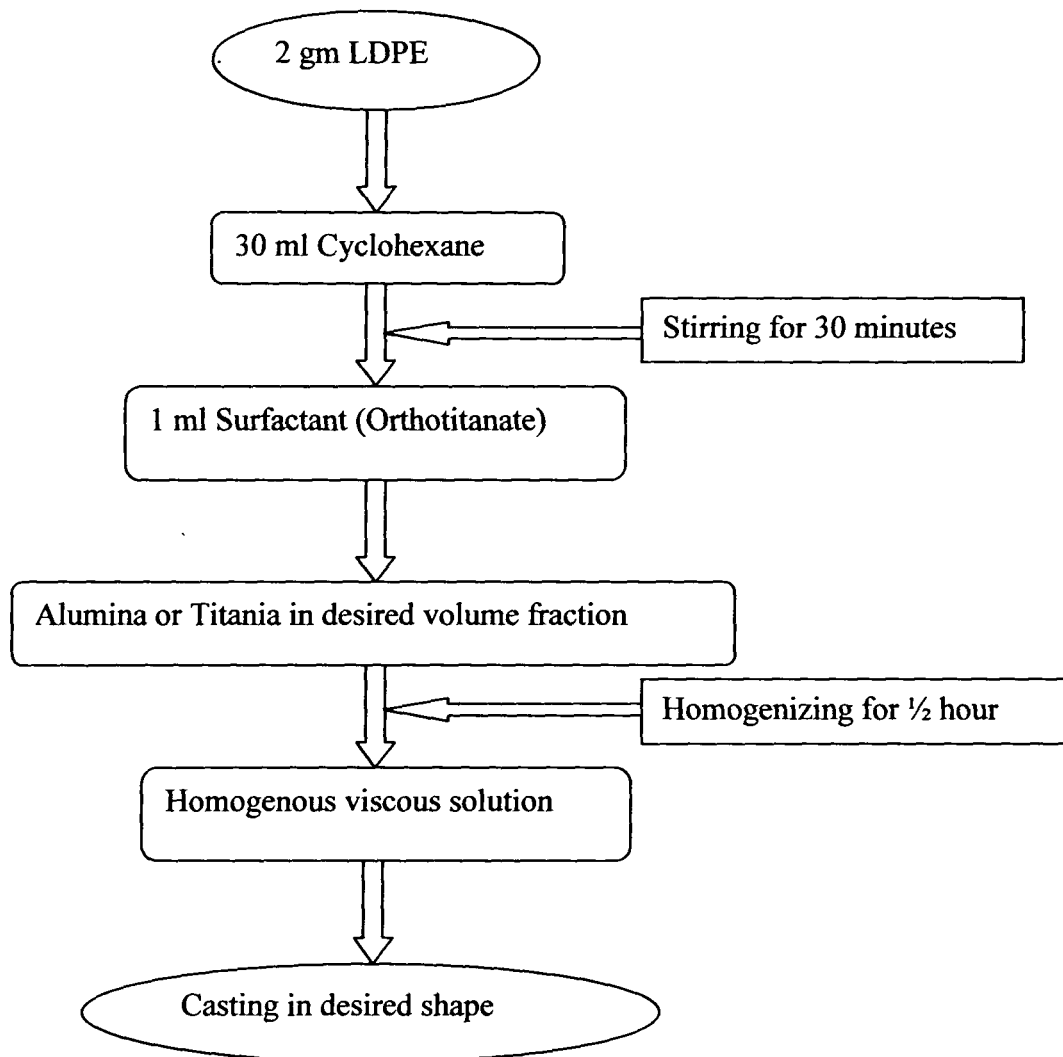
Figure 2.2   Schematic of composite synthesis

2.3 MICROSTRUCTURAL STUDIES

Along with the intrinsic properties of the constituents, distribution and the size of inclusions and change in the structural configuration of the inclusion particles in the composite matrix are the key factors that affect the propagation of electromagnetic wave, passing through the composite material. Microstructural studies provide the internal structural detail of the composite, determining its utility as substrate in microwave applications. Techniques used for micro-structural studies are described subsequently.

Adaptation of different patch geometries to achieve broadband operation of microstrip antenna on customized composite material in X-band

18

2.3.1 X-ray diffraction

X-ray diffraction studies are an important tool for structural analysis and gives information of various phases present in the specimen. X-ray diffraction patterns of alumina, titania, LDPE-alumina composite and LDPE-titania composite are recorded at 2θ values using Rigaku X-Ray Diffractometer, model: MINIFLEX using Cu K_α line of wavelength $\lambda = 1.541841$ Å.

Figure 2.3 shows the XRD pattern of pure titania particles and figures 2.4 (a-b) show the XRD patterns of LDPE-titania composite for 2 % and 4 % VF of titania. The system shows peaks at 25°, 38°, 45°, 48°, 54°and 63°. According to JCPDS (file no. 03-0380) data, this XRD pattern corresponds to brookite phase of titania. It shows that titania retains its crystalline properties in the composite. Alumina is crystalline in nature and shows distinct peaks at 17°, 20°, 38°, 45°, 65°, 68° and 78° [16]. Figures 2.5 (a-d) show the XRD spectra of pure alumina and LDPE-alumina composite with increase in volume fraction of alumina. XRD of LDPE-alumina system shows six peaks at Bragg angles 17.5°, 21.5°, 27°, 46°, 66.5° and 77° confirming that the alumina particles filled polymer matrix does not lose its crystalline properties.
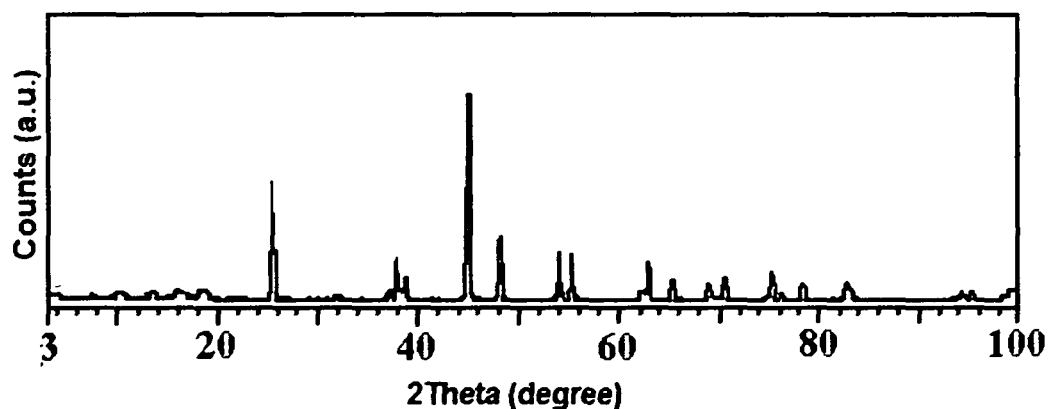
Figure 2.3   XRD pattern of pure titania

Adaptation of different patch geometries to achieve broadband operation of microstrip antenna on customized composite material in X-band

19
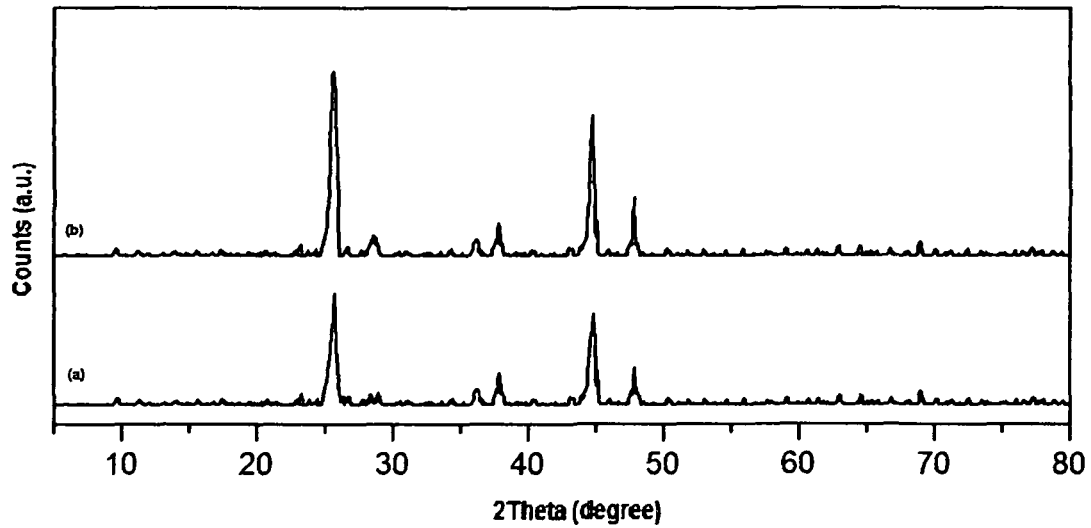
Figure 2.4   XRD pattern of (a) 2 % VF of titania in LDPE
                                (b) 4 % VF of titania in LDPE
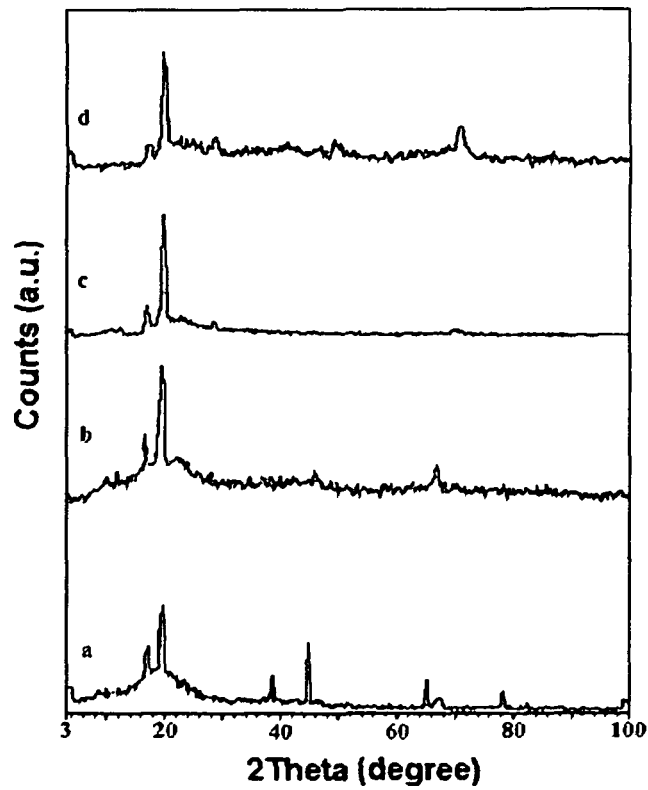
Figure 2.5   XRD pattern of (a) pure alumina
                                (b) 2 % VF of alumina in LDPE
                                (c) 3 % VF of alumina in LDPE
                                (d) 4 % VF of alumina in LDPE

Adaptation of different patch geometries to achieve broadband operation of microstrip antenna on customized composite material in X-band

20

2.3.2 Scanning Electron Micrograph results

Scanning electron micrography (SEM) is a sensitive technique to study the distribution pattern of the inclusions in the polymer matrix. SEM image has been obtained using the JEOL-JSM-6390 system. The surface of each samples are platinum coated using a sputtering unit before taking the micrographs.
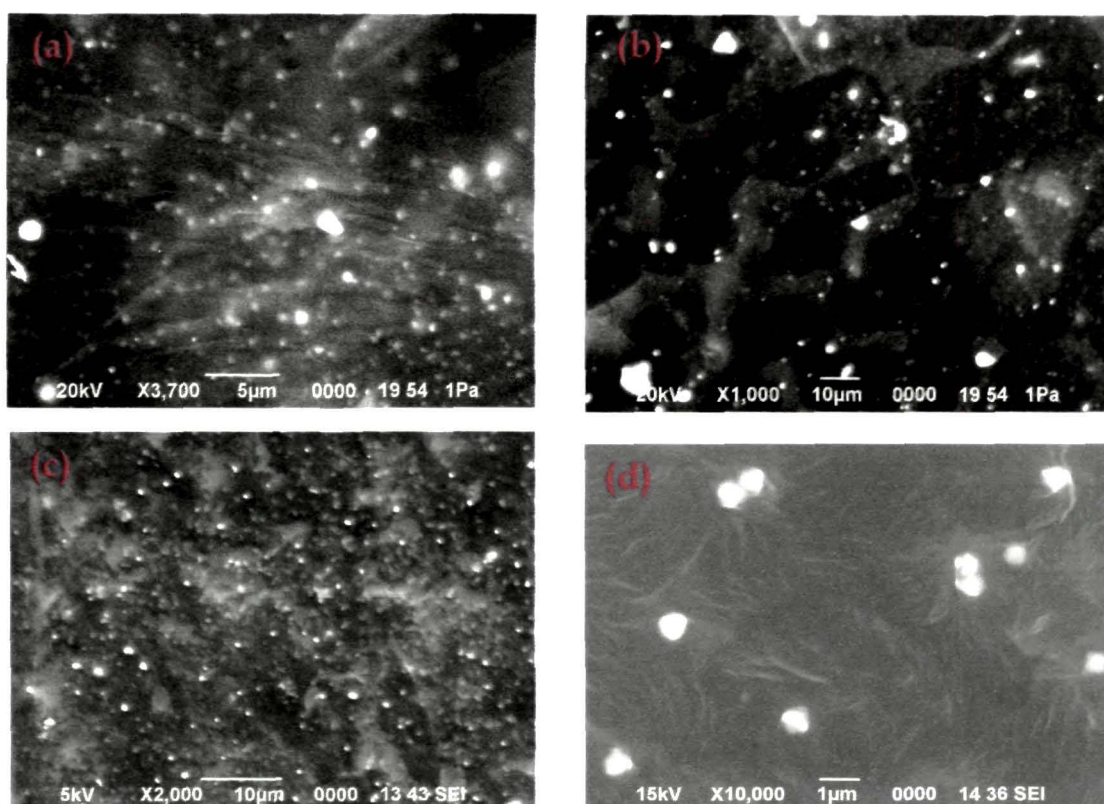
Figure 2.6   SEM micrographs of composites with LDPE and 4 % VF

         (a) and (b) Alumina
         (c) and (d) Titania.

The micrographs are taken at 10^{-11} A probe current and 20 KV accelerating voltage at different resolutions. Figures 2.6 (a–b) and 2.6 (c-d) show the SEM micrographs of 4 % VF of alumina and 4 % VF of titania in LDPE composite, respectively.

Adaptation of different patch geometries to achieve broadband operation of microstrip antenna on customized composite material in X-band

21

From the SEM images, most of the particles appear spherical in shape and almost homogeneously distributed over the matrix. The sizes of the titania particle is about 1 μm and that of alumina varies in the 1-5 μm range.

2.4 OTHER RELEVANT PROPERTY STUDIES

Physical and thermal properties of composites (substrate materials) are important for microwave applications. Relevant characteristics are evaluated and described in the following subsections.

2.4.1 Density and water absorbance studies

It is essential to reduce the size and weight of microwave electronic parts for space and telecommunication applications. Density and porosity of the composite gives an idea of the compactness of the material and its applicability as alternate light- weight material.

The densities of the samples are measured with Archimedes's principle. The samples of dimension 10 mm × 20 mm × 5 mm are prepared and weight measured in air, W_{air}. The composite is suspended in water and apparent immersed weight of the sample is measured, referred as W_{app}. The experimental bulk density (d_s) of the composite is measured by the Archimedes' principle and is given by

$$d_s = \frac{W_{air}}{W_{air} - W_{app}} \times D_{water} \qquad (2.2)$$

or

$$d_s = \frac{W_{air}}{W_{app}} \times D_{water} \qquad (2.3)$$

where

W_{air} = Weight of the sample in air (gm)

W_{app} = Weight of the sample in air - weight of the displaced water (gm)

D_{water} = Density of water at room temperature (=0.997 g/cc at 25 °C)

Adaptation of different patch geometries to achieve broadband operation of microstrip antenna on customized composite material in X-band

22

Water absorbance studies of the material help in determining the porosity of the material in humid and wet environmental conditions in which the system can work without affecting its microwave performance. Percentage of water absorbance of the composite is measured by dipping the sample in distill water for 48 hours and pat drying and measuring the weight thereafter. The percentages of water absorption of the composites are determined according to the expression

$$\text{Water absorbance (\%)} = \frac{W_t - W_0}{W_0} \times 100 \tag{2.4}$$

where W_t and W_0 are the weights of the wet and dry composites respectively.

The results of density and water absorbance are tabulated in table 2.2. None of the samples exhibited any appreciable water absorbance except for the 6% VF of titania in LDPE composite, which exhibited a mere 0.01% water absorbance. Water absorbance measurements were taken at an accuracy of two decimal places, so the 0.01% water absorbance value for 6% VF TiO_2 in LDPE composite may be due to weight measurement errors (0.01% is equivalent to 1 part in 10,000).

Table 2.2   Density and water absorbance of the two composites

% Volume fraction of filler	Alumina filled LDPE composite		Titania filled LDPE composite	
	Density (gm/cc)	Water absorbance (%)	Density (gm/cc)	Water absorbance (%)
0	0.91	0	0.911	0
1	1.05	0	0.916	0
2	1.18	0	0.923	0
3	1.25	0	0.927	0
4	1.31	0	0.931	0
5	1.41	0	0.936	0
6	1.52	0	0.941	0.01

Adaptation of different patch geometries to achieve broadband operation of microstrip antenna on customized composite material in X-band

23

2.4.2 Thermal property studies

Effective thermal properties of composite materials depend on the intrinsic microscopic properties of the filler dielectric, homogeneity of distribution and compactness of filler in the matrix [17, 18].

2.4.2.1 Design of modified Lee's method to measure thermal conductivity

Heat transfer in particulate composites takes place via the polymer-filler interface, giving rise to an enhanced thermal conductivity with the increase in number of reinforced particles. There are different techniques for thermal conductivity measurements in insulators. Lee's method is the most popular one, but it suffers from the need of bulky steam system for heating and high possibility of radial heat flow. The set up is indigenously designed and fabricated in the laboratory by using more robust components: guarded hot plate, solid state transducer and amplifier for acquiring data. The theory of the instrument is based on Lee's method.
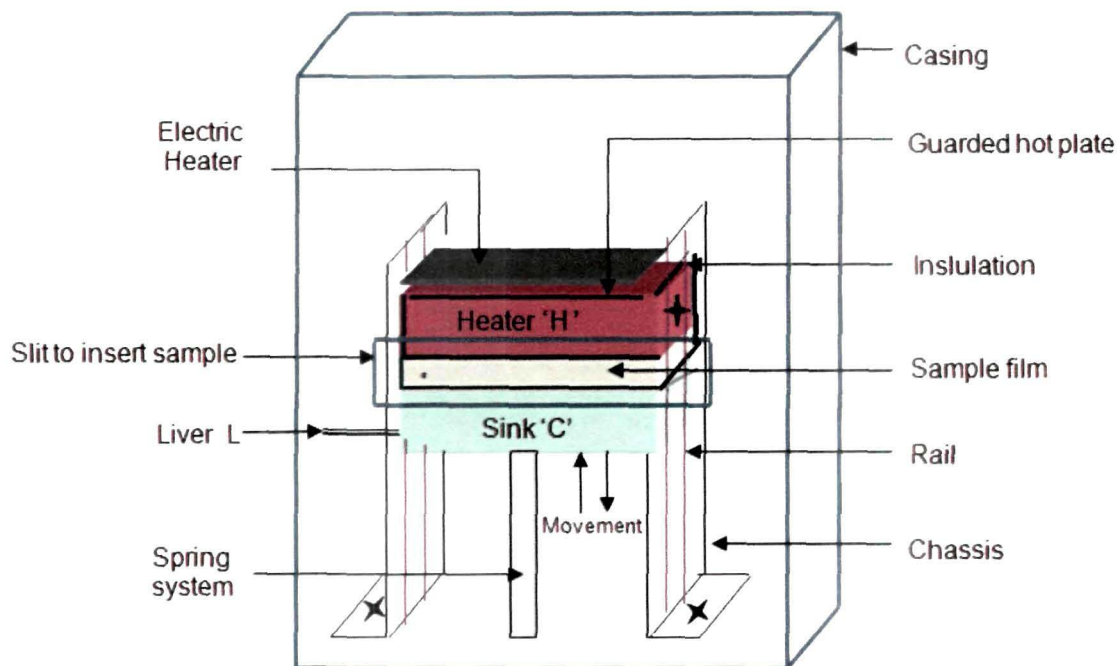
Figure 2.7   Schematic diagram of thermal conductivity measurement set-up

Adaptation of different patch geometries to achieve broadband operation of microstrip antenna on customized composite material in X-band

24

The instrument consists of two brass slabs where one acts as heat source and other as sink. The sample to be tested is placed between the source and the sink. The exposed portion of the source and sink is covered with heat insulating-seal to ensure no radial heat flow. A thermostatic electric heater is used to heat the source and sink is kept at room temperature. A spring system is attached to the other end of sink to ensure good contact between source, sample and sink with the advantage of easy placement of the sample. A non-conducting casing is used for mounting the system. The schematic diagram of the instrument is shown in figure 2.7.

Temperature of the slabs is measured using a transistor as a transducer element. It works based on Peltier effect. The system can measure both absolute and relative temperatures of the slabs using a switch. The area of sample is kept same as the area of the slab. The source is heated and heat conducts through the sample to the sink. The rate at which heat (Q) conducts through the specimen is equal to the rate at which the sink losses heat and is given by,

$$Q = \frac{KA(\theta_1 - \theta_2)}{d} \tag{2.5}$$

where,

K is the coefficient of thermal conductivity of the specimen

A is the area of sample

d is the thickness of sample

θ_1 and θ_2 are temperatures of the source and sink at steady state

If M is the mass of the slab, 'S' is specific heat of the slab material, the rate of cooling of the sink at θ_2 is

Adaptation of different patch geometries to achieve broadband operation of microstrip antenna on customized composite material in X-band

25

$$Q = MS\left(\frac{d\theta}{dt}\right)_{\theta=\theta_2}$$ (2.6)

where, $d\theta/dt$ is the time rate of fall of temperature at θ_2

From equation 2.5 and 2.6

$$\frac{KA(\theta_1 - \theta_2)}{d} = MS\left(\frac{d\theta}{dt}\right)_{\theta=\theta_2}$$ (2.7)

$$K = \frac{dMS\left(\frac{d\theta}{dt}\right)_{\theta=\theta_2}}{A(\theta_1 - \theta_2)}$$ (2.8)

The rate of cooling is found by heating the sink to a temperature above θ_2. The sample is then placed between the source and sink and source is heated. The temperature of the source is allowed to reach an equilibrium temperature with the sink. The time of fall of temperature (t), of the sink is noted at regular intervals. The slope of the tangent drawn to this plot gives the value of rate of fall of temperature.

2.4.2.2 Coefficient of thermal expansion measurement set up

Thermal expansion coefficients of the prepared samples are measured with Comparator method. The experimental setup, developed in the laboratory is shown in figure 2.8. The setup consists of a glass cavity containing inlet and outlet for steam. A glass rod is used as holder to place the sample inside the cavity. A thermometer is placed near the sample to measure its temperature. A traveling microscope of least count 0.01 mm monitors the change in dimension of the sample.

The length of the sample is made manifolds than the cross sectional dimensions so as the change can be taken linearly. Prior to placing the sample the change in length of the glass for the same increase in temperature is

Adaptation of different patch geometries to achieve broadband operation of microstrip antenna on customized composite material in X-band

26

observed which is found to be negligible as compared to the change in the sample length.
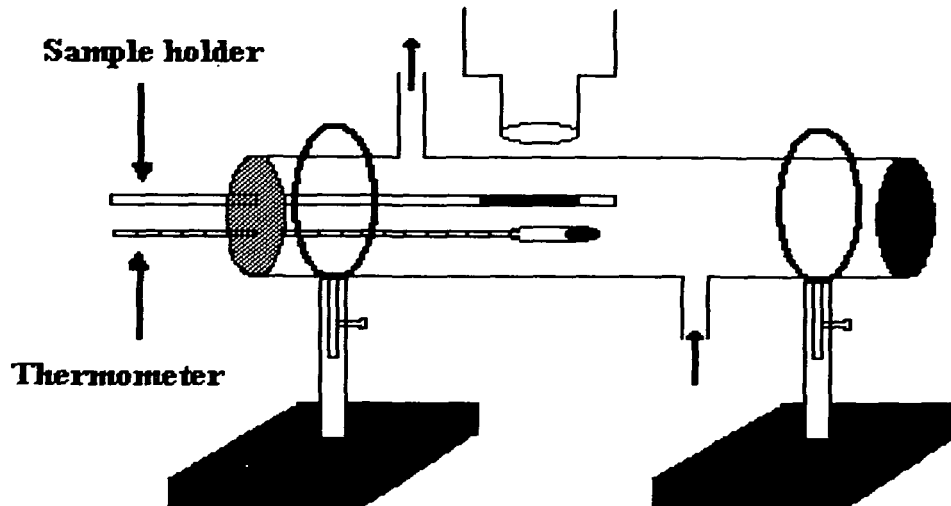
Figure 2.8   Setup for measurement thermal expansion coefficient

The initial length of the sample is L_1 (say) at room temperature, t_1 °C. After passing steam at 100 °C through the cavity the temperature reaches steady value (t_2 °C) and the new linear dimension is L_2. The thermal expansion coefficient (α) can be determined as

$$\alpha = \frac{L_2 - L_1}{L_1 \times (t_2 - t_1)} \text{ per °C.}$$

2.4.2.3 Thermal conductivity and coefficient of thermal expansion measurement

        results

The thermal conductivity and thermal expansion coefficient of the prepared samples measured with the above two techniques are shown in figures 2.9 and 2.10, respectively.

Adaptation of different patch geometries to achieve broadband operation of microstrip antenna on customized composite material in X-band

27
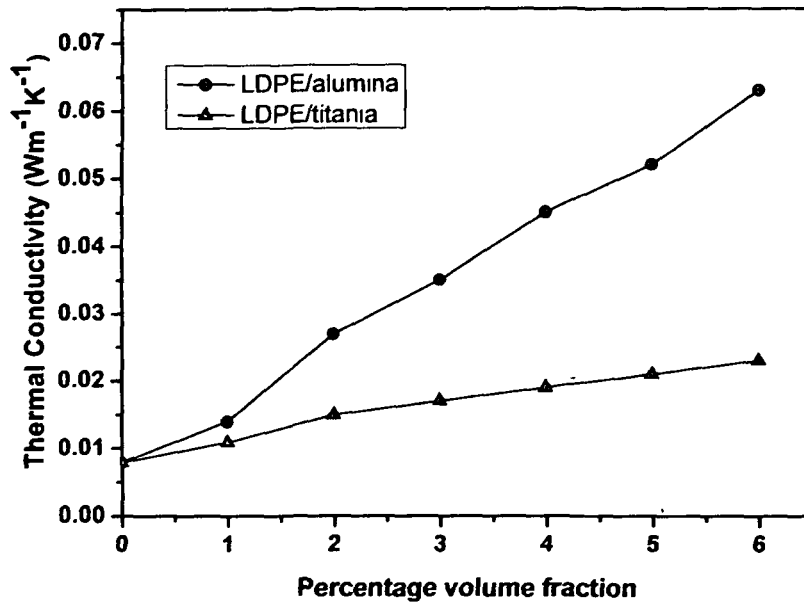
Figure 2.9   Thermal conductivity of developed composites
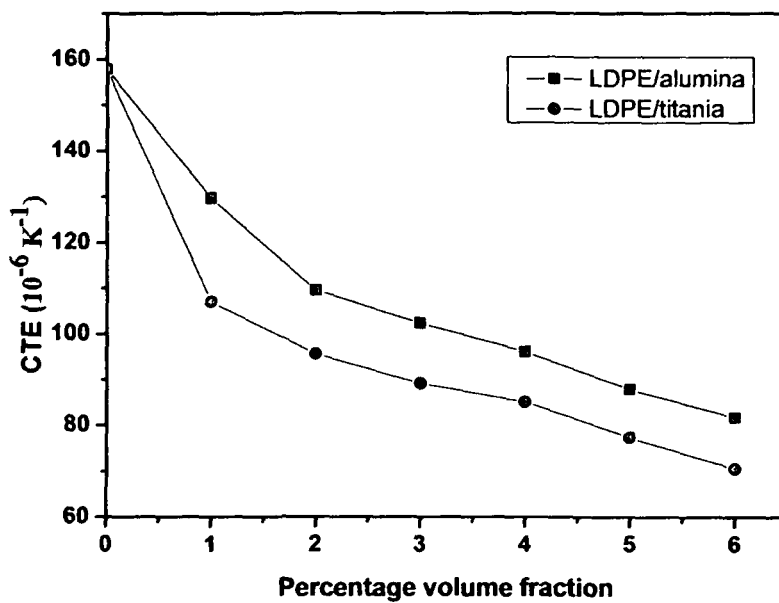
Figure 2.10   Coefficient of thermal conductivity of developed composite

2.5 MICROWAVE CHARACTERIZATION OF THE COMPOSITES

Broadband antenna applications make it essential to measure the complex permittivity of materials over a wide range of frequencies. It helps in determining important characteristics such as edge impedance, feed point location etc. The complex effective permittivity depends on the permittivity of

Adaptation of different patch geometries to achieve broadband operation of microstrip antenna on customized composite material in X-band

28

each constituent in the composite matrix, the volume fraction of inclusions and eventually on the spatial arrangement in the mixture [22-25]. Most accurate method is the cavity perturbation method which is a resonant method, but has the limitation of single frequency operation [28, 29]. Broadband characterization of the dielectric properties of material is possible using nonresonant methods. Nicolson and Ross developed a transmission/reflection technique for obtaining the complex permittivity of linear materials over a broad range of microwave frequencies. Both these techniques are adopted to determine the complex permittivity of the composites.

2.5.1 Measurement of complex permittivity using cavity perturbation technique

A TE$_{103}$ cavity is designed at 9.68 GHz to measure the complex permittivity of the composites. An iris is used to couple the oscillations excited within the cavity with outside microwave measurement system as shown in figure 2.11(a). The diameter of iris hole for critical coupling in the cavity is found to be 8.42 mm. The quality factor (Q) of the cavity is obtained by sweeping the cavity in the frequency range 8.2 GHz to 12.4 GHz using Agilent E8362C VNA as shown in figure 2.11(b).
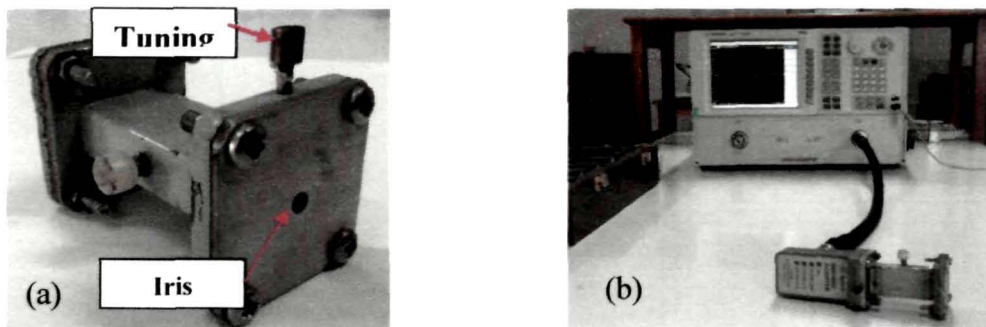
Figure 2.11   (a) A TE$_{103}$ rectangular resonant cavities with tuning screw and iris hole
(b) Cavity perturbation measurement of complex permittivity

A tuning screw is used to compensate for any mismatch due to loading, causing shift in the resonant frequency of the cavity (figure 2.11). The Q of the cavity is calculated using the formula given as

Adaptation of different patch geometries to achieve broadband operation of microstrip antenna on customized composite material in X-band

29

$$Q = \frac{\text{Re}sonant\ frequency}{3dB\ band\ width} = \frac{f_r}{(f_2 - f_1)} \qquad (2.9)$$

f_2 and f_1 are the frequencies corresponding to 3 dB point, such that $f_2 > f_1$ and f_1 is the resonant frequency. The Q for the TE_{103} reflection cavity is experimentally found to be 1833.52.

The composite sample of dimension 1 mm^3 sizes is inserted into the TE_{103} cavity at the maximum electric field position using a Teflon sample holder. The 1 mm^3 sample is cut from a composite sheet of thickness 1 mm. The composite sheet is initially moulded with a thickness of 1mm. The sample sheet is placed on a polished steel plate and pressed using a special arrangement with a 0.9 mm × 0.9 mm flat steel piece. The arrangement is mounted on a milling machine and the sides cut by a sharp surgical blade mounted on a cutter mount of the milling machine with least count 0.02 mm. The cutting is carried out by moving the X axis bed of the machine and then the sample rotated each time by 90° to cut the other three sides one by one. The dimensions were checked using slide calipers (Mitutoyo) of least count 0.001cm.

On insertion of the samples, the resonant frequency of empty cavity and Q factor alters due to change in the overall capacitance and conductance of the cavity without perturbing the inductance. If f_1 and f_0 are the resonant frequencies with and without the samples, the real (ε_r') and imaginary part of permittivity (ε_r'') are given by,

$$\varepsilon_r' = 1 + \frac{f_0^2 - f_1^2}{f_1^2} \frac{V_c}{4V_s} \qquad (2.10)$$

$$\varepsilon_r'' = \frac{V_c}{4V_s} \left[\frac{f_0^2}{f_1^2} \left(\frac{1}{Q_1} - \frac{1}{Q_0} \right) \right] \qquad (2.11)$$

where, V_s is the volume of the sample, V_c is the volume of the cavity, Q_1, Q_0 are the respective quality factors of the cavity with and without the sample. Through this technique microwave characterization can be done for only one frequency corresponding to resonant frequency of the cavity.

Adaptation of different patch geometries to achieve broadband operation of microstrip antenna on customized composite material in X-band

30

Measured results of real and imaginary part of complex permittivity of different composites are shown in figure 2.12 and figure 2.13, respectively.
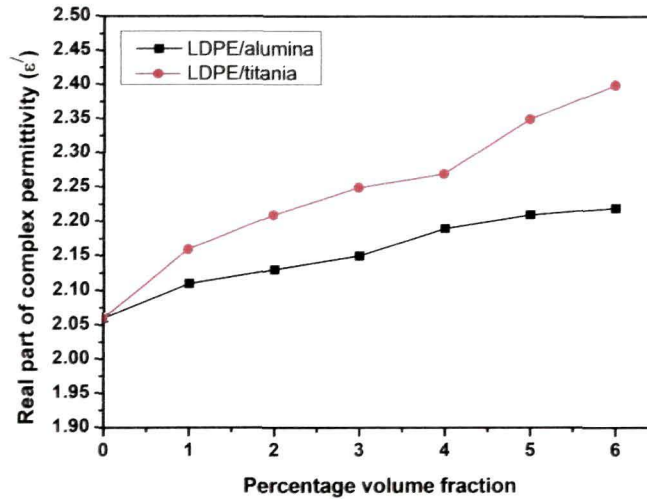
Figure 2.12 Real part of complex permittivity of developed composite determined using cavity perturbation method
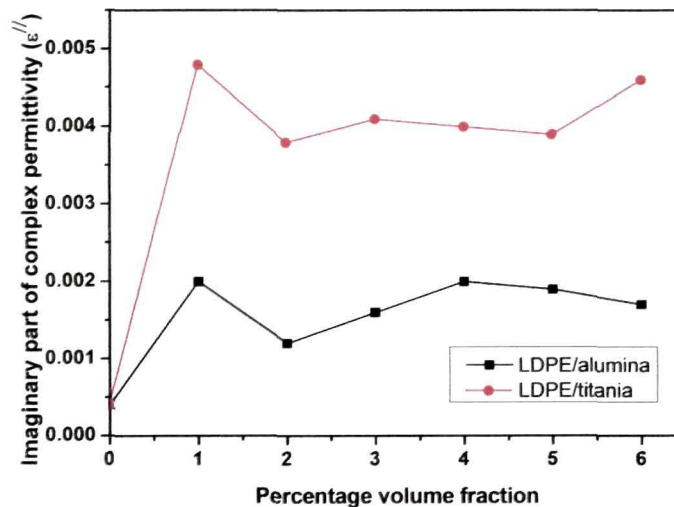
Figure 2.13 Imaginary part of complex permittivity of developed composite determined using cavity perturbation method

2.5.2 Measurement of complex permittivity using Nicolson-Ross technique

The working principle of Nicholson-Ross method [31-33] is based on transmission/reflection method. Figure 2.14 shows a typical measurement configuration for a transmission/reflection method. A sample of rectangular

Adaptation of different patch geometries to achieve broadband operation of microstrip antenna on customized composite material in X-band

31

shape with permittivity $\varepsilon = \varepsilon_0 \varepsilon_r$ and permeability $\mu = \mu_0 \mu_r$ is inserted into a segment of transmission line with characteristic impedance Z_c. Let d and Z be the thickness and the new characteristic impedance of the segment in which the material is installed.
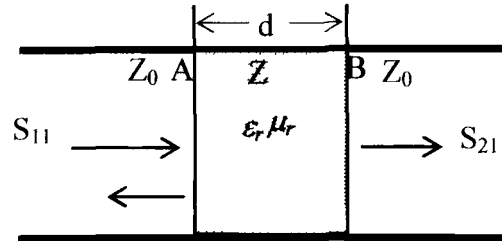
Figure 2.14   A schematic diagram of transmission/reflection method with rectangular shape material inserted

The characteristic impedance $Z=\sqrt{\mu_r/\varepsilon_r}\,Z_0$ where μ_r and ε_r are complex quantities if the material is lossy in nature. For an infinite thickness d the reflection coefficient of the microwave at the air-sample interface (A) is given as,

$$\Gamma = \frac{Z - Z_0}{Z + Z_0} = \frac{\sqrt{\dfrac{\mu_r}{\varepsilon_r}} - 1}{\sqrt{\dfrac{\mu_r}{\varepsilon_r}} + 1} \tag{2.12}$$

If the thickness d is finite, the transmission coefficient through the segment AB is given as

$$T = \exp\left[-j\left(\frac{\omega}{c}\right)\sqrt{\mu_r \varepsilon_r}\, d \right] \tag{2.13}$$

The scattering coefficient S_{21} and S_{11} of the slabs are given as

$$S_{21}(\omega) = \frac{(1 - \Gamma^2)T}{1 - \Gamma^2 T^2} \tag{2.14}$$

$$S_{11}(\omega) = \frac{(1 - T^2)\Gamma}{1 - \Gamma^2 T^2} \tag{2.15}$$

Let

$$V_1 = S_{21} + S_{11} \tag{2.16}$$

$$V_2 = S_{21} - S_{11} \tag{2.17}$$

If $\qquad X = \dfrac{1 - V_1 V_2}{V_1 - V_2}$ $\hfill$ (2.18)

Then using equations (2.14)-(2.18), the reflection coefficient can be found as

$$\Gamma = X \pm \sqrt{X^2 - 1} \hfill (2.19)$$

For equation (2.19), the appropriate sign is chosen such that $|\Gamma| \leq 1$.

Similarly, using equations (2.14)-(2.18), the transmission coefficient T can be found as

$$T = \frac{V_1 - \Gamma}{1 - V_1 \Gamma} \hfill (2.20)$$

Rearranging equation (2.12), let

$$\frac{\mu_r}{\varepsilon_r} = \left(\frac{1 + \Gamma}{1 - \Gamma}\right)^2 = c_1 \hfill (2.21)$$

Rearranging equation (2.13), let

$$\mu_r \varepsilon_r = -\left[\frac{c}{wd}\ln\left(\frac{1}{T}\right)\right]^2 = c_2 \hfill (2.22)$$

From equations (2.21) and (2.22),

$$\varepsilon_r = \sqrt{\frac{c_2}{c_1}} \hfill (2.23)$$

$$\mu_r = \sqrt{c_1 c_2} \hfill (2.24)$$

Right-hand side of equation (2.23) and (2.24) are complex term. Separating real and imaginary parts, the complex permittivity and permeability values can be obtained.

The measurement set up for X-band permittivity characterization consists of an Agilent E8362C vector network analyzer, Agilent WR-90 X11644A rectangular waveguide line. Using the S parameter results obtained from the VNA, Agilent 85071E software calculates the complex permittivity and permeability for the composites.

Adaptation of different patch geometries to achieve broadband operation of microstrip antenna on customized composite material in X-band

33

The set up for measuring the complex permittivity and permeability of the materials in X-band is shown in figure 2.14. Prior to measurements, the system is calibrated using Thru–Reflect–Line (TRL) method.
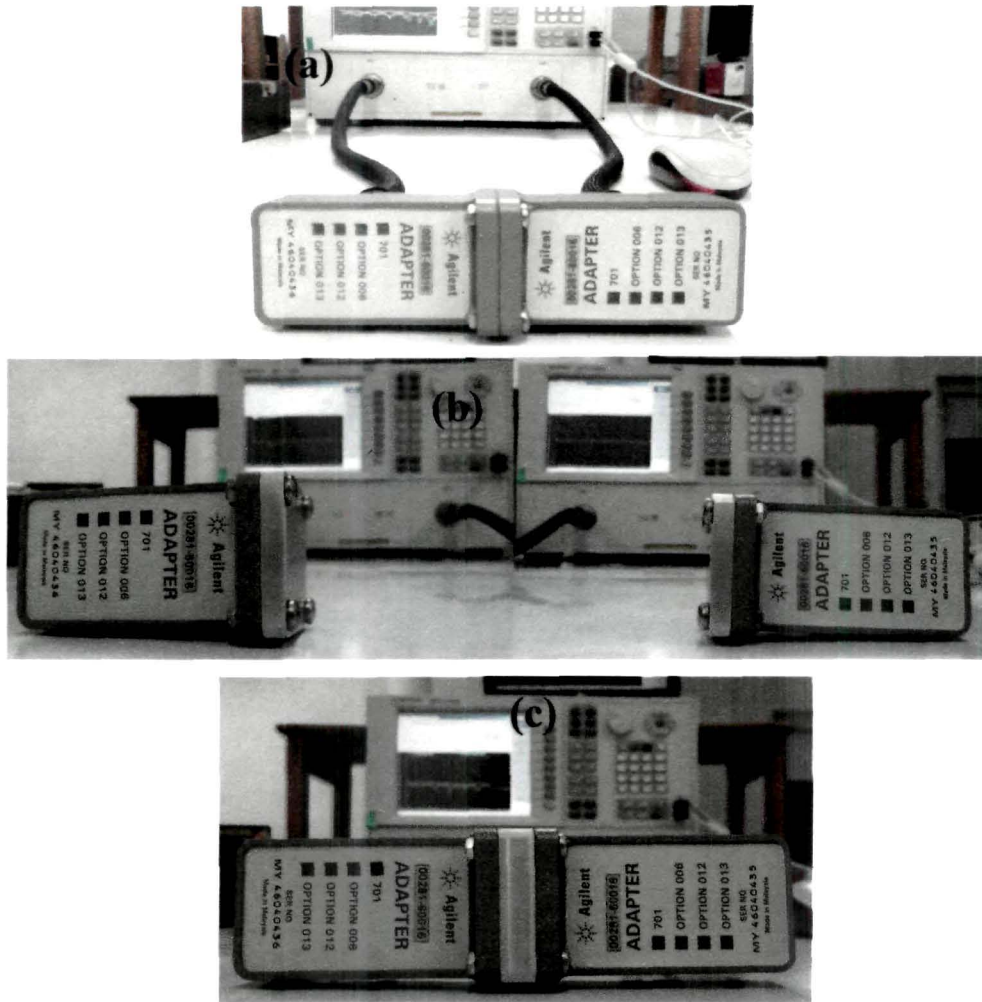
Figure 2.15   TRL calibration using Agilent WR90-X11644A calibration kit
(a) Thru-calibration, (b) reflect-calibration and (c) Line-calibration

In thru calibration, the two ports are connected directly at the desired reference plane as shown in figure 2.15 (a), whereas for reflect calibration, the ports are terminated with a load such that high reflection occurs (figure 2.15 (b)). The two ports are connected by a quarter wavelength segment in line calibration (figure 2.15 (c)). After TRL calibration, the composite sample of dimension 10.38 mm x 22.94 mm x 3.7 mm is inserted in the sample holder of length 9.78 mm and the complex permittivity and

Adaptation of different patch geometries to achieve broadband operation of microstrip antenna on customized composite material in X-band

34

permeability are measured. Measured complex permittivities of the composite materials are shown in figure 2.16 to 2.19.
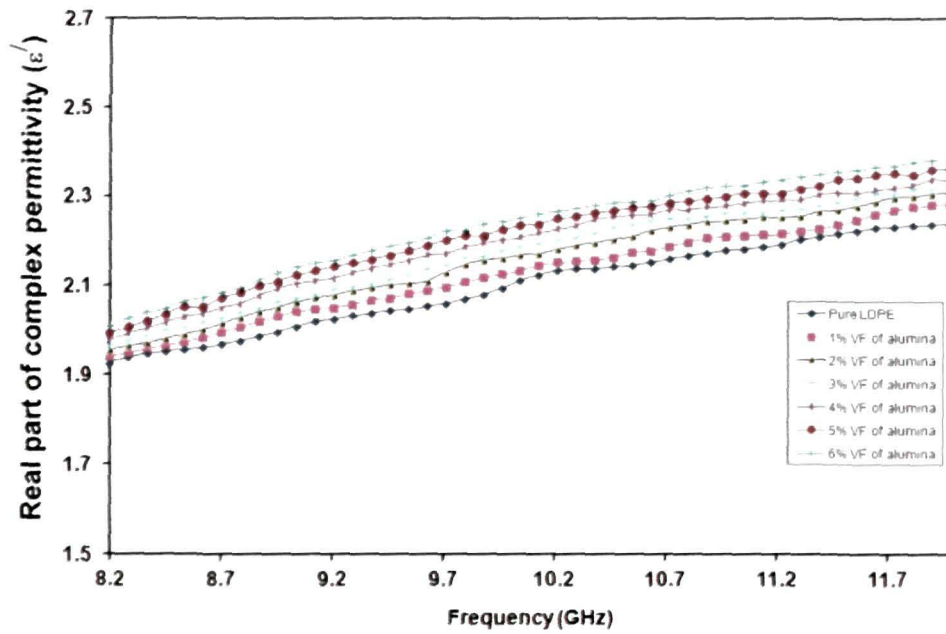
Figure 2.16   Real part of permittivity of LDPE/alumina composite
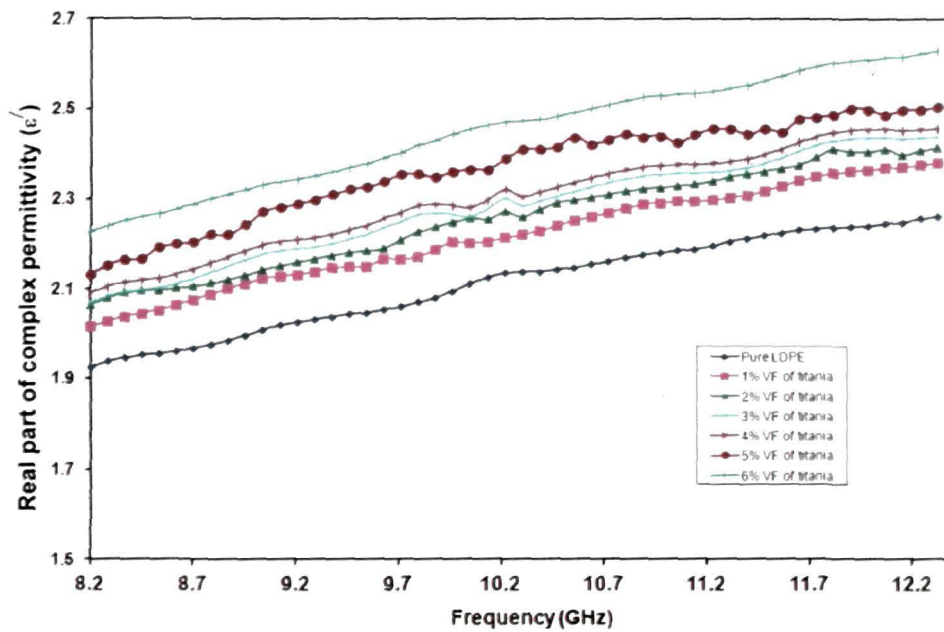
Figure 2.17   Real part of permittivity for LDPE/titania composite

Adaptation of different patch geometries to achieve broadband operation of microstrip antenna on customized composite material in X-band

35
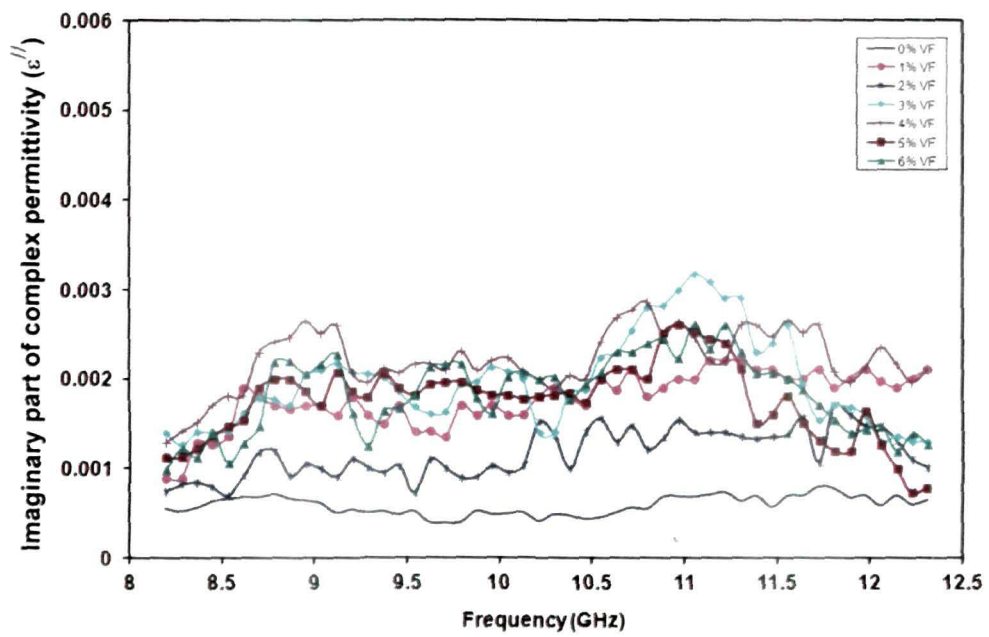
Figure 2.18   Imaginary part of permittivity for LDPE/alumina composite
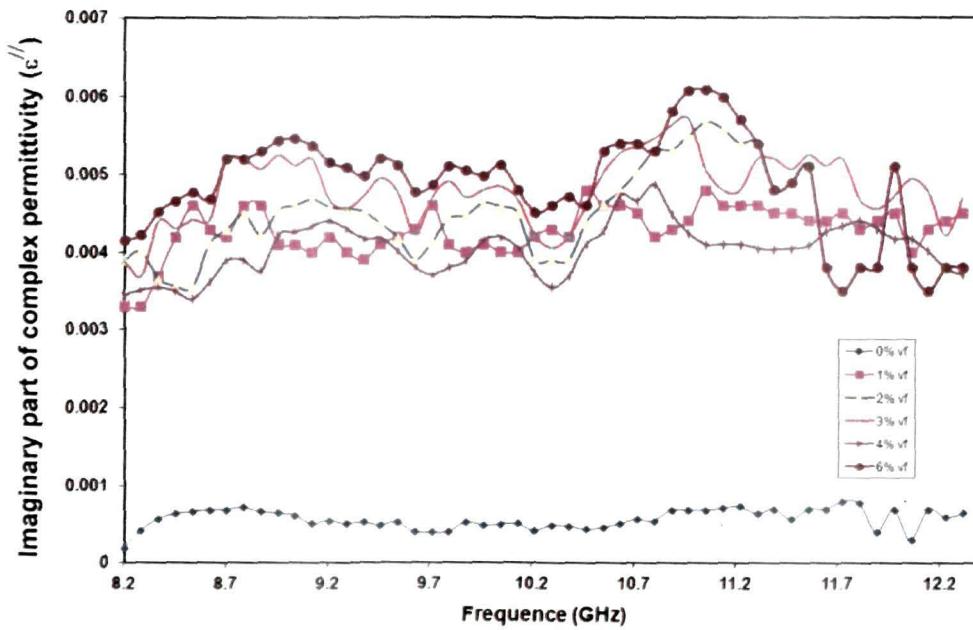
Figure 2.19   Imaginary part of permittivity for LDPE/titania composite

Adaptation of different patch geometries to achieve broadband operation of microstrip antenna on customized composite material in X-band

36

2.5.3 Comparison of measured complex permittivity using cavity perturbation technique and Nicolson-Ross technique

The measured values of real and imaginary parts of all the composites are determined using both techniques and compared at 9.68 GHz. The values show good agreement with each other.

Table 2.3   Comparison of real and imaginary part of complex permittivity for LDPE/alumina composite at 9.68 GHz

% Volume	Cavity Perturbation Technique		Nicolson-Ross Technique	
fraction of filler	$\varepsilon/$	$\varepsilon//$	$\varepsilon/$	$\varepsilon//$
0	2.06	0.0004	2.061	0.0004
1	2.11	0.002	2.109	0.0018
2	2.13	0.0012	2.127	0.001
3	2.15	0.0016	2.147	0.0017
4	2.19	0.002	2.188	0.0022
5	2.21	0.0019	2.209	0.0019
6	2.22	0.0017	2.215	0.0018

Table 2.4   Comparison of Real and imaginary part of complex permittivity for LDPE/titania composite at 9.68 GHz

% Volume	Cavity Perturbation Technique		Nicolson-Ross Technique	
fraction of filler	$\varepsilon/$	$\varepsilon//$	$\varepsilon/$	$\varepsilon//$
0	2.06	0.0004	2.061	0.0004
1	2.16	0.0048	2.162	0.0041
2	2.21	0.004	2.208	0.0045
3	2.25	0.0041	2.255	0.0048
4	2.27	0.0038	2.273	0.0042
5	2.35	0.0039	2.347	0.0047
6	2.4	0.0046	2.398	0.0051

2.6 DISCUSSION AND CONCLUSIONS

LDPE/titania and LDPE/alumina composite materials for microstrip antenna substrate applications are successfully fabricated and analyzed. Microstructural analysis reveals that the particulate inclusions are homogenously distributed in the host matrix and are sufficiently isolated from

---

Adaptation of different patch geometries to achieve broadband operation of microstrip antenna on customized composite material in X-band

37

each other. Polymer composite systems show enhanced thermal conductivity and thermal dimensional stability with the increase in filler percentage. The sizes of the reinforced particles are much smaller than the probing wavelength (~3 cm in the present investigation) hence, the scattering losses that may occur, can be assumed to be negligible therefore the permittivity of the materials depends mainly on the volume fraction of the inclusions and dielectric properties of the parent materials.

Table 2.5   Comparison of properties of few conventional substrate materials with the developed composites

Material	$\varepsilon/$ (at 10 GHz)	$\varepsilon//$ (at 10 GHz)	Thermal conductivity (W/cmK)	Coefficient of thermal expansion	Water absorbance (%)
PTFE*	3.01	0.0013	0.51	17-40	<0.1
RT-Duroid*	6.15	0.0027	0.49	34-120	0.05
Glass Epoxy*	3.38	0.0021	0.71	46	0.06
2 % VF of titania in LDPE**	2.23	0.0036	0.027	109.65	0
2% VF of alumina in LDPE**	2.14	0.0011	0.015	95.7	0

*Hall, P.S. and James, J.R., *Handbook of Microstrip Antennas*, (London, Peter Peregrinus Ltd. 1989)

**Measured values

Complex permittivity studies of the composite material shows that the permittivity of the material can be tailored by varying the content of particulate inclusions. The permittivity values of the composite show that the material can be used as substrates for microstrip antennas in X band.

Referring to the table 2.7, it can be seen that the developed composite substrate materials have dielectric properties comparable to those of the commercially available substrates. It is worth mentioning that the loss component ($\varepsilon/$) is in fact lower for LDPE/alumina composite, while for

Adaptation of different patch geometries to achieve broadband operation of microstrip antenna on customized composite material in X-band

38

LDPE/titania composite it is only marginally higher. The particulate composites provide an advantage of tailoring the properties to desired requirements, by varying the content of inclusions. These tailored composites can be efficient substitutes to conventional substrates like Glass Epoxy, PTFE etc.

Adaptation of different patch geometries to achieve broadband operation of microstrip antenna on customized composite material in X-band

39

References

1. Murthy, V. R. K., Sunderam, S. and Viswanathan, B., *Microwave Materials*, (Delhi, Narosa Publishing House, 1990).

2. Bahl, I. and Ely, K., Modern Microwave Substrate Materials, *Microwave Journal*, **33**, 131 (1990).

3. Traut, G. R., Clad Laminates of PTFE Composites for Microwave Antennas, *Microwave Journal*, **23**, 47 (1980).

4. Hall, P.S. and James, J.R., *Handbook of Microstrip Antennas*, (London, Peter Peregrinus Ltd. 1989).

5. Donnet, J. B., Bansal, R. C., and Wang, M. J., *Carbon Black, Science and Technology*, (Florida, CRC press, 1983).

6. Deka, Juti R. and Bhattacharyya, N. S., Microwave characterization of alumina filled polystyrene composite, *Proc. 2nd IASTED Int. Conf. Antennas, Radar, and Wave Propagat.*, Banff, Alberta, Canada, (2005).

7. Molefi, J. A., Luyt, A. S., Krupa, I., Comparison of LDPE, LLDPE and HDPE as matrices for phase change materials based on a soft Fischer-Tropsch paraffin wax, *Thermochimica Acta*, **500**, 88–92 (2010).

8. *http://www.dynalabcorp.com/technical_info_ld_polyethylene.asp*

9. Dey, A., De, S., De, A. and De, S. K., Characterization and dielectric properties of polyaniline nanocomposites, *Nanotechnol.* **15**, 1277 (2004).

10. Singh, P., Babbar, V. K., Razdan, A., Puri, R. K. and Goel, T. C., Complex permittivity, permeability, and X-band microwave absorption of CaCoTi ferrite composites, *J. Appl. Phys.* **87**, 4362-4366 (2000).

11. Chen Y. J., Cao, M. S., Wang, T. H. and Wan, Q., Microwave absorption properties of the ZnO nanowire-polyester composites, *Appl. Phys. Lett.* **84**, 3367-3369 (2004).

12. Lim, K. M., Lee, K. A., Kim, M. C., and Park, C. G., Complex permeability and electromagnetic wave absorption properties of amorphous alloy-epoxy composites, *J. Non-Cryst. Solids.* **351**, 75-83 (2005).

Adaptation of different patch geometries to achieve broadband operation of microstrip antenna on customized composite material in X-band

40

13. Wang J. W., Shen, Q. D., Yang, C. Z., and Zhang, Q. M., High Dielectric Constant Composite of P(VDF–TrFE) with Grafted Copper Phthalocyanine Oligomer, *Macromolecules.* **37**, 2294-2298 (2004).

14. Nan, C. W., Physics of inhomogeneous inorganic materials, *Prog. Mater. Sci.* **37**, 1-116 (1993).

15. Neelakanta, P.S., *Handbook of Electromagnetic Materials: Monolithic and Composite Versions and Their Applications,* (CRC Press, Boca Raton, FL, pp. 133, 1995).

16. Klug, H.P. and Alexander, L.E., *X-ray Diffraction Procedures for Poly Crystalline and Amorphous Materials,* (Chapter 9, Wiley Interscience, New York, 1974).

17. Kulijanin, J., Vučković, M., Čomor, M.I., Influence of CdS-filler on the thermal properties of polystyrene, *Eur. Polym. J.*, **38**, 1659 (2002).

18. Todd, M. G. and Shi, F. G., Characterizing the interphase dielectric constant of polymer composite materials: Effect of chemical coupling agents, *J. Appl. Phys.*, **94**, 4551 (2003).

19. Hong, J. I., Schadler, L. S., Siegel, R. W. and Martensson, E., Rescaled electrical properties of ZnO/Low density polyethylene nanocomposites, *Appl. Phys. Lett.* **82**, 1956 (2003).

20. Sichel, E.K., ed., *Carbon Black- Polymer Composites: the physics of electrically conducting composites,* (New York, M. Dekker, 1982).

21. Mittal, K.L., ed., *Silanes and Other Coupling Agents,* (Utrecht the Netherlands Adhesion Society, VSP, 2, 2000).

22. Duncan M. Price, Mark Jarratt, Thermal conductivity of PTFE and PTFE composites, *Proc. 28th Conf. North Am. Thermal Analysis Soc.*, Orlando, Florida, 579 (2000).

23. Sareni, B., Krahenbuhl, L., Beroual, A. and Brosseau, C., Complex effective permittivity of a lossy composite material, *J. Appl. Phys.*, **80**, 4560 (1996).

Adaptation of different patch geometries to achieve broadband operation of microstrip antenna on customized
composite material in X-band

41

24. Sareni, B., Krahenbuhl, L., Beroual, A. and Brosseau, C., Effective dielectric constant of random composite materials, *J. Appl. Phys.*, **81**, 2375 (1997).

25. Todd, M. G. and Shi, F. G., Molecular basis of the interphase dielectric properties of microelectronic and optoelectronic packaging materials, *IEEE Trans. Compon. Packag. Technol.*, **26**, 667 (2003).

26. Jarvis, J. B., Geyer, R. G., Grosvenor, Genezic, M. D., Jones, C. A., Riddle, B., Weil, C. M., and Krupka, J., Dielectric characterization of low-loss materials: A comparison of technique, *IEEE Trans. Dielectr. Electr. Insul.*, **5**, 571 (1998).

27. Budinski, K.G., and Budinski, M.K., *Engineering Materials Properties and Selection* (Pearson Prentice Hall, 2006).

28. Carter, R. G. Accuracy of microwave cavity perturbation measurements, *IEEE Trans. Microw. Theory Tech.* **49**, 918-923, 2001.

29. Chao, S. H. Measurements of microwave conductivity and dielectric constant by the cavity perturbation method and their errors, *IEEE Trans. Microw. Theory Tech.* **33**, 519-526, 1985.

30. Krupka, J. Frequency domain complex permittivity measurements at microwave frequencies, *Meas. Sci. Technol.* **17**, 55-70, 2006.

31. Nicolson, A.M., and Ross, G.F. Measurement of the intrinsic properties of materials by time-domain techniques, *IEEE. T. Instrum. Meas.* **19**, 377-382, 1970.

32. TRL/LRM Calibration, Agilent E5070B/E5071B ENA Series RF Network Analyzers, 1st Edition, Agilent Technologies, No. 16000-95026, Japan, 2004

33. Engen, G. F., and Hoer, C. A. Thru-reflect-line: An improved technique for calibrating the dual six-port automatic network analyzer, *IEEE Trans. Microw. Theory Tech.* **27**, 987-993, 1979.

Adaptation of different patch geometries to achieve broadband operation of microstrip antenna on customized composite material in X-band

42

CHAPTER III

RECTANGULAR PATCH ANTENNA ON SINGLE LAYER AND GRADED COMPOSITE SUBSTRATE

3.1 Introduction

3.2 Design and Fabrication of Rectangular Patch Microstrip Antenna

3.2.1 Design formulation of rectangular patch

3.2.2 Determination of feed point

3.2.3 Software for numerical simulation

3.3 Antenna Performance Measurement Set up

3.3.1 S_{11} measurement set up

3.3.2 Radiation pattern measurement set up

3.3.3 Calculation of Directivity

3.4 Fabrication and Measurement of Rectangular Patch Microstrip Antenna on Single Layer Composite Substrate

3.4.1 Preparation of substrate for microstrip antenna

3.4.2 Fabrication of microstrip patch antenna

3.4.3 S_{11} parameter and radiation pattern studies for rectangular patch antenna

3.5 Design and Fabrication of Rectangular Patch Microstrip Antenna on Graded Composite Substrate

3.5.1 Fabrication of graded composite substrate

3.5.2 Design of rectangular patch antenna on graded composite substrate

3.5.3 S_{11} and radiation pattern measurement for the rectangular patch antenna on graded substrate

3.6 Conclusions

References

3.1 INTRODUCTION

This chapter describes studies on the developed composite materials for their applicability as substrates for microstrip antennas. Rectangular patch is the simplest geometry to design [1-5] and hence, a rectangular radiator is designed and analyzed on the composite material. The performance is analyzed by varying the material properties of the composite.

Complex permittivity of substrate material plays a critical role in antenna operation. By varying the substrate permittivity, one can control the size of the radiator and radiation performance of microstrip antennas [13-18]. Substrate material with low permittivity may be used to increase the bandwidth of operation, but very low permittivity material increases the dimensions of the microstrip patch antenna (MPA), which poses difficulty for use in handheld devices. Increase in permittivity of the substrate material increases the Q of the antenna and hence its impedance bandwidth is reduced [3, 10]. With a view to increase the bandwidth and directivity of operation of rectangular patch antenna without increasing the complexity in design and patch dimensions, substrate grading is investigated. This may also suppress the surface wave propagation.

3.2 DESIGN AND FABRICATION OF RECTANGULAR PATCH MICROSTRIP ANTENNA

Rectangular patch antennas are designed using transmission line model (TLM) [7-9]. The dimensions of the radiating patch can be estimated using this technique.

3.2.1 Design formulation of rectangular patch

TLM represents the microstrip antenna as two slots of width W and height h, separated by a transmission line of length L [7-9] as shown in figure 3.1 (a). The dielectric constant, ε_r (real part of complex permittivity) is an important parameter in calculating these two dimensions.

Adaptation of different patch geometries to achieve broadband operation of microstrip antenna on customized composite substrate in X-band

The value of effective dielectric constant ε_{reff} can be expressed as [10]:

$$\varepsilon_{reff} = \frac{\varepsilon_r + 1}{2} + \frac{\varepsilon_r - 1}{2}\left[1 + 12\frac{h}{W}\right]^{-\frac{1}{2}} \tag{3.1}$$

where, ε_r stands for dielectric constant of substrate, h represent height of dielectric substrate, and W is the width of the patch.

(a)

(b)   (c)
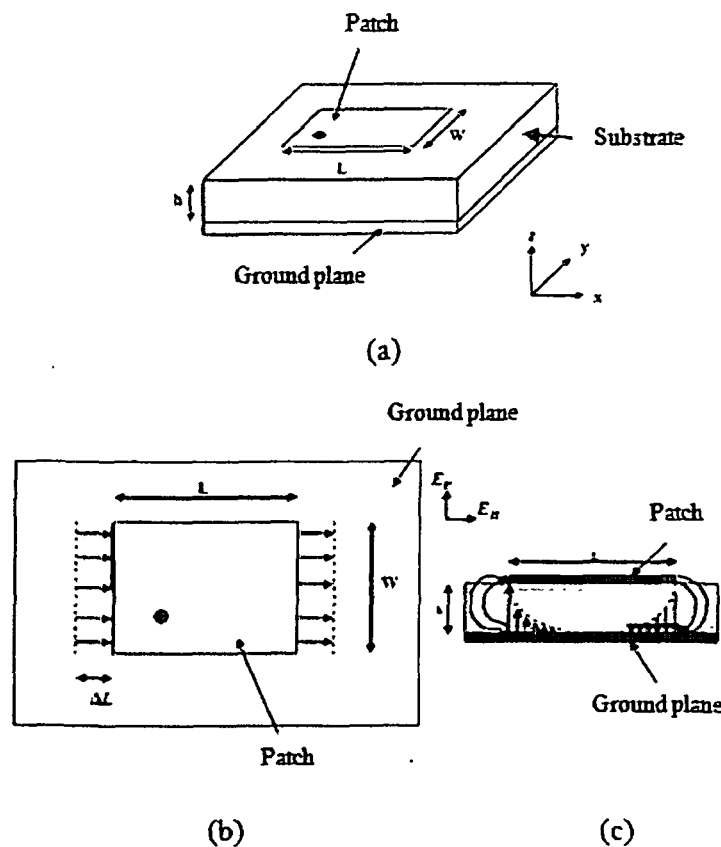
Figure 3.1   (a) Coaxially fed microstrip antenna (b) Top view of the antenna

                (c) Cross sectional view of the antenna

The edges along the width are the two radiating slots, which are 'L' distance apart and excited in phase and radiating in the space above the ground plane. The fringing fields along the width can be modeled as radiating slots and electrically the patch of the microstrip antenna looks greater than its physical dimensions (figure 3.1 (b-c)). The dimensions of the patch along its length have now been extended on each end by a distance ΔL, which is given empirically by Hammerstad [8] as,

Adaptation of different patch geometries to achieve broadband operation of microstrip antenna on customized composite substrate in X-band

44

$$\Delta L = 0.412 \ \frac{\left(\varepsilon_{reff} + 0.3\right)\left(\dfrac{W}{h} + 0.264\right)}{\left(\varepsilon_{reff} - 0.258\right)\left(\dfrac{W}{h} + 0.8\right)} \tag{3.2}$$

The effective length of the patch L_{eff} now becomes,

$$L_{eff} = L + \Delta L \tag{3.3}$$

For a given resonance frequency f_0, the effective length is given in [7] as

$$L_{eff} = \frac{c}{2 f_0 \sqrt{\varepsilon_{reff}}} \tag{3.4}$$

For efficient radiation, the width W can be represented as [9]

$$W = \frac{c}{2 f_0 \sqrt{\dfrac{\varepsilon_r + 1}{2}}} \tag{3.5}$$

The patch dimension is calculated using equations 3.1-3.5. The dimensions are further optimized using numerical simulations to obtain the desired antenna performance.

3.2.2 Determination of feed point

The rectangular patch antenna is fed coaxially at the point where the input impedance is 50 Ω. The location of the feed point can be found out using the two slot model for microstrip antenna [7-12].

The resonant radiation conductance G_r for a patch fed at an edge can be determined from the radiated power as

$$P_r = \frac{1}{2} G_r (E_0 h)^2 = \frac{1}{2} G_r V_0^2 \tag{3.6}$$

$$R_r = \frac{1}{G_r} \tag{3.7}$$

Where, R_r is the radiation resistance.

The expressions for R_r with an estimated accuracy of 10 % average for $h \leq 0.03\lambda_0$ and $\varepsilon_r \leq 5$ can be expressed as,

$$R_r = \frac{V_0^2}{2P_r} = \varepsilon_{reff} \frac{Z_0^2}{120 I_2} \tag{3.8}$$

Adaptation of different patch geometries to achieve broadband operation of microstrip antenna on customized composite substrate in X-band

45

Where, Z_0 is the characteristic impedance of the microstrip line of which the patch is a segment and

$$I_2 = (k_0 h)^2 \left[0.53 - 0.03795 \left(k_0 \, W/2 \right)^2 - 0.03553/\varepsilon_{reff} \right] \tag{3.9}$$

where, $k_0 = 2\pi/\lambda_0$, is the wave number.

If the patch is fed at a distance x_f from one of the radiating edges, the input resistance can be expressed as,

$$R_{in} = R_r \cos^2 \left(\pi x_f / L \right) \tag{3.10}$$

The distance, x_f, is selected such that the value of R_{in} is equal to the feed line impedance, usually taken to be 50 Ω. The y position of the feed can be taken at any point along the width of the patch which is usually taken to be $W/2$.

The approximate dimensions calculated using TLM technique are further optimized using numerical modeling software CST Microwave Studio.

3.2.3 Software for numerical simulation

Computer-aided design (CAD) is emerging as a norm in microstrip antenna design. This is because the use of such softwares helps to reduce development time by serving as a tool in the design process. Another reason is the increase in complexity in designs where accurate prediction of system performance can only be made with the help of CAD software packages.

In this work, CST Microwave Studio is used to model microstrip antenna structures. CST Microwave Studio is a full-featured software package for electromagnetic analysis and design in the high frequency range. It simplifies the process of analyzing the structure by providing a powerful solid 3D modeling. After the component has been modeled, a fully automatic meshing procedure is applied before the simulation process is started. CST Microwave Studio is part of the CST Design Studio Suite.

Since no method works equally well in all the application domains, the software contains four different simulation techniques (transient solver,

Adaptation of different patch geometries to achieve broadband operation of microstrip antenna on customized composite substrate in X-band

46

frequency domain solver, integral equation solver, eigenmode solver) to best fit the particular application. The most flexible tool is the transient solver, which can obtain the entire broadband frequency behavior of the simulated structure from only one computation run (in contrast to the frequency step approach of many other simulators). It is based on the Finite Integration Technique (FIT). All the simulations in this work are done in transient solver mode to cover the entire X-band.

3.3 ANTENNA PERFORMANCE MEASUREMENT SET UP

To analyze the performance of an antenna, S_{11} and radiation pattern measurements are to be carried out on the fabricated antennas. The set ups for measurement are described below.

3.3.1 S_{11} measurement set up

S_{11} measurements are carried out over the X-band using Agilent PNA series vector network analyzer (VNA) E8362C.

Calibration of the VNA is done using Agilent 85052 D calibration kit. The actual reflection coefficient is found from the measured value using equation [13].

$$S_{11M} = E + E_{RT}\left[\frac{S_{11A}}{1 - E_S S_{11A}}\right]$$

(3.11)

Schematic for the measurement is shown in figure 3.2.

E = Directivity
E_{RT} = Reflection tracking
E_S = Source Match
S_{11M} = Measured
S_{11A} = Actual
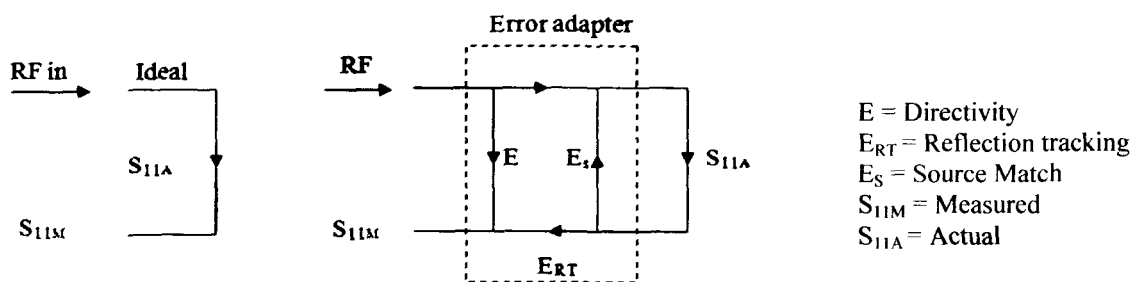
Figure 3.2   Schematic of S_{11} measurement scheme

There are three systematic errors. In order to solve the individual error terms, measurement of three known calibration standards is carried out: a

Adaptation of different patch geometries to achieve broadband operation of microstrip antenna on customized composite substrate in X-band

47

short, an open, and a broad band load (Z_o). Calibrated value is stored in the system and used to solve the equations 3.11 yielding the systematic error terms and this allows deriving the actual S_{11} parameter of the antenna from measurements.

All the antennas for measurement are fed coaxially. The photograph of the measurement system is shown in figure 3.3.

Network
Analyzer

Calibration
Kit

Antenna under
Test
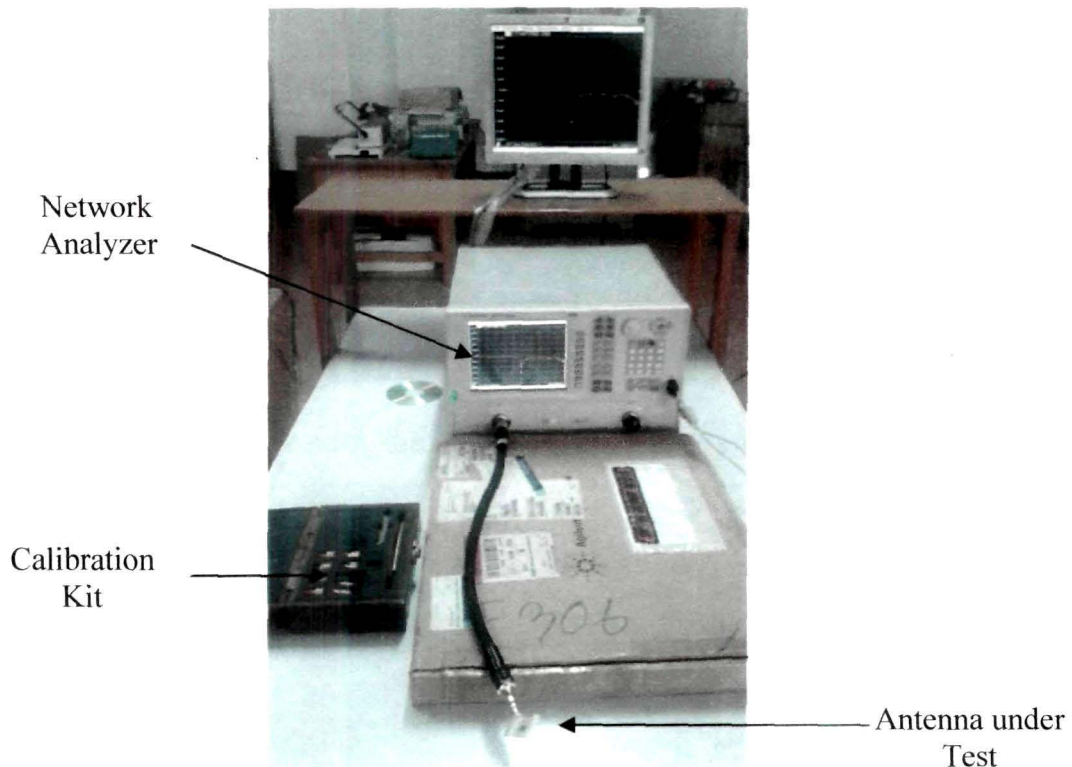
Figure 3.3   Antenna S_{11} measurement set up using VNA

3.3.2 Radiation pattern measurement set up

The E-plane and H-plane radiation pattern measurements are carried out using an automated measurement setup with a PC controlled turn table figure 3.4. An Agilent MXG-N5183A signal generator is used as the source to feed the transmitting X-band horn antenna while the received power from the test antenna mounted on the PC controlled turn table is measured by Anritsu spectrum analyzer. The system is calibrated using two standard horn antenna in receiving and transmitting ends.

Adaptation of different patch geometries to achieve broadband operation of microstrip antenna on customized composite substrate in X-band

48

Radiation pattern measurements are taken in open space so that the effect of reflection of microwave signals from the walls can be avoided.
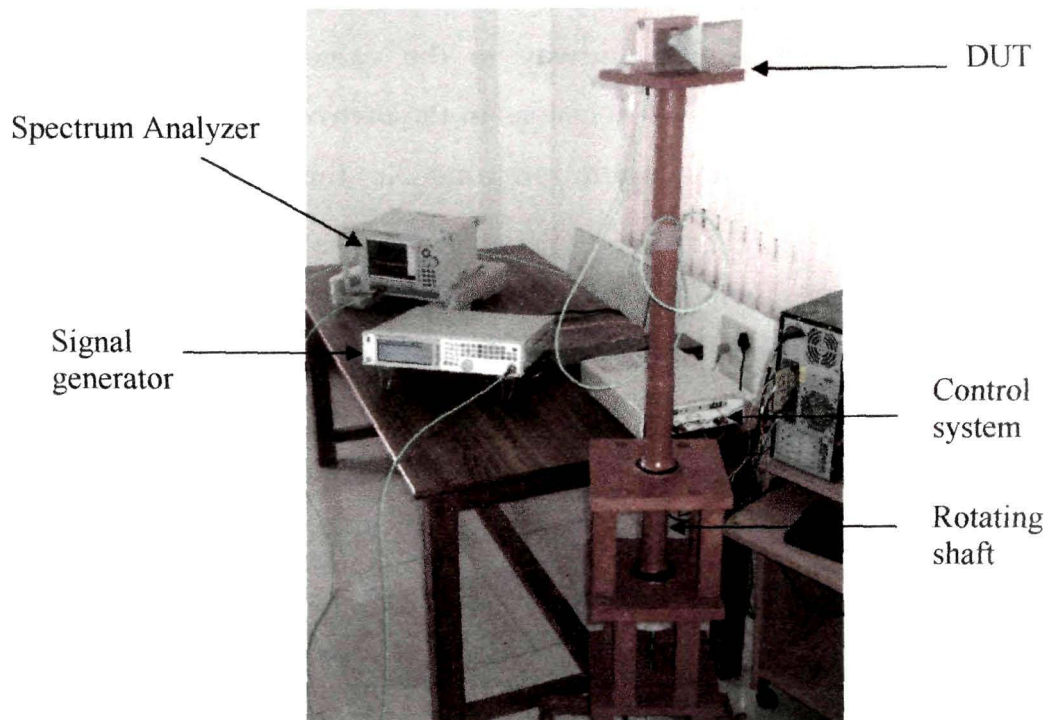
Figure 3.4   Antenna radiation pattern measurement set up

3.3.3 Calculation of Directivity

The directivity (D) is calculated from the radiation pattern as [15],

$$D \approx \frac{32400}{\Theta_{1d}\Theta_{2d}}$$

(3.12)

Where, Θ_{1d} is the half power beamwidth in E-plane and Θ_{2d} is the half power beamwidth in H-plane. D is a unitless quantity and is expressed in dBi as [16],

$$D_{dBi} = 10 \cdot \log_{10}[D]$$

(3.13)

3.4 FABRICATION AND MEASUREMENTS OF RECTANGULAR PATCH MICROSTRIP ANTENNA ON SINGLE LAYER COMPOSITE SUBSTRATE

3.4.1 Preparation of substrate for microstrip antenna

The synthesis process of polymer composite material, described in Chapter II, in the final stage, the material with different VF is casted on a

Adaptation of different patch geometries to achieve broadband operation of microstrip antenna on customized composite substrate in X-band

49

square mold of dimension 4 cm × 4 cm × 2 mm. Rectangular patch antenna is fabricated on 2 % VF of alumina in LDPE and 2 % VF of titania in LDPE composite substrates. The samples are chosen, as the permittivity value of these composites lies almost midway to the values of pure LDPE and composites with 6 % VF of the inclusions in the matrix. Dielectric parameters of the composites and the optimized antenna dimensions are given in table 3.1.

The antennas are fed coaxially at 50 Ω impedance matching point, which is at 2.1 mm from the radiating edge for the microstrip antenna with dimension as given in the table 3.1. Figure 3.5 (b) shows the fabricated antenna on composite substrate. Performance studies of the fabricated antennas are carried out in the X-band of microwave frequencies.

Table 3.1   Optimized Design parameters of rectangular microstrip antenna on LDPE/alumina and LDPE/titania composite substrate at 10 GHz

Substrate	ε'	ε''	f_0 (GHz)	h (mm)	W (mm)	L (mm)
2% VF of alumina in LDPE	2.14	0.0011	10	2	11.9	8.6
2% VF of titania in LDPE	2.23	0.0036	10	2	11.4	8.3
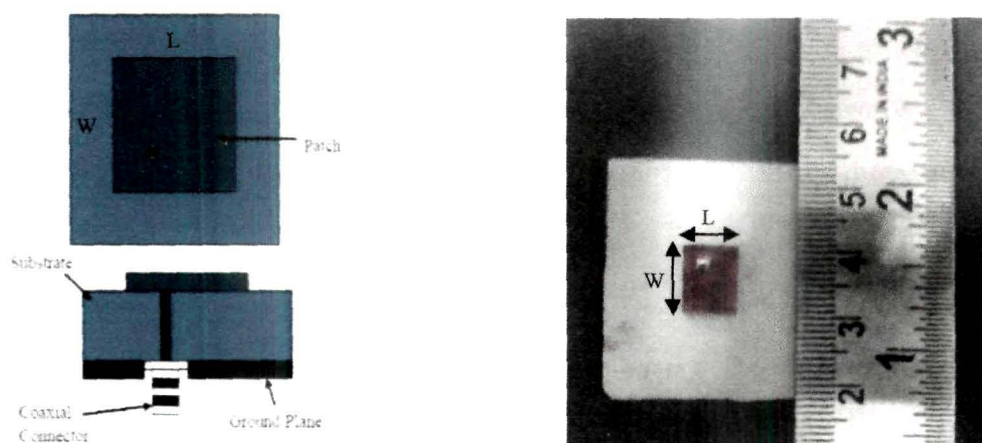
Figure 3.5   (a) Layout of a coaxially fed microstrip antenna

(b) Coaxially fed microstrip antenna fabricated on composite substrate.

Adaptation of different patch geometries to achieve broadband operation of microstrip antenna on customized composite substrate in X-band

50

3.4.2 Fabrication of microstrip patch antenna

Radiating patches of dimensions given in table 3.1 is fabricated on the composite substrates. The fabrication of copper patch on the dielectric composite substrate is performed in two steps by rolling technique [14], as described in the following paragraphs.

In the first step of the process, the substrate is thoroughly cleaned with acetone to remove oil and grime from the surface. Subsequently, the substrate is dried at 30 °C in a vacuum oven. A thin layer of cyanoacrylate epoxy resin (CER), of thickness less than 20 micron (99.95% less than the probing wavelength), is used on both sides of the substrate as an adhesive. It is observed with the cavity resonator method that the loaded frequency of the substrate does not shift its position on brushing thin layer of CER adhesive on both sides of the substrate. Copper sheet of thickness 0.4 mm is placed on both sides of the substrate, and rolled at pressure 6 torr for one hour, to obtain the metalized substrate.

Both sides of the metalized substrate are masked with an adhesive tape. The artwork of microstrip patch in accordance with the design formulae (table 3.1) is drawn on one surface of the masked substrate by specially designed sharp tool with precision of 0.02 mm attached to milling machine whose least count is 0.002 mm. The adhesive tape from all the side of the microstrip patch drawn is peeled off and is dipped in a slightly acidic ferric chloride (FeCl$_3$ + HCl) bath. Ferric chloride solution is continuously stirred for uniform etching of the copper. To prevent the sample from over etching, which may cause corroded edge of the microstrip patch, the concentration of ferric chloride solution is gradually reduced with time. The whole system is then taken out from the solution and washed with distilled water to remove any traces of ferric chloride solution. The tape on the bottom side is lifted carefully to release ground plane side. To determine any discrepancies in the

Adaptation of different patch geometries to achieve broadband operation of microstrip antenna on customized composite substrate in X-band

51

line pattern, the microstrip patch is observed under a microscope of least count 0.01 mm. This process of transferring artwork on the substrate, avoids the underneath etching of copper, thus keeping the dimension of the patch accurate and hence the frequency of operation remains same as designed.

Antenna performance measurements are carried out on the rectangular patch antennas fabricated on LDPE/alumina and LDPE/titania composites in X-band.

3.4.3 S_{11} parameter and radiation pattern studies for rectangular patch antenna

Figure 3.6 – 3.7 gives the measured and simulated S_{11} results for rectangular patch antennas on the 2 % VF of alumina in LDPE and 2 % VF of titania in LDPE composite substrates.
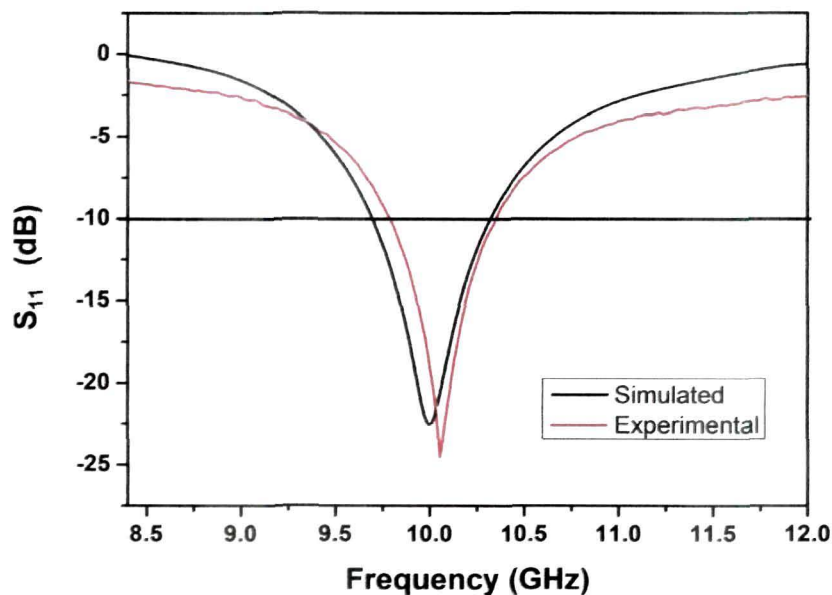
Figure 3.6   Measured and simulated S_{11} results for rectangular patch antenna on 2 % VF of alumina in LDPE composite substrate

Adaptation of different patch geometries to achieve broadband operation of microstrip antenna on customized composite substrate in X-band

52
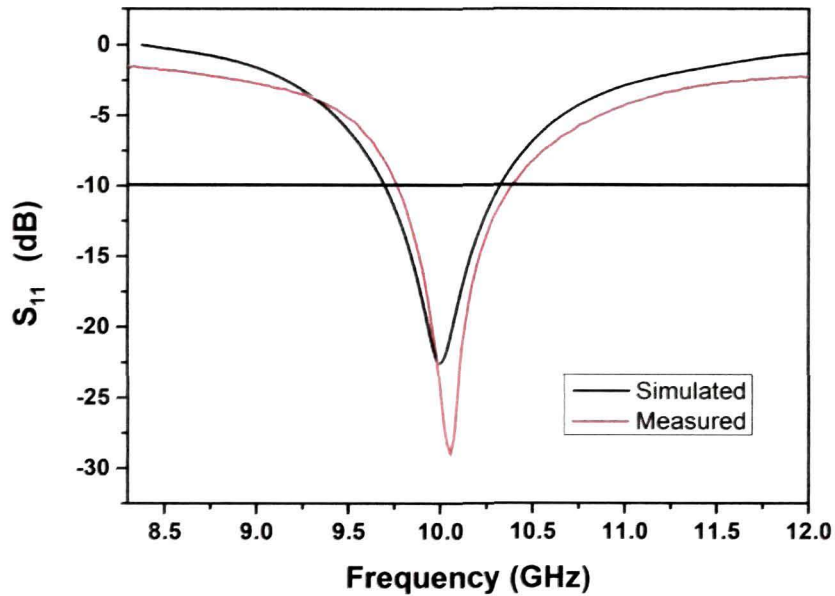
Figure 3.7   Measured and simulated S_{11} results for rectangular patch antenna on 2 % VF of titania in LDPE composite substrate

Figure 3.8 - 3.9 show radiation pattern in E and H plane of microstrip antenna fabricated on LDPE/alumina and LDPE/titania composites.
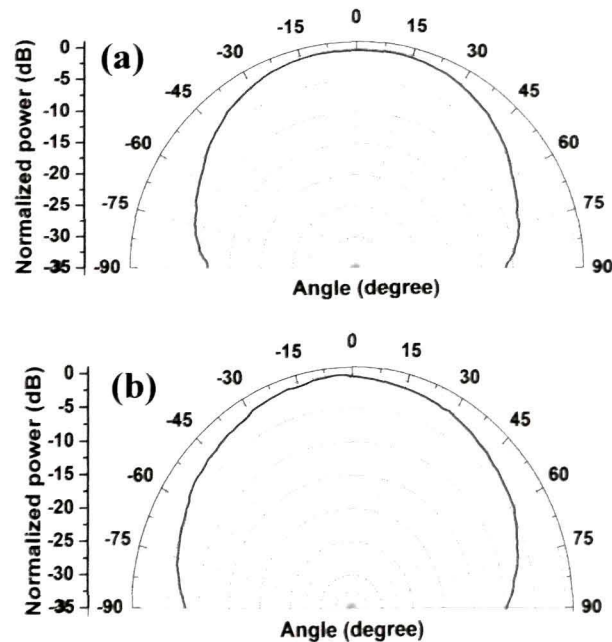
Figure 3.8   Measured (a) E-plane and (b) H-plane radiation pattern of rectangular patch antenna on 2 % VF of alumina in LDPE composite substrate

Adaptation of different patch geometries to achieve broadband operation of microstrip antenna on customized composite substrate in X-band

53
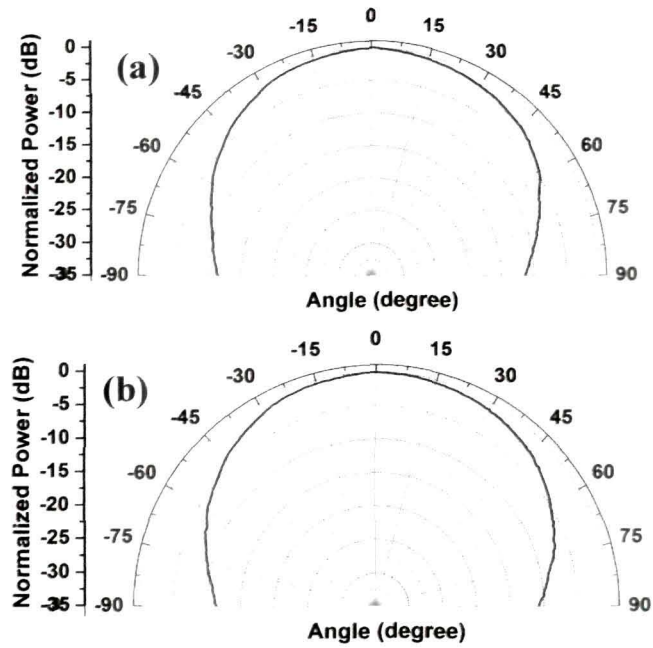
Figure 3.9   Measured (a) E-plane and (b) H-plane radiation pattern of rectangular patch antenna on 2 % VF of titania in LDPE composite substrate

Comparison of S_{11} parameter of microstrip antennas on LDPE/Titania and LDPE/alumina substrates are shown in figure 3.10.
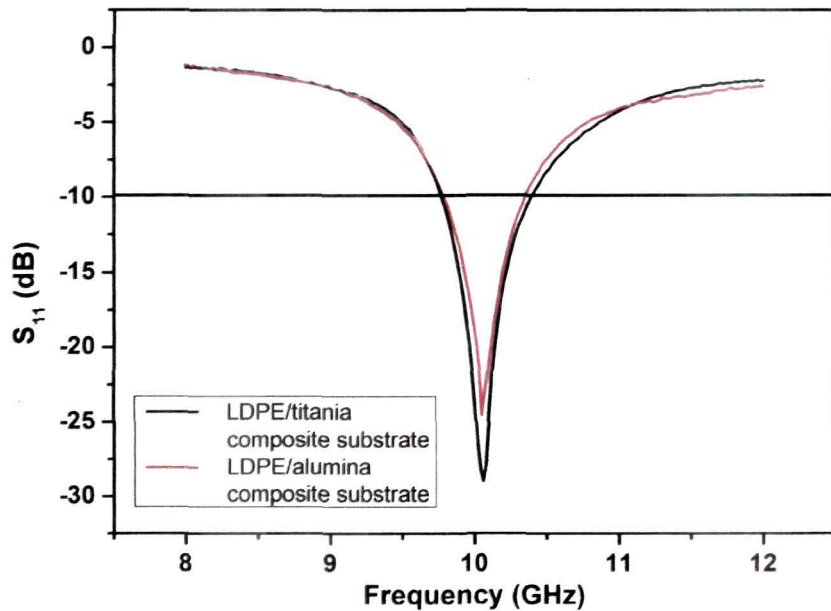
Figure 3.10   Measured S_{11} results for rectangular patch antenna on LDPE/alumina and LDPE/titania composite substrates

Adaptation of different patch geometries to achieve broadband operation of microstrip antenna on customized composite substrate in X-band

54

The performance parameters determined from the S_{11} measurement and radiation pattern studies are tabulated in table 3.2.

Table 3.2   Antenna performance parameters

Substrate		Patch dimension (mm²)	Ground plane dimension (mm²)	Resonating frequency (GHz)	S_{11} at center frequency (dB)	-10 dB operational bandwidth	Directivity (dBi)
2 % VF of alumina in LDPE	Expt	11.9 × 8.6	35 × 30	10.06	-24.52	5.6 %	5.91
	Sim	11.9 × 8.6	35 × 30	10.00	-22.5	5.8%	-
2 % VF of titania in LDPE	Expt	11.4 × 8.3	35 × 30	10.04	-29.1	6 %	6.29
	Sim	11.4 × 8.3	35 × 30	10.00	-22.5	6.1%	-

Antenna designed on titania in LDPE substrate shows better S_{11} characteristics and directivity (table 3.2) than alumina in LDPE substrate. For further investigations, LDPE/titania is used as substrates for microstrip antennas. Moreover addition of a small amount of titania in the matrix can sufficiently alter the dielectric properties of the composite as compared to the addition of same amount of alumina in the matrix.

3.5 DESIGN AND FABRICATION OF RECTANGULAR PATCH MICROSTRIP ANTENNA ON GRADED COMPOSITE SUBSTRATE

MPA with graded layer substrate is investigated for enhancement of return loss and band width of operation. Unlike other multilayer structure reported in [17-21], the permittivity of the substrate immediately below the radiator is kept lowest, increasing towards the ground plane (figure 3.10). To obtain the variation in permittivity in the layers, percentage volume fraction of titania is changed for the different layers in the substrate. Percentage volume fraction of titania is increased in the subsequent layers below, to give a graded permittivity substrate structure.

3.5.1 Fabrication of graded composite substrate
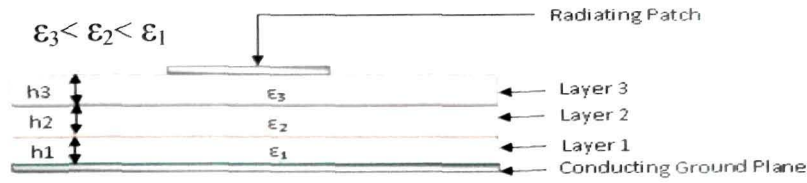
Figure 3.11   Schematic diagram of MPA on graded substrate

The graded composite substrate is synthesized using different layers of composite material with different VF of filler. Figure 3.11 shows the schematic of the microstrip antenna on graded substrate. Layer 1 (0.5 mm thick) is of 4 % VF of TiO_2 in LDPE, layer 2 (0.5 mm thick) is of 3 % VF of TiO_2 in LDPE and layer 3 is of 2 % VF of TiO_2 in LDPE (1 mm thick). Individual layers of required thickness are fabricated separately using the process described in the chapter II. The three layers are compressed under pressure of up to 0.3 kg/cm² in a compression mould and temperature is slowly increased till 90 °C, just enough for the layer to coalesce into a uniform structure without losing its form. The temperature is immediately reduced thereafter so that a smooth transition of grading is obtained without affecting the concentration of inclusions across the boundaries and hence the permittivity of individual layers.

To verify that the thickness of the layers does not change during the graded substrate formation, the relative dielectric permittivity of the graded substrate structure (ε_{rc}) is calculated using the multilayer formulation as used in [22, 23] and compared with experimental results. The theoretical relative dielectric permittivity for three layer substrate is expressed as,

$$\varepsilon_{rc} = \frac{\sum_{i=1}^{3} h_i}{\sum_{i=1}^{3} \frac{h_i}{\varepsilon_{ri}}} \tag{3.14}$$

Adaptation of different patch geometries to achieve broadband operation of microstrip antenna on customized composite substrate in X-band

56

where h_i the height of the ith layer and ε_{ri} is is the dielectric permittivity of the ith layer. Using the permittivity values for different composites as determined in chapter II (section 2.5.2) ε_{rc} is calculated using equation 3.14. The experimental results for permittivity determined for graded substrate using Nicolson-Ross method is almost same (99.9 % accurate) as that calculated for three layer geometry using equation 3.14. The measured and calculated relative permittivity is plotted in figure 3.12. The result indicates that during graded substrate formation the thickness of individual layer remains the same, as expected.
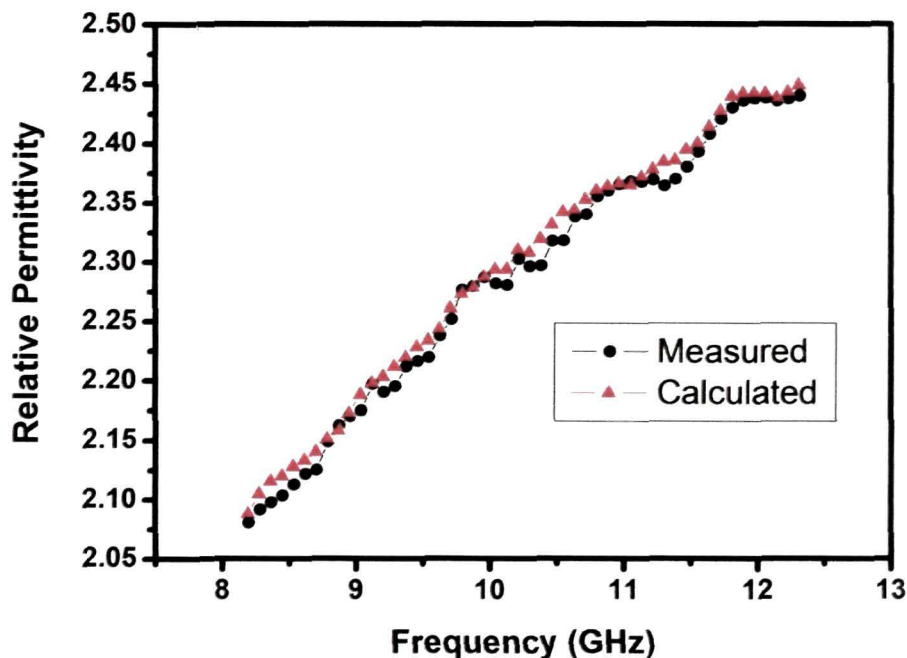
Figure 3.12   Calculated and measured permittivity for the graded substrate

3.5.2 Design of rectangular patch antenna on graded composite substrate

A rectangular microstrip patch antenna on the developed substrate is designed at 10 GHz using the equations 3.1-3.7 and then optimized using CST Microwave studio. The geometry of the radiator is determined using permittivity value, ε_{rc}, of the graded substrate in transmission line model. The

Adaptation of different patch geometries to achieve broadband operation of microstrip antenna on customized composite substrate in X-band

57

dimension of the radiator patch is found to be 11.2 mm × 8.1 mm. The antennas are fed coaxially at 50 Ω impedance matched point.

3.5.3 S_{11} and radiation pattern measurement for the rectangular patch antenna on graded substrate

Figure 3.13 shows the simulated and measured S_{11} characteristics of the rectangular patch antenna fabricated on graded composite substrate. The measured resonant frequency is shifted by 0.1 GHz from the simulated value.
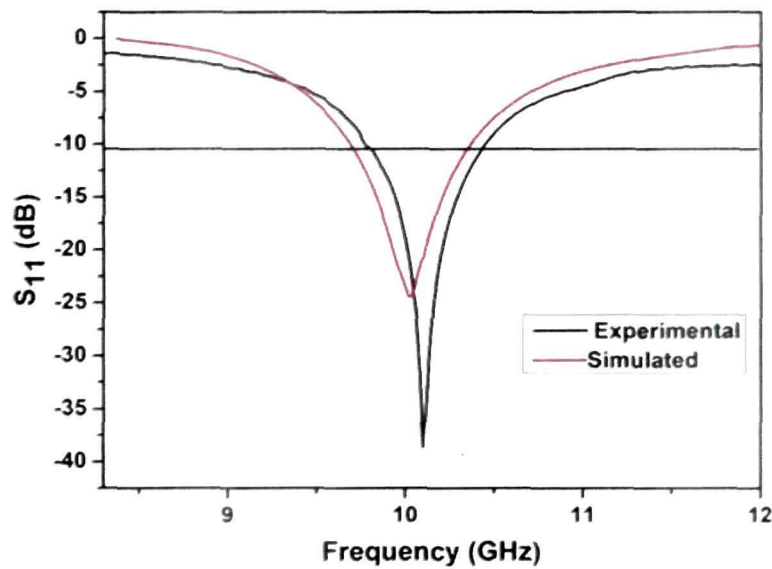
Figure 3.13   Simulated and measured S_{11} results for rectangular patch antenna on graded substrate

The performance of the antenna fabricated on graded substrate is compared with MPAs designed at same frequency but fabricated on single composition viz. 2 %, 3 % and 4 % VF of TiO_2 in LDPE substrate (figure 3.14). The height of substrate is kept same for all the four MPAs i.e. 2 mm. Comparison of performance of all the antennas is given in table 3.3.

Adaptation of different patch geometries to achieve broadband operation of microstrip antenna on customized composite substrate in X-band

58
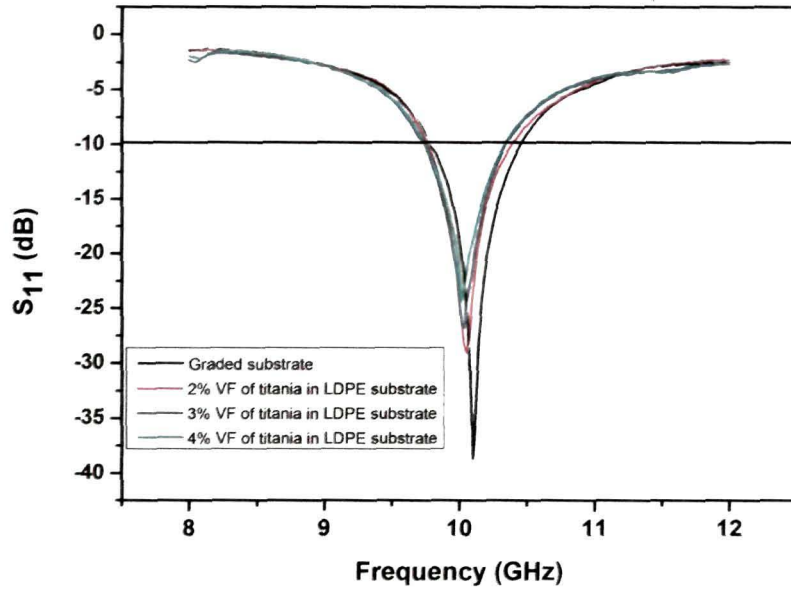
Figure 3.14   Comparison of measured S_{11} results for rectangular patch antenna on different substrate

Radiation patterns are measured at 10 GHz. Co polar and cross polar E-plane and H-plane patterns are shown in figure 3. 15 (a-b).
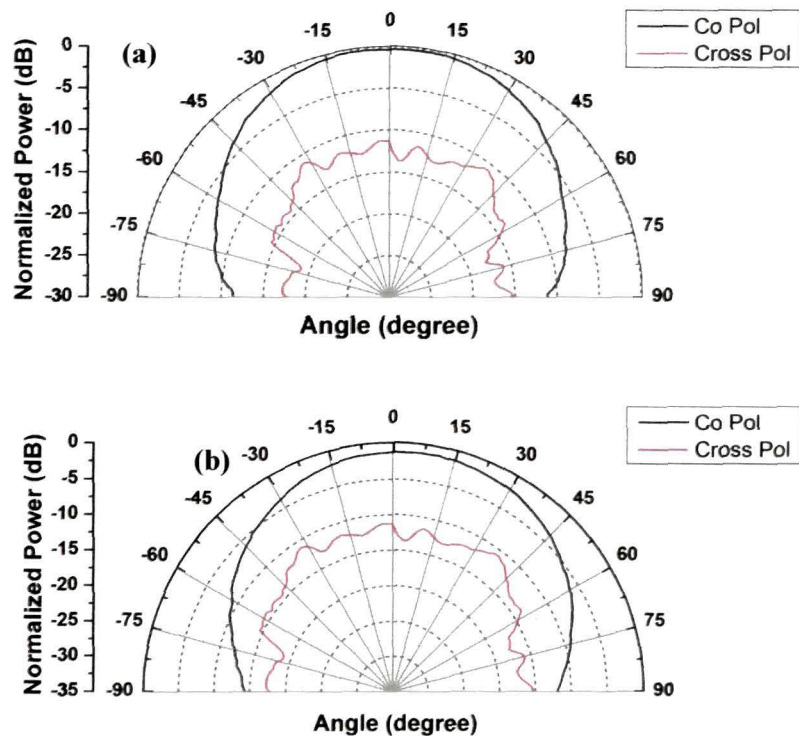
Figure 3.15   Measured (a) E-plane and (b) H-plane radiation pattern of rectangular patch antenna on graded composite substrate

Adaptation of different patch geometries to achieve broadband operation of microstrip antenna on customized composite substrate in X-band

59

From the E-plane and H-plane measured patterns, the directivity of the rectangular patch antenna on grade substrate at 10 GHz is found out to be 9.91 dBi. Table 3.3 compares the performance of rectangular patch antenna designed at 10 GHz on different substrates.

Table 3.3 S_{11} parameter result comparison

Substrate		Permittivity at 10 GHz	Patch dimenssion (mm^2)	Resonating frequency (GHz)	S_{11} at the resonating frequency (dB)	-10dB bandwidth
2%VF of titania in LDPE		2.23	11.4×8.3	10.06	-29	6.06 %
3%VF of titania in LDPE		2.28	11.2×8.1	10.04	-26.8	5.87 %
4%VF of titania in LDPE		2.39	10.9×7.8	10.02	-22.4	5.78 %
Graded	Expt	2.27	11.2×8.1	10.1	-38.6	6.73 %
	Sim	-	11.2×8.1	10.0	-23	6.75%

3.6 CONCLUSIONS

Studies carried out, indicate that, alumina in LDPE and titania in LDPE composites are suitable substrates for microstrip antennas. The microstrip antenna designed on the graded substrate resonates at the design frequency confirming the formation of the individual layers of the graded substrate with the desired thickness. Graded composite material developed as substrate for microstrip antenna shows an enhanced S_{11} performance and bandwidth as compared to single composition substrate. The directivity values are also high for antenna on graded substrate. All these are achieved with the antenna size being reduced marginally in comparison to the antenna on 2% VF of titania in LDPE substrate (4% reduction in area) (Table 3.1). Instead of using commercially available substrates, where the material properties cannot be altered, graded particulate composite substrates may form a new technological alternative, where the substrate properties can be tailored easily by altering the filler content in the matrix. In all the future investigations of this work, graded composite material is used as substrate for antenna designs.

Adaptation of different patch geometries to achieve broadband operation of microstrip antenna on customized composite substrate in X-band

60

References

[1]   Wong, K.-L., *Compact and Broadband Microstrip Antennas*, (John Wiley & Sons, 2002).

[2]   Zürcher, J. F. and Gardiol, F. E., *Broadband Patch Antennas*, (Artech House, Boston, 1995).

[3]   Kumar, G. and Ray, K.P., *Broadband Microstrip Antennas*, (Artech House, Boston, 2003).

[4]   Carver, K.R. and Mink, J.W., Microstrip Antenna Technology, *IEEE Trans. Antennas Propag.* **29**, 2-24, (1981).

[5]   Pozar, D.M., Microstrip Antennas, *Proc. IEEE*, **80**, 79-91, (1992).

[6]   Zurcher, J. F., The SSFIP: A global concept for high performance broadband planar antennas, *Electron. Lett.*, **24**, 1433-1435, (1988).

[7]   Sengupta, D.L., Transmission Line Model Analysis of Microstrip Antennas, *Electromagnetics*, **4**, 355-376, (1984).

[8]   Hammerstad, E.O., Equations for Microstrip Circuit Design, *Proc. Fifth European Microwave Conf.*, 268-272, (1975).

[9]   Bahl, I.J. and Bhartia, P., *Microstrip Antennas*, (Artech House, Dedham, MA, 1980).

[10] Balanis, C.A., *Advanced Engineering Electromagnetics*, (John Wiley & Sons, New York, 1989).

[11] Kara, M., Formulas for the Computation of Physical Properties of Rectangular Microstrip Antenna Elements with Various substrate Thicknesses, *Microwave and Opt. Technol. Lett.*, **12**, 234-239, (1996).

[12] Jackson, D.R. and Alexopoulos, N.G., Simple Approximate Formulas for Input Resistance, bandwidth and Efficiency of a Resonant Rectangular Patch, *IEEE Trans. On Antennas and Propagat.*, **AP-39**, 407 – 410, (1991).

[13] http://cp.literature.agilent.com/litweb/pdf/5965-7917E.pdf, *Agilent Network Analyzer Basics*

Adaptation of different patch geometries to achieve broadband operation of microstrip antenna on customized composite substrate in X-band

61

[14] Laverghetta, T. S., *Microwave Materials and Fabrication Techniques*, (Third Edition, Artech House, 2002).

[15] Balanis, C.A., *Antenna Theory Analysis and Design*, (Second edition, John Wiley and Sons, 2005).

[16] Kraus, J.D., and Marhefka, R.J., *Antennas for All Applications*, (Third Edition, Tata McGraw Hill, 2003).

[17] Croq, F. and Pozar, D. M., Millimeter-wave design of wide-band aperture-coupled stacked microstrip antennas, *IEEE Trans. Antennas Propag.*, **39**, 1170-1176, (1991).

[18] Liu, Z.-F., Kooi, P.-S., Li, L.-W., Leong, M.-S.and Yeo, T.-S., A Method for Designing Broadband Microstrip Antennas in Multilayered Planer Structures, *IEEE Trans. Antennas Propag.*, **47**, 1416-1420, (1999).

[19] Kim, J.H., Kim, H.C. and Chun, K., Performance Enhancements of a Microstrip Antenna with Multiple Layer Substrates, *Int'l. Sympos. Signal, Systems and Electronics*, 319-322, (2007).

[20] Sharma, A. and Singh, G., Design of Single Pin Shorted Three-Dielectric Layered Substrates Rectangular Patch Microstrip Antenna for Communication Systems, *Progress in Electromagnetic Research Letters*, **2**, 157-165, (2008).

[21] Malathi, P. and Kumar, R., Design of Multilayer Rectangular Microstrip Antenna using Artificial Neural Networks, *Int'l. J. Recent Trends Eng.*, **2**, 53-57, (2009).

[22] Ali, W.K.W. and AI-Charchafchi, S.H., Using Equivalent Dielectric Constant to Simplify the Analysis of Patch Microstrip Antenna with Multi Layer Substrates, *IEEE AP-S Int'l. Sympos.*, **2**, 676-679, (1998).

[23] Jha, K.R. and Singh, G., Analysis and design of rectangular microstrip antenna on two-layer substrate materials at terahertz frequency, *J. Comput. Electron.* **9**, 68-78, (2010).

Adaptation of different patch geometries to achieve broadband operation of microstrip antenna on customized composite substrate in X-band

62

CHAPTER IV

TRANSVERSE LINE TERMINATED E-ARM PATCH ANTENNA ON GRADED COMPOSITE SUBSTRATE

4.1 Introduction

4.2 Design of E-Shaped Patch on Graded Composite Substrate

4.2.1 Dimensions of the E-shaped patch

4.2.2 S11 and Radiation pattern measurement results for the E-shaped patch

4.3 Design of Transverse Line Terminated E-Arm Patch Antenna

4.3.1 Dimensions of the Transverse Line terminated E-arm patch

4.3.2 Fabrication of the Transverse Line Terminated E-arm Patch with Hot Press Lamination Method

4.3.3 S11 and radiation pattern measurement results for transverse line terminated E-arm patch antenna

4.4 Conclusions

References

4.1 INTRODUCTION

Bandwidth enhancement can be achieved by various techniques described in chapter 1. Stacked patches, parasitic patches and slot couplings are techniques used on the same plane [1-3]. Slots on the radiator patch modify the patch topology within the patch area maintaining a single-layer radiating structure. Also, profile of antenna remains thin and additional resonant frequencies can be obtained, resulting in bandwidth improvement. Examples include E-shaped patch antennas, T-shaped patch antennas, U-slot patch antennas, V-slot patch antennas etc [4-10]. U-shaped patch have been reported to demonstrate broadband performance for microstrip antennas [6]. Better bandwidth over the U-shaped patch is obtained for E-shaped patches as discussed in [7]. In addition E-patches are simple to design, with two parallel slots incorporated in simple rectangular patch geometry to introduce a second resonant mode, resulting in a dual band operation [4-8]. The dimensions of the slots and feed point location control the performance of the design.

Single broad band performance can be achieved by using a T-shaped strip patch antenna in which the radiating patch is constructed by a T-shaped strip with a microstrip feed line. Performance of this type of antenna can be enhanced by tuning the length of individual segments of the T-shaped patch [9, 10].

Both the techniques of E-shaped patch and T-shaped strip patch are combined in this novel approach. First the E-shaped patch is designed and optimized for its performance with dimensions of E-arms and feed positions, and then the arms of E are terminated in transverse sections i.e. T-type stubs. The design is further optimized with the dimensions of the terminating stubs. A comprehensive parametric study has been carried out to understand the

Adaptation of different patch geometries to achieve broadband operation of microstrip antenna on customized composite substrate in X-band

63

effects of various dimensional parameters on the performance of the final design. Simulations are performed using CST Microwave Studio software. The final optimized design of transversely terminated E- arm patch antenna is fabricated and the measured S_{11} results are compared with simulated results. All the antennas are fabricated on the graded substrate developed as discussed in chapter III.

4.2 DESIGN OF E-SHAPED PATCH ON GRADED COMPOSITE SUBSTRATE

Figure 4.1 gives the geometry of the E-shaped patch. Technique developed by Ang et.al. [4] is used to model a simple E-shaped patch on graded substrate operating in X-band.

(a)   (b)
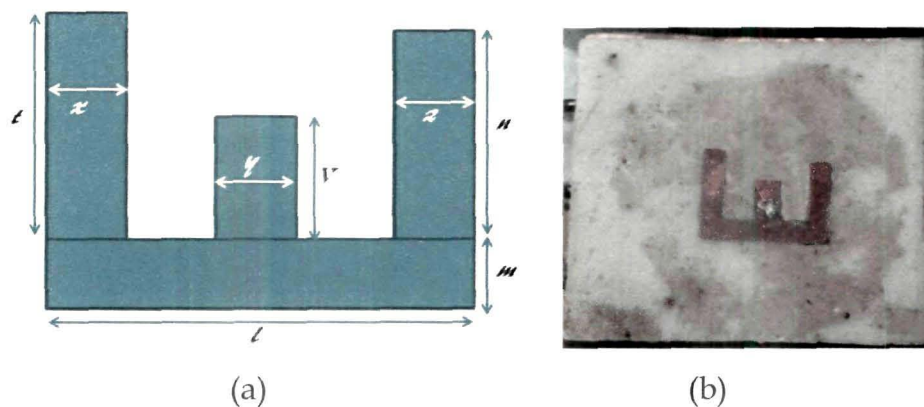
Figure 4.1   (a) Geometry of E-shaped patch
                   (b) Fabricated coaxially fed E-shaped patch antenna

4.2.1 Dimensions of the E-shaped patch

The dimensions of different strips constituting the E-shaped patch are given in table 4.1. A patch is designed on the graded substrate by metalizing copper strip on it and drawing the E-shaped patch artwork on the mask tape on the strip by the process described in chapter III section 3.4.2. The antenna is fed coaxially at 1.6 mm distance from the base of the middle strip.

Adaptation of different patch geometries to achieve broadband operation of microstrip antenna on customized composite substrate in X-band

64

Table 4.1   Design parameter of E-shaped patch

Design frequency (GHz)	Substrate thickness (mm)	*l* (mm)	*m* (mm)	*n* (mm)	*t* (mm)	*V* (mm)	*x* (mm)	*y* (mm)	*z* (mm)
10	2	14.1	1.9	7	7.9	4.6	2.1	2.1	2.1

4.2.2 S_{11} and Radiation pattern measurement results for the E-shaped patch
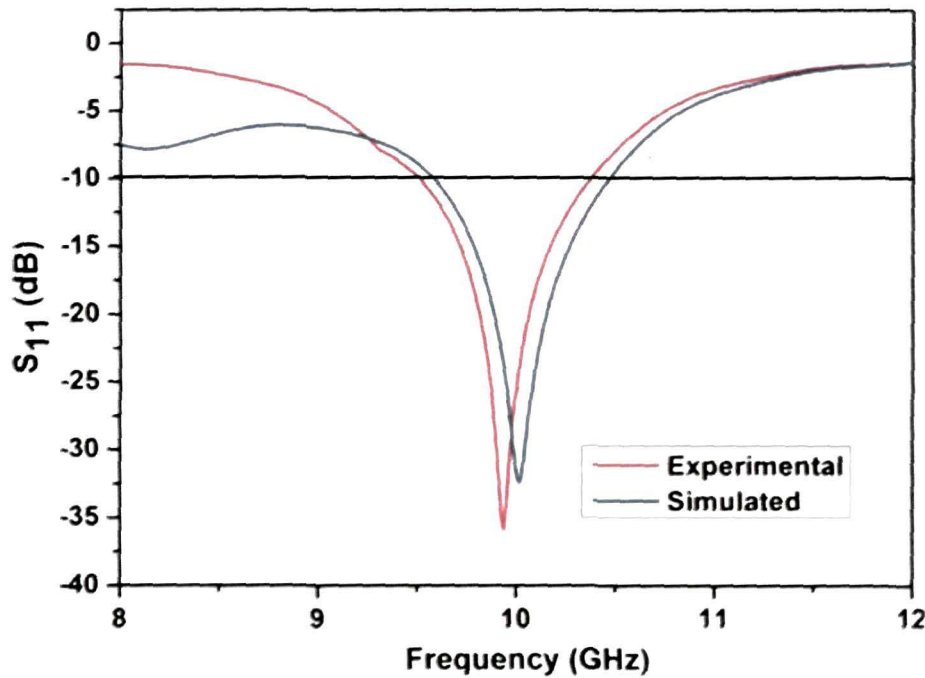
Figure 4.2   Measured and simulated S_{11} results for E-shaped patch antenna

The S_{11} result of the simple E-shaped patch is shown in figure 4.2. It shows that the antenna can perform in a single band centered at 9.95 GHz with an operating bandwidth (- 10 dB) of 9.1 %. The bandwidth is enhanced by 2.4 % in comparison to the simple rectangular patch antenna designed at the same frequency on the same substrate.

The results of radiation pattern measurements are shown in figure 4.3. Directivity of the E-shaped antenna is found to be 11.09 dBi, which is higher than the simple rectangular patch antenna.

Adaptation of different patch geometries to achieve broadband operation of microstrip antenna on customized composite substrate in X-band

65
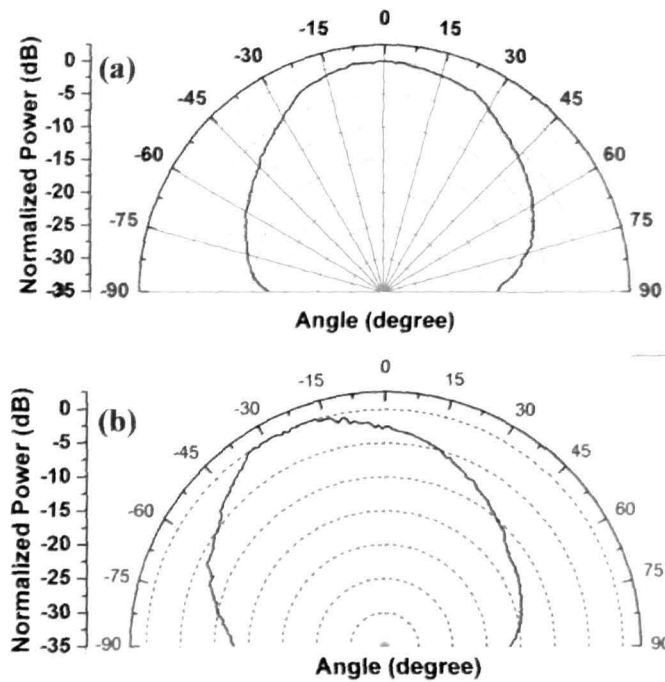
Figure 4.3   (a) E-plane and (b) H-plane radiation pattern results for E-shaped patch antenna at 10 GHz

4.3 DESIGN OF TRANSVERSE LINE TERMINATED E-ARM PATCH ANTENNA

The optimized design of different strips constituting the patch for E-shaped patch at 10 GHz, mentioned in section 4.1, is considered for implementation of the new design. All the three E-arms are terminated in transverse lines; the design of the structure is done in two modules,

a) Starting from the simple rectangular patch, the basic E-shaped patch is derived and then combined with the technique of T-strip shaped patch, three horizontal stubs (terminations) are added to the three arms of the fundamental E-shaped patch.

b) The dimensions of all the terminations as well as the feed point locations are optimized.

4.3.1 Dimensions of the transverse line terminated E-arm patch

Technique of broadening operational bandwidth by using T-shaped patch is given by Yang et.al. [9]. Combining this idea in the above mentioned design of E-shaped patch antenna, a new patch geometry is studied to obtain broad operational bandwidth in X-band. Figure 4.4 gives the geometry of

---

Adaptation of different patch geometries to achieve broadband operation of microstrip antenna on customized composite substrate in X-band

66

transverse line terminated E-arm patch with three transverse strips. The simulated dimensions of different transverse terminations constituting the E-shaped patch are given in table 4.2. The antenna is fed coaxially at 1.6 mm distance from the base of the lower horizontal strip and 1.2 mm distance from the left side ('m' side) of the lower horizontal strip.

(a)   (b)
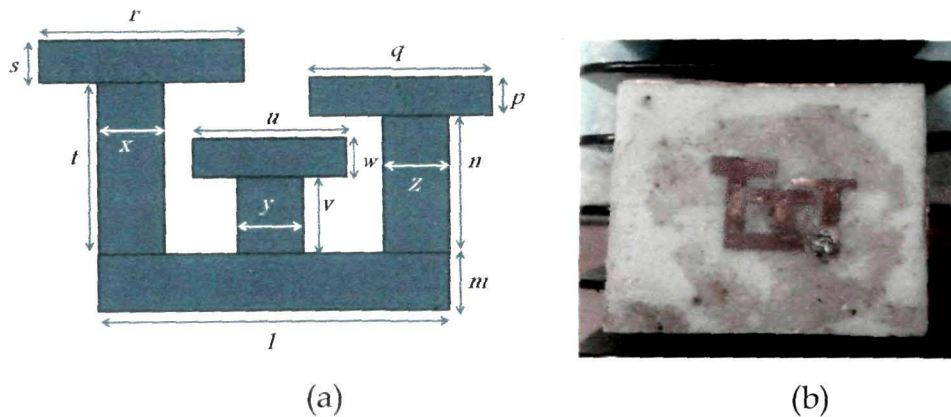
Figure 4.4   (a) Geometry of transverse line terminated E-arm patch
(b) Fabricated coaxially fed transverse line terminated E-arm patch antenna

Table 4.2   Design parameter of transverse line terminated E-arm patch

Design frequency (GHz)	Substrate thickness (mm)	*l* (mm)	*m* (mm)	*n* (mm)	*p* (mm)	*q* (mm)	*r* (mm)
10	2	14.1	1.9	7	1.1	8.2	8.3

s (mm)	*t* (mm)	*u* (mm)	*v* (mm)	*w* (mm)	*x* (mm)	*y* (mm)	*z* (mm)
2.1	8.2	8.1	7.9	4.6	2.1	2.1	2.1

4.3.2 Fabrication of transverse line terminated E-arm patch with hot press lamination method

The masking tape technique employed for fabrication of simple patch antenna in chapter III (section 3.4.2) is difficult to use in layout involving complex artwork due to limitation in precision of movement of tool. Hot press lamination method is used for such layout. The computer generated artwork is transferred on the metallized substrate. Leaving the patch geometry the rest of the metal is subsequently etched. Fabrication and etching of the patch design is done using the following processes

Adaptation of different patch geometries to achieve broadband operation of microstrip antenna on customized composite substrate in X-band

67

1. Metallization of copper on the substrate

2. Preparation and transfer of patch artwork

3. Transferring the artwork to the metal surface by hot press lamination

4. Etching and removal of mask

Metallization of copper on the substrate

The metallization process is performed in two steps by rolling technique as described in chapter section 3.4.2. in which a thin uniform copper foil of thickness 0.4 mm is taken. The treated copper foil is pasted over the substrate using thin layer of cyanoacrylate epoxy resin of thickness less than 20 micron. The copper and the substrate system is kept under pressure of 6 torr for 1 hour for good adhesion.

Preparation and transfer of patch artwork

A positive artwork enlarged 10 times that of patch dimension is made in MS Word software. The exact sized printout of this is taken on glossy paper in a very high quality laser printer at 10% reduction, to get the actual dimension and accuracy of the layout. The printouts are examined thoroughly through a microscope with least count of 0.01 mm to ensure its uniformity and freedom from edge distortion.

The mask (artwork) is aligned properly on one side of the metallized substrate. Then hot press at temperature 80 °C and pressure 6 torr is rolled over it. It takes about 5-7 minutes for complete transfer of the artwork to metal surface. Following which, the masking paper is removed.

Etching the artwork

A masking tape is placed on the bottom side of the metallized sample system exposing a circular hole of diameter 3 mm at the location for coaxial feed point. The system is then dipped in a slightly acidic ferric chloride

Adaptation of different patch geometries to achieve broadband operation of microstrip antenna on customized composite substrate in X-band

68

(FeCl$_3$ + HCl) bath. Uniform etching is ensured by continuously stirring the etching solution. Undercutting and jagged edges is minimized by diluting the ferric chloride solution over the time. The whole system is then washed with distilled water to remove any traces of ferric chloride solution. The mask of the microstrip patch and the masking tape from the bottom is carefully removed. The edge smoothness of the microstrip patch is confirmed under a traveling microscope with least count of 0.01 mm. The photograph of the patch patterns are shown in figure 4.4 (b).

4.3.3 S_{11} and radiation pattern measurement results for transverse line terminated E-arm patch antenna
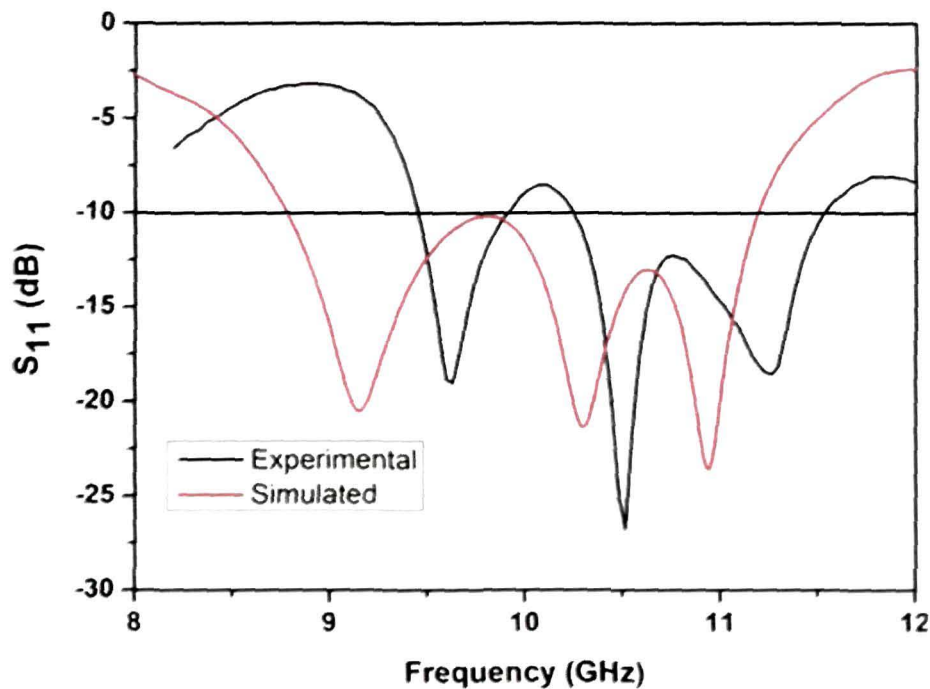
Figure 4.5   Measured and Simulated S_{11} results for transverse line terminated E-arm patch antenna

Simulated S_{11} results show the -10 dB operational bandwidth to be 24 % but the practical antenna performs in two frequency bands. The bandwidth at 9.67 GHz is 4.56 % while for the higher 10.5 GHz frequency, the bandwidth is found to be 11.8 %. Excluding a small band of 0.34 GHz, transverse line

Adaptation of different patch geometries to achieve broadband operation of microstrip antenna on customized composite substrate in X-band

69

terminated E-arm patch performs over the frequency range of 9.458 GHz to 11.532 GHz.

　　　Figure 4.6 – 4.8 show the radiation pattern of the antenna both in E and H plane at 9.6 GHz, 10.5 GHz and 10.9 GHz.
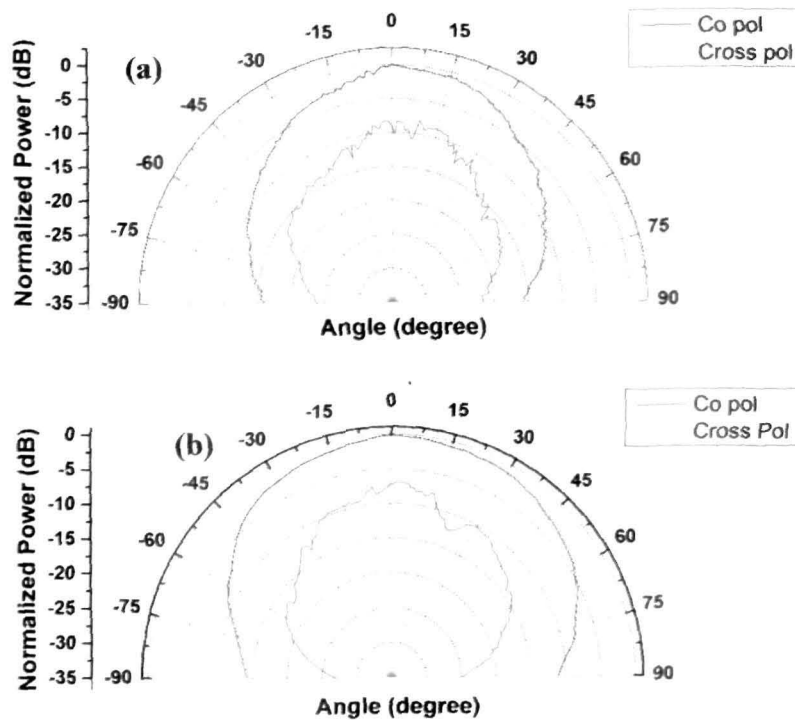
Figure 4.6　　　(a) E-plane and (b) H-plane radiation pattern results for transverse line terminated E-arm antenna at 9.6 GHz

Adaptation of different patch geometries to achieve broadband operation of microstrip antenna on customized composite substrate in X-band

70
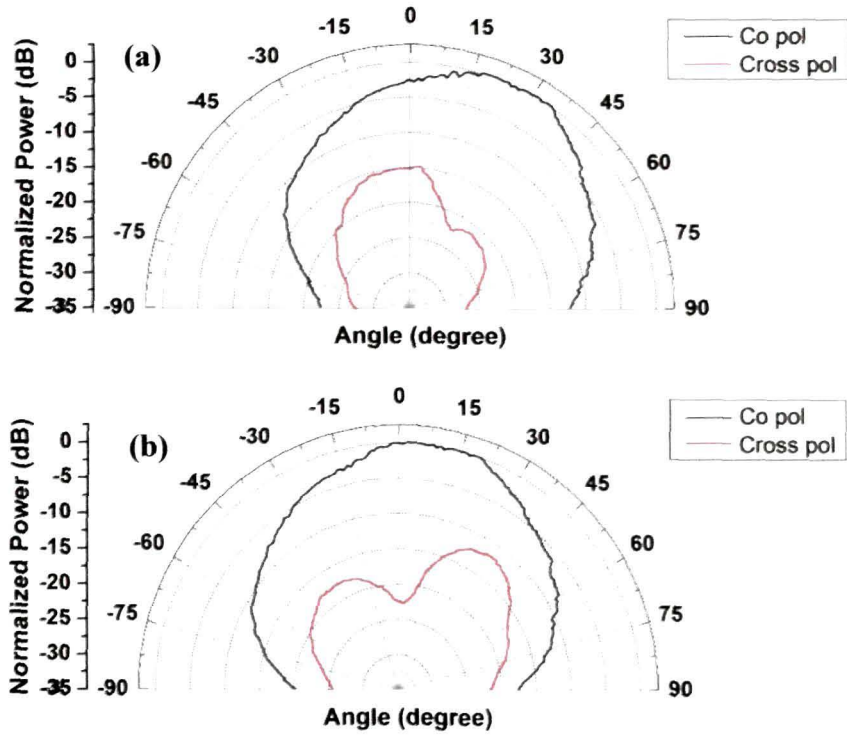
Figure 4.7   (a) E-plane and (b) H-plane radiation pattern results for transverse line
terminated E-arm antenna at 10.5 GHz
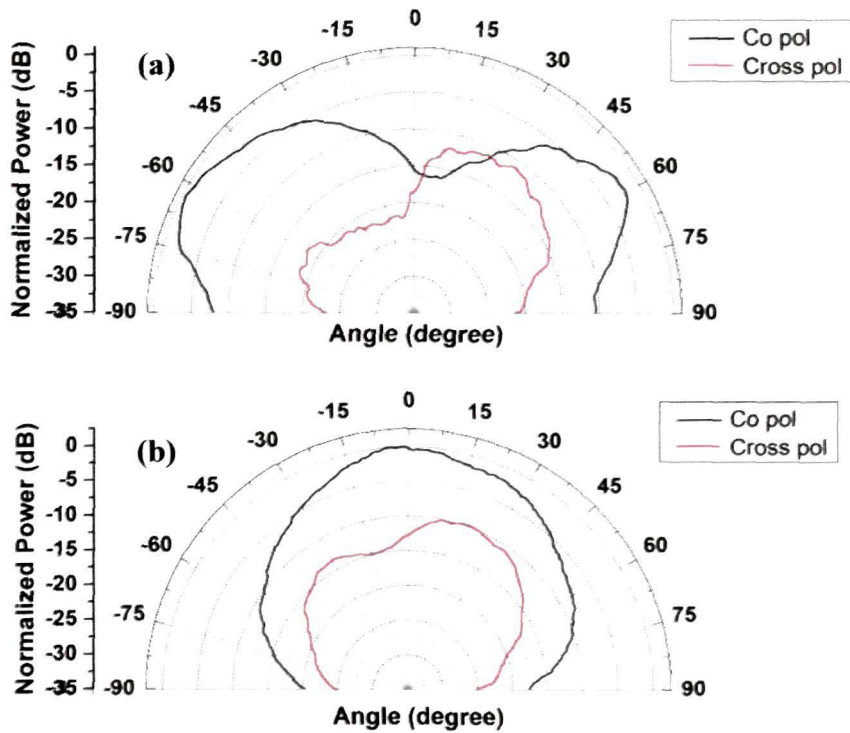
Figure 4.8   (a) E-plane and (b) H-plane radiation pattern results for transverse line
terminated E-arm antenna at 10.9 GHz

**Adaptation of different patch geometries to achieve broadband operation of microstrip antenna on customized
composite substrate in X-band**

71

The radiation pattern studies show that, with change in frequency the direction of the main lobe changes. The directivity of the antenna is increasing from 9.7 dBi at 9.6 GHz to 13.1 dBi at 10.9 GHz. The variation in radiation pattern with change in operational frequency may be qualitatively analysed using change in surface current distribution through out the patch geometry with change in frequency [12, 13]. The surface current variation can be observed from the simulated results. This is because of the assymetry in the patch geometry. The simulated surface current distribution at different frequencies are shown in figure 4.9 (a)– (c).
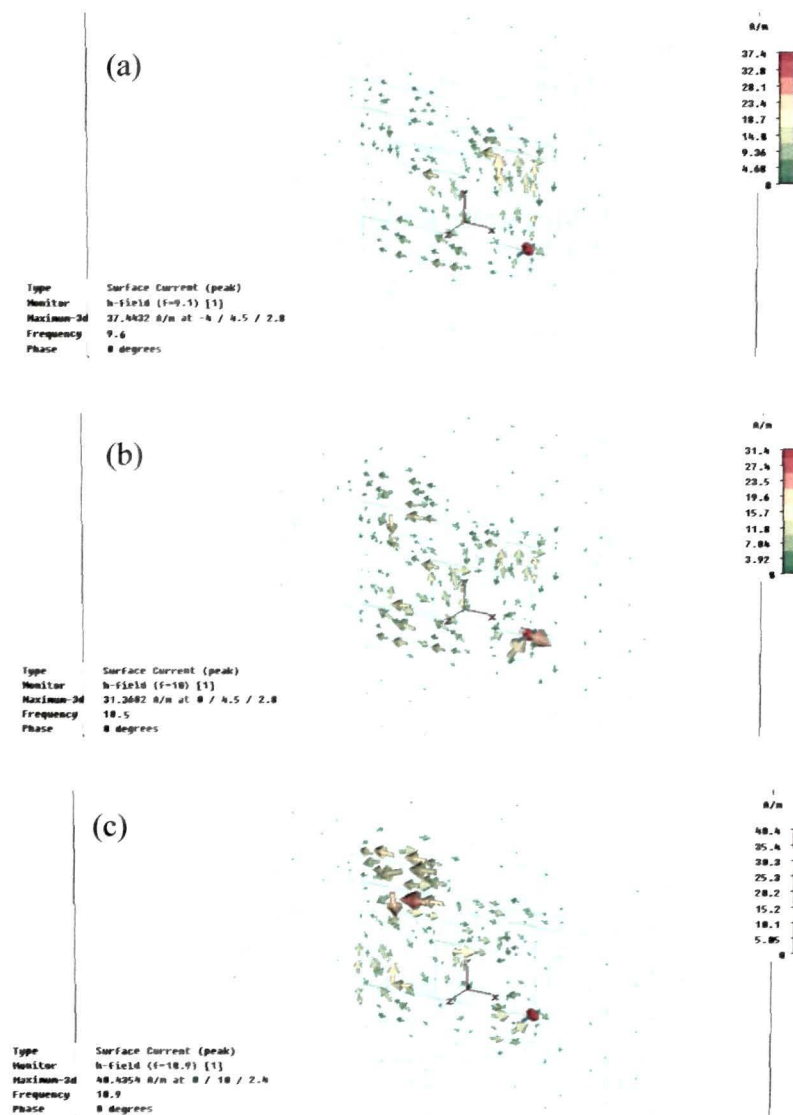
Figure 4.9   Simulated surface current distribution over the transverse line terminated E-arm patch at (a) 9.6 GHz (b) at 10.5 GHz and (c) at 10.9 GHz

Adaptation of different patch geometries to achieve broadband operation of microstrip antenna on customized composite substrate in X-band

72

4.4 CONCLUSIONS

E-shaped patch design fabricated on graded composite substrate shows bandwidth enhancement of 3.1 % over the simple rectangular patch designs with same substrate. Transverse termination of E-arms further enhances the bandwidth by almost 5.5 %, resulting in a overall bandwidth enhancement of as much as 8.6 %. This design is simple and efficient technique for broadband performance in the X-band.

Modifying the dimensions of all the strips can controll the performance of operation and resonating frequency. The change in radiation patterns of the modified E-shaped patch is useful for the systems where different devices working in the same environment placed at different directions are to be controlled by using a single antenna.

Adaptation of different patch geometries to achieve broadband operation of microstrip antenna on customized composite substrate in X-band

73

References

[1] Wong, K.-L., Compact and Broadband Microstrip Antennas, (John Wiley & Sons, 2002).

[2] Zürcher, J. F. and Gardiol, F. E., Broadband Patch Antennas, (Artech House, Boston, 1995).

[3] Kumar, G. and Ray, K.P., Broadband Microstrip Antennas, (Artech House, Boston, 2003).

[4] Ang, B.-K. and Chung, B.-K., A Wideband E-shaped Microstrip Patch Antenna for 5-6 GHz Wireless Communications, *Progress in Electromagnetid Research*, 75, 397-407, (2007).

[5] Yang, F., Zhang, X. X., Ye, X., and Rahmat-Samii, Y., Wide-band E-shaped patch antennas for wireless communications, *IEEE Trans. Antennas Propagat.*, 49, 1094–1100, (2001).

[6] Huynh, T. and Lee, K. F., Single-layer single-patch wideband microstrip antenna, *Electron. Lett.*, 31, 1310–1312, (1995).

[7] Ge, Y., Esselle, K. P., and Bird, T. S., E-shaped patch antennas for high-speed wireless networks, *IEEE Trans. Antennas Propagat.*, 52, 3213–3219, (2004).

[8] Ge, Y., Esselle, K. P., and Bird, T. S., A compact E-shaped patch antenna with corrugated wings, *IEEE Trans. Antennas Propagat.*, 54, 2411–2413, (2006).

[9] Yu, A. and Zhang, X. X., A method to enhance the bandwidth of microstrip antennas using a modified E-shaped patch, *Proceedings of Radio and Wireless Conference*, 261–264, Aug. 10–13, (2003).

[10] Yang, C.-F., Hseih, C.-Y. and Cheng, C.-M., Design Small-Size and Wide-Band T-shaped patch Antenna on Ceramic Substrate, *WCNC 2007 Proceedings*, (2007).

[11] Kim, M. K., Kim, K., Suh, Y. H., and Park, I., A T-shaped microstrip-line-fed wide slot antenna, *Proc. IEEE Antennas Propagat. Soc. Int. Symp.*, 3, 1500-1503, (2000).

[12] Qlu, M., and He., S., High directivity patch antenna with both photonic band gap substrate and photonic band gap cover, *Microwave and Optical Technology letters*, 3, 41-44, (2001).

[13] Zulkifli, F.Y., Rahardjo, E.T., and Haranto, D., Radiation properties enhancement of triangular patch microstrip array using hexagonal defected ground structure, *PIER M*, 5, 101-109, (2009).

Adaptation of different patch geometries to achieve broadband operation of microstrip antenna on customized composite substrate in X-band

74

CHAPTER V

AMALGAMATED RECTANGULAR AND V-SLOTTED SEMICIRCULAR MICROSTRIP PATCH ANTENNA

5.1 *Introduction*

5.2 *Design of a Circular Patch Microstrip Antenna*

5.2.1 *Dimensions of the circular patch*

5.2.2 S_{11} *and radiation pattern results of the circular patch antenna*

5.3 *Unequal Arm Length Cross Slot on Circular Patch Antenna*

5.3.1 S_{11} *and radiation pattern results of the unequal arm length cross slotted circular patch antenna*

5.3.2 *Measurement of axial ratio*

5.4 *V-slotted Semicircular Patch Amalgamated with Rectangular Patch Antenna*

5.4.1 *Design and study of amalgamated V-slotted semicircular- rectangular patch antenna*

5.4.2 S_{11} *and radiation pattern results*

5.5 *Conclusions*

References

5.1 INTRODUCTION

Broadband performance of rectangular microstrip patch antennas can also be achieved by using additional microstrip patches directly coupled to the radiating or nonradiating edges of a rectangular microstrip antenna [1-9]. In this design the central patch is fed mostly by coaxial feed and additional patches are gap coupled with the central patch. Researchers have studied different designs with multiple numbers of gap coupled rectangular patch elements to achieve broadband performance [5-9]. The broad bandwidths in these designs are obtained at the cost of increase in the patch dimension.

In wireless communication systems, where relative orientations between the transmitting and radiating antenna cannot be maintained, for example in mobile communication systems, a practical compromise is to use circular polarization at one end with linear at the other or circular polarization at both ends [1-3].

Circular polarization in compact antenna designs, can be achieved by including an embedded cross-slot of unequal arm lengths [2, 3], embedding a Y-shaped slot of unequal arm lengths [4], inserting slits or spur lines at the patch boundary [5-13], truncating patch corners or tips [14-17], introducing small peripheral cuts at the boundary of a circular patch [18], adding a tuning stub [19-21] or a bent tuning stub [22]. The main disadvantage of the CP MSAs is their narrow bandwidth characteristic [1-3]. The impedance bandwidth of a typical microstrip patch antenna, defined by -10 dB return loss, is around 3-4 %, while its 3 dB - axial ratio (AR) bandwidth is less than 1 % [10-13]. The AR bandwidth of the CP antenna is usually less than its impedance bandwidth; this limits the operational frequency bandwidth of the antenna. Thus, the approach to enhance the bandwidth of the CP MSA consists of a broad banding of its AR bandwidth. There are some methods to enhance the AR bandwidth of the CP MSA: by multiple resonances due to parasitic patches; by means of complex (usually balanced) feeds; using an air gap or foam with low dielectric constant as a patch substrate; by using photonic band gap structures. [1-3, 10-16].

Adaptation of Different Patch Geometries to Achieve Broadband Operation of Microstrip Antennas on
Customized Substrate in X-band

75

The work is focused on developing antennas for handheld devices, where both compact size and bandwidth are important consideration. Single feed circular patch antennas with its small size as compared to its rectangular counterpart are good candidates [1, 2] as compact antennas. Cross slot with unequal arm lengths is introduced on circular patch to achieve circular polarization operation, but the bandwidth is low.

Designs of composite microstrip antenna structures with rectangular microstrip patches parasitically coupled to circularly polarized semicircular patch antennas have been investigated to improve upon the bandwidth performance.

The antenna configuration studied considers a single feed rectangular patch as the centre element resonating at 10 GHz (design conducted in chapter III on graded substrate) with two parasitically fed slotted semicircular patches on the radiating edge. A circular patch antenna at 10 GHz is designed, and its performance studied on the substrate (chapter III, section 3.5). Cross slot design on the circular patch is optimized by varying the arm lengths of slot for maximum bandwidth of operation. The bifurcated unit of the circular patch i.e. two semicircular patches with unequal V-shaped arm slot are capacitively coupled as parasitic element with the centre rectangular patch along the radiating edges.

The developed antenna is studied for its broadband circular polarization operation over the X-band.

5.2. DESIGN OF A CIRCULAR PATCH MICROSTRIP ANTENNA
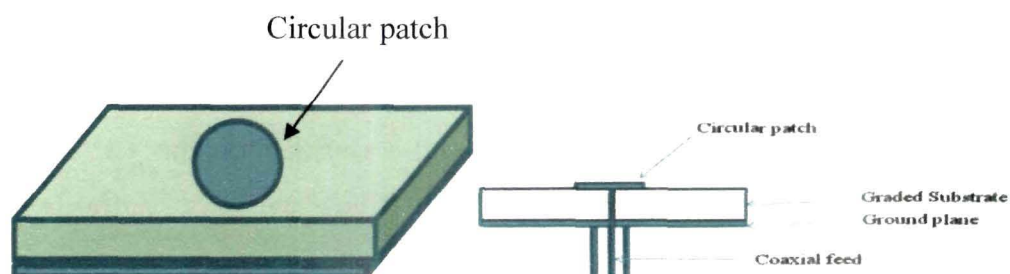
Figure 5.1   Schematic diagram of coaxially fed circular patch antenna

A circular patch is designed using the cavity model [2, 3, 12]. Here the antenna is modeled as a cylindrical cavity, bounded at its top and bottom by

Adaptation of Different Patch Geometries to Achieve Broadband Operation of Microstrip Antennas on Customized Substrate in X-band

76

electric walls and on its edge by magnetic walls. The fields within the dielectric region correspond to TM$_{nm}$ modes. The wave equation for electric field within the cavity is,

$$\left(\nabla^2 + k^2\right)\underline{E} = 0 \tag{5.1}$$

The solution of this equation in cylindrical coordinate is

$$E_z = E_0 J_n(k\rho)\cos(n\phi) \tag{5.2}$$

$$H_\rho = \frac{j}{\omega\mu\rho}\frac{\partial E_z}{\partial\phi} = -\frac{jn}{\omega\mu\rho}E_0 J_n(k\rho)\sin(n\phi) \tag{5.3}$$

$$H_\phi = -\frac{j}{\omega\mu}\frac{\partial E_z}{\partial\rho} = -\frac{jk}{\omega\mu}E_0 J_n{}'(k\rho)\cos(n\phi) \tag{5.4}$$

$$E_\rho = E_\phi = H_z = 0 \tag{5.5}$$

The magnetic wall boundary condition is given by

$$H_\phi(\rho = a) = 0 \tag{5.6}$$

as,

$$J_n{}'(ka) = 0 \tag{5.7}$$

The disk metallization radius can be determined using

$$J_n{}'\left(k_0 a\sqrt{\varepsilon_r}\right) = 0 \tag{5.8}$$

For the lowest order mode, n=1, the first root of the above equation comes out to be 1.841, hence

$$a = \frac{1.841}{k_0\sqrt{\varepsilon_r}} = \frac{8.794}{f_r\sqrt{\varepsilon_r}} \tag{5.9}$$

Due to fringing field effect, the effective radius, a, of a circular patch is greater than its physical radius, a_p. The semiemperical relationship between a and a_p is given by relation [1, 13],

$$a = a_p\left[1 + \frac{2h}{\pi a\varepsilon_r}\left\{\ln\left(\frac{a_p}{2h}\right) + (1.141\varepsilon_r + 1.77) + \frac{h}{a_p}(0.268\varepsilon_r + 1.65)\right\}\right]^{1/2} \tag{5.10}$$

Adaptation of Different Patch Geometries to Achieve Broadband Operation of Microstrip Antennas on Customized Substrate in X-band

77

5.2.1 Dimension of the circular patch

The circular patch is designed and fabricated at 10 GHz on the graded composite substrate with relative permittivity (ε_r) of 2.29. Using the equations 5.9-5.10, the physical radius of the circular patch is found to be 0.45 cm. Optimization of patch dimension and feed point location is carried out using CST Microwave Studio at 10 GHz for maximum S_{11}. The optimized patch radius is found to be 0.49 cm.

A circular patch antenna of radius 0.49 cm is fabricated on the graded substrate using the patch metallization process discussed in chapter IV (section 4.3.2). Figure 5.2 shows the circular patch antenna fabricated on the graded composite substrate. The patch is fed coaxially at a distance 2.8 mm from the center of the patch with a probe with diameter 0.5 mm.
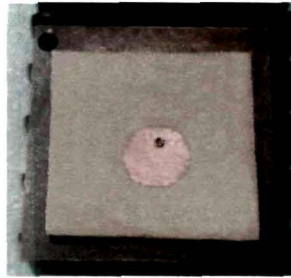
Figure 5.2   Simple circular patch antennas at 10 GHz on graded composite substrate

5.2.2 S_{11} and radiation pattern results of the circular patch antenna

The simulated and experimental results for S_{11} are plotted in figure 5.3.
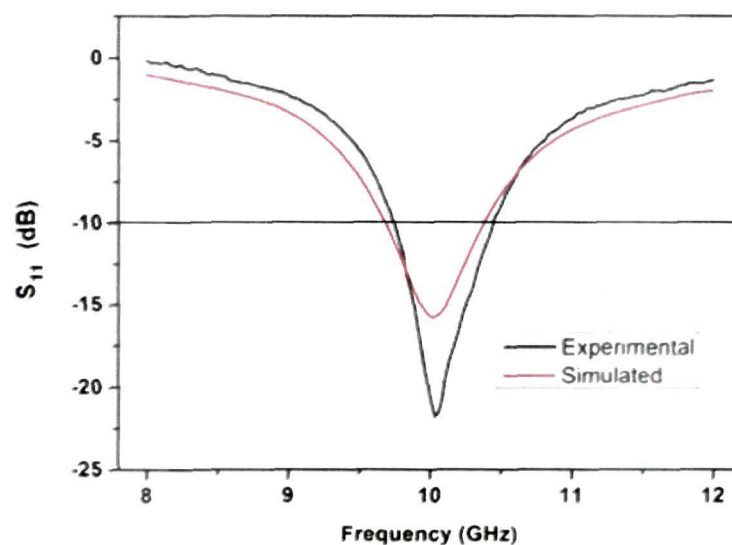
Figure 5.3   Simulated and experimental S_{11} parameter for simple circular patch antenna on graded substrate

Adaptation of Different Patch Geometries to Achieve Broadband Operation of Microstrip Antennas on Customized Substrate in X-band

78

The antenna resonates at 10.04 GHz with -10 dB bandwidth of 6.8 %. The radiation pattern of the circular patch is investigated at 10 GHz using the set up described in the chapter III. The radiation pattern is shown in figure 5.4. The directivity of the antenna is 7.21 dBi.
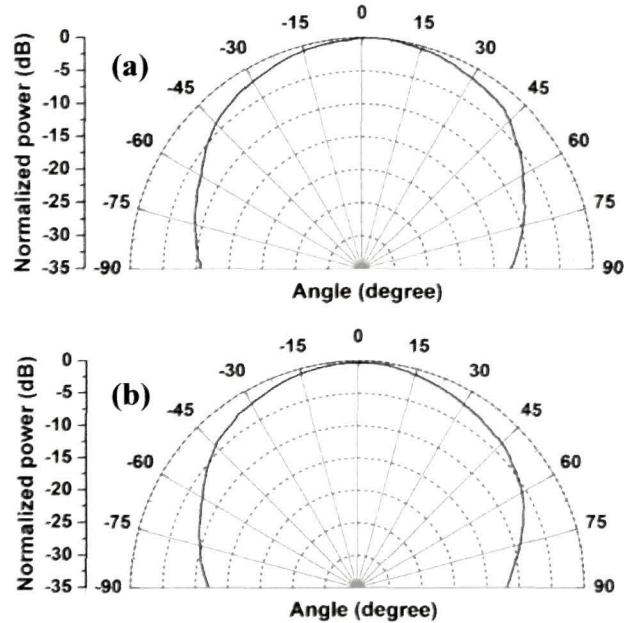
Figure 5.4 Measured co polar (a) E-plane and (b) H-plane radiation pattern for slotted circular patch antenna on graded substrate at 10 GHz

5.3 Unequal arm length cross slot on circular patch antenna

Unequal cross slot on the radiating patch is designed to obtain circularly polarized patch antenna. The dimensions of the slot arms are optimized for maximum -10 dB bandwidth.
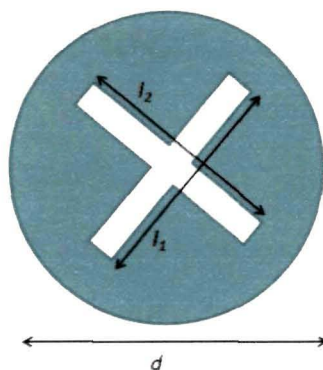
Figure 5.5   Schematic diagram of a cross slotted microstrip antenna

Figure 5.5 shows the schematic design of the slotted circular patch and the dimension parameters of the patch are tabulated in table 5.1.

Adaptation of Different Patch Geometries to Achieve Broadband Operation of Microstrip Antennas on Customized Substrate in X-band

79

Table 5.1   Design parameters for cross slotted microstrip antenna

Parameters	Magnitude (mm)
d	9
l_1	6.1
l_2	4.9
w_1	1.0
w_2	1.0

The geometrical structure of the slotted circular patch antenna and the fabricated patch are shown in figure 5.6 (b) and (c).

(a)   (b)   (c)
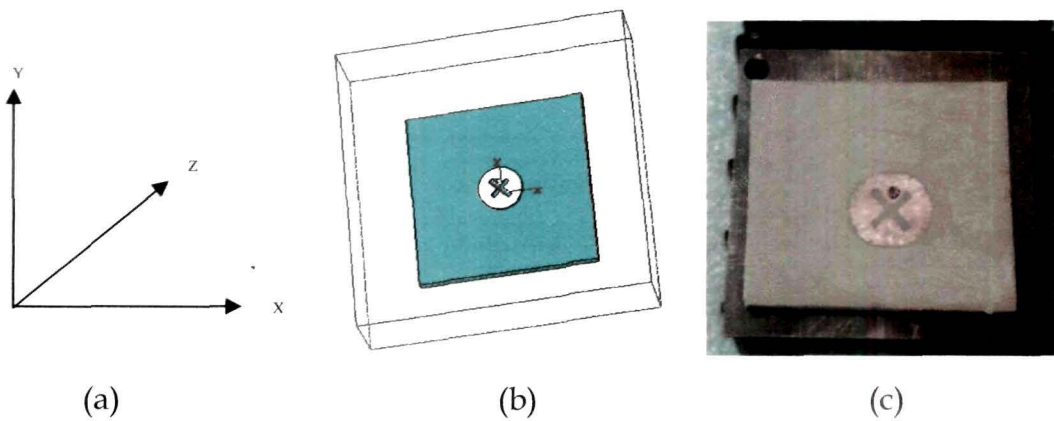
Figure 5.6   (a) Reference coordinate system (b) Slotted circular patch antenna geometrical structure (c) Fabricated patch

5.3.1 S_{11} and radiation pattern results of the unequal arm length cross slotted circular patch antenna

Simulated and measured S_{11} results for the slotted circular patch antenna plotted in figure 5.7 show that the -10 dB bandwidth of the circular patch antenna increases but resonant frequency shifts marginally. The patch resonates at 9.9 GHz.

Adaptation of Different Patch Geometries to Achieve Broadband Operation of Microstrip Antennas on Customized Substrate in X-band

80
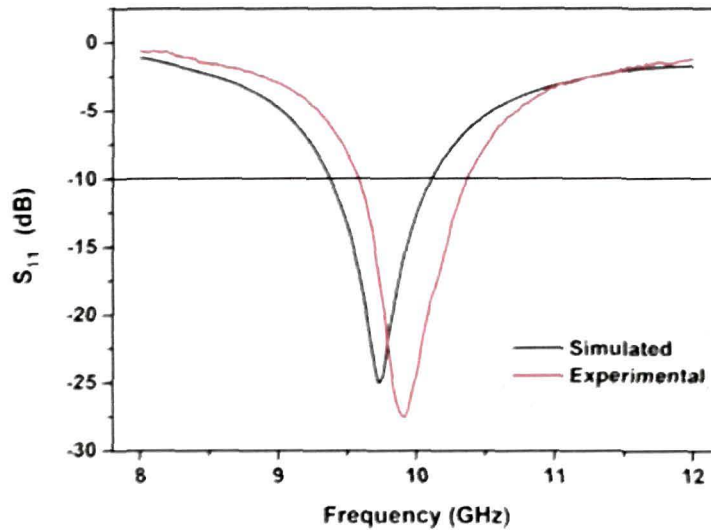
Figure 5.7   Simulated and experimental S_{11} results for slotted circular patch antenna

The radiation pattern of the slotted circular patch antenna is studied at 10 GHz.

The radiation pattern measurement results are shown in figure 5.8 -5.9.

Figure 5.8   Measured radiation pattern in (a) the XZ-plane and (b) YZ-plane for slotted circular patch antenna on graded substrate at 10 GHz in receiving mode and standard transmitting antenna polarization is in the XZ plane (reference figure 5.6 (a))

Adaptation of Different Patch Geometries to Achieve Broadband Operation of Microstrip Antennas on Customized Substrate in X-band

81

Figure 5.9   Measured radiation pattern in (a) the XZ-plane and (b) YZ-plane for slotted circular patch antenna on graded substrate at 10 GHz in receiving mode and standard transmitting antenna polarization is in the YZ plane (reference figure 5.6 (a))

From the radiation pattern, the directivity of the antenna is found out to be 7.51 dBi and 7.1 dBi for the two orthogonal polarization planes at 10 GHz.

5.3.2 Measurement of axial ratio

The axial ratio is determined for the whole operating frequency band. In general, polarization of EM wave is considered to be elliptical.
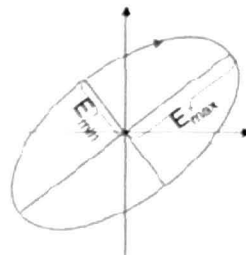
Figure 5.10   Polarization ellipse of electric field vector

Plane polarization and circular polarization are special cases of elliptical polarization. Axial ratio is defined as,

Adaptation of Different Patch Geometries to Achieve Broadband Operation of Microstrip Antennas on Customized Substrate in X-band

82

$$\text{Axial ratio} = E_{max}/E_{min}$$

The axial ratio is measured in the direction of maximum radiation over the operating frequency band. The antenna under test is kept in receiving mode. The transmitting horn antenna is rotated in angular steps of 2 degrees over a complete 360° rotation about the line of sight.

Transmitting antenna rotates around the line of sight

Line of sight

Receiving antenna rotates on a horizontal plane
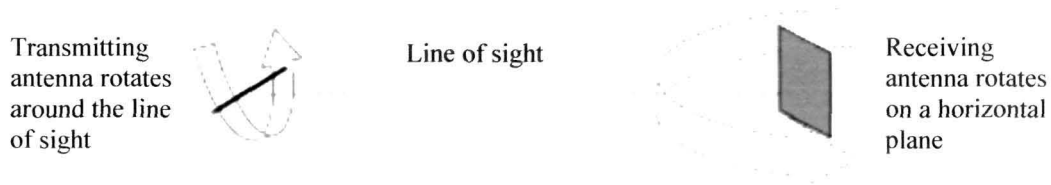
Figure 5.11   Schematic of the measurement set up

In case of cross slotted circular patch antenna, the E_{max} and E_{min} are observed in the two orthogonal planes and axial ratio is calculated over the operating band.
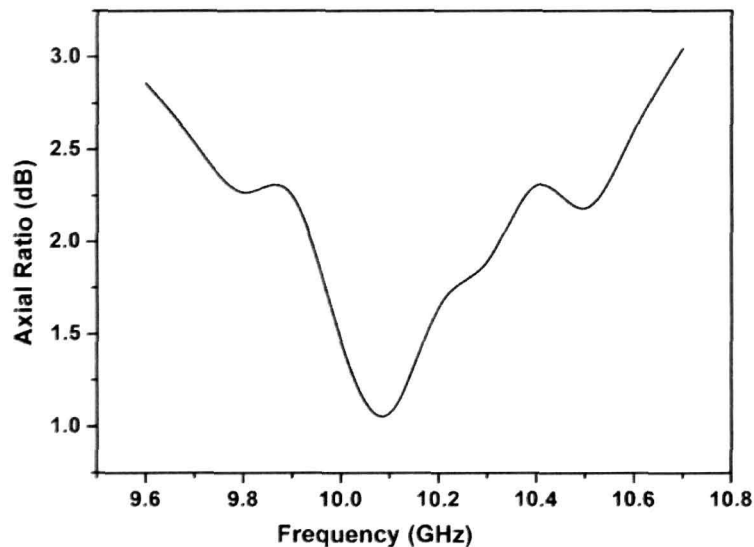
Figure 5.12 Measured axial ratio for slotted circular patch antenna on graded substrate

The axial ratio is observed to be less than 3 dB from 9.6 GHz to 10.6 GHz (figure 5.12).

Table 5.2 gives the measured results of the S_{11} measurements for the simple circular patch antenna and slotted circular patch antenna

Adaptation of Different Patch Geometries to Achieve Broadband Operation of Microstrip Antennas on Customized Substrate in X-band

83

Table 5.2 Comparison of S_{11} results of simple and slotted circular patch antennas

Design	Design frequency (GHz)	Resonating Frequency (GHz)	S_{11} at resonating frequency (dB)	-10 dB bandwidth	Directivity (dBi)
Simple circular patch	10	10.04	-21.79	6.8 %	7.21
Slotted circular patch	10	9.9	-27.48	7.5 %	7.51

5.4 AMALGAMATED RECTANGULAR AND V-SLOTTED SEMICIRCULAR PATCH ANTENNA

The slotted circular patch discussed in the previous section is bifurcated to form two V-slotted semicircular patch of same radius. Literature shows that a semicircular patch resonates at the same frequency as its circular counter part of same radius [18, 19]. In the new approach, the two V-slotted semicircular patches are incorporated as the parasitic section gap coupled is a rectangular patch antenna, capacitively coupled to the centre rectangular patch.

5.4.1 Design and study of amalgamated rectangular and V-slotted semicircular patch antenna

The schematic diagram of the patch geometry is shown in figure 5.13a. The dimensions of the rectangular patch, slots on the semicircular patch, gap between the rectangular and the semicircular patches, angle of inclination of the slots to the base of the semicircular patch and the feed point location are optimized using simulation. The optimized dimensions are indicated in figure 5.13b. Figure 5.13c shows photograph of the fabricated structure.

Adaptation of Different Patch Geometries to Achieve Broadband Operation of Microstrip Antennas on Customized Substrate in X-band

84

(a)   (b)   (c)
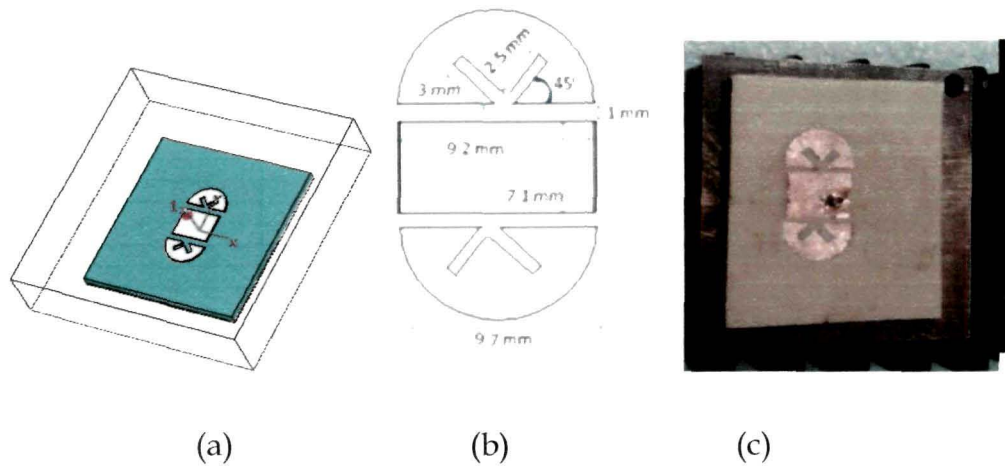
Figure 5.13 V-slotted semicircular patch coupled rectangular patch microstrip antenna

Simulated results of S_{11} parameter for different gap dimension between the rectangular and the semicircular patches are shown in figure 5.14.
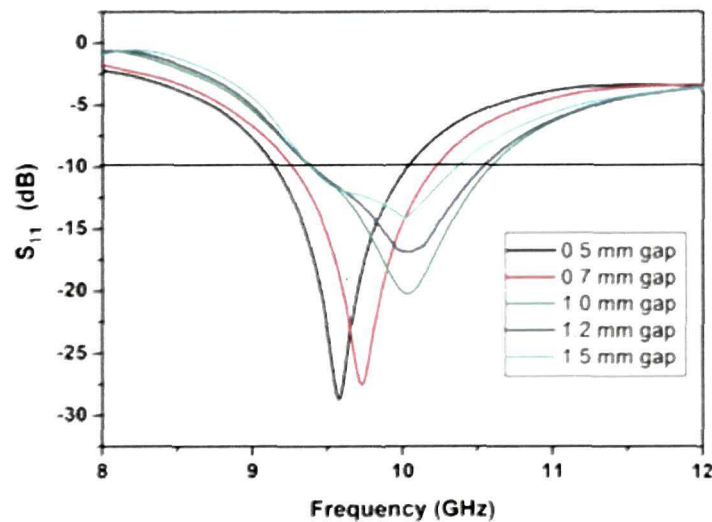
Figure 5.14 Simulated S_{11} results for slotted semicircular patch coupled rectangular patch antenna on graded substrate for different gap dimension

Results show that the antenna system with 1 mm gap between the semicircular and the rectangular patch performs with largest -10 dB bandwidth. The metallization of the patch geometry is done over the graded substrate using the technique discussed in chapter IV (section 4.3.2). The design is investigated for its performance in X-band by taking the measurements of S_{11} parameter and the radiation pattern at 10 GHz.

Adaptation of Different Patch Geometries to Achieve Broadband Operation of Microstrip Antennas on Customized Substrate in X-band

85

5.4.2 S₁₁ and radiation pattern results of amalgamated rectangular and V-slotted semicircular patch antenna
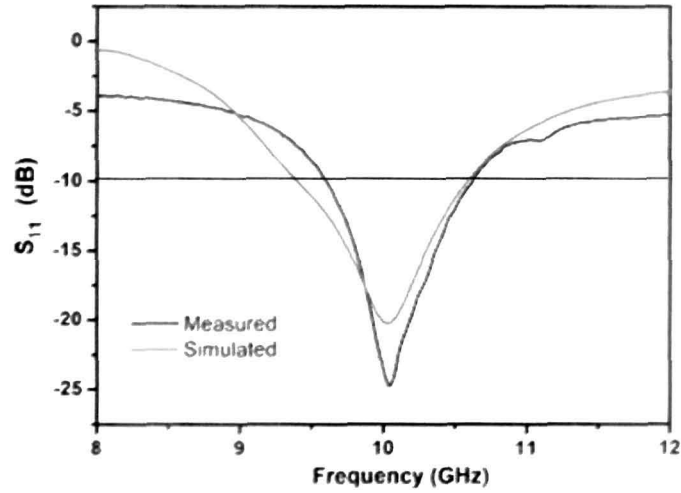
Figure 5.15 Simulated and experimental S_{11} results for slotted semicircular patch coupled rectangular patch antenna on graded substrate

The simulated and measured S_{11} results for the design with 1mm gap between the rectangular patch and the semicircular patches as shown in figure 5.15 show close agreement with each other. An enhancement of 9.4 % bandwidth of operation of the antenna is observed. The comparison of measured S_{11} results for simple rectangular antenna and simple circular patch antenna with the new design is given in table 5.3.

Table 5.3   Comparison of S_{11} results for developed antennas

Design	Design frequency (GHz)	Resonating Frequency (GHz)	S_{11} at resonating frequency (dB)	-10 dB bandwidth
Simple rectangular patch	10.0	10.1	-38.6	6.73 %
Simple circular patch	10.0	10.04	-21.79	6.8 %
Slotted circular patch	10.0	9.9	-27.48	7.5 %
Slotted semicircular patch amalgamated with rectangular patch	10.0	10.05	-24.9	9.4 %

The simulated performance of the proposed antenna is compared with the conventional design of the gap coupled rectangular patch antenna.

Adaptation of Different Patch Geometries to Achieve Broadband Operation of Microstrip Antennas on Customized Substrate in X-band

86

Comparative performance evaluation for the two designs is carried out for equivalent overall sizes of the two antennas (figure 5.16). Simulated S_{11} results using CST Microwave Studio (figure 5.17) is centered at 11 GHz and -10 dB bandwidth is 2.3 % only, while the amalgamated patch shows much superior performance with -10 dB bandwidth of 9.4 %.

(a)   (b)
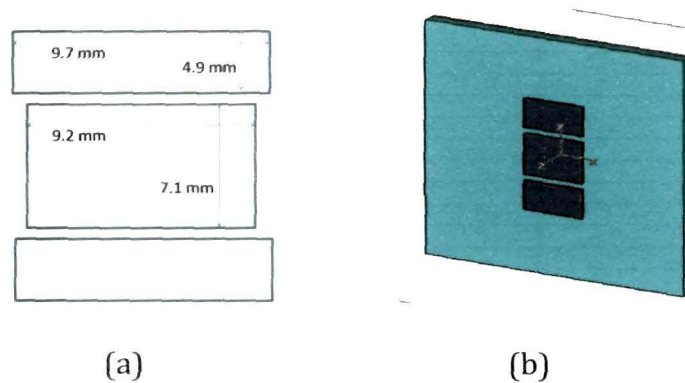
Figure 5.16 (a) Schematic of the patch system (b) Schematic of the rectangular patch coupled microstrip antenna
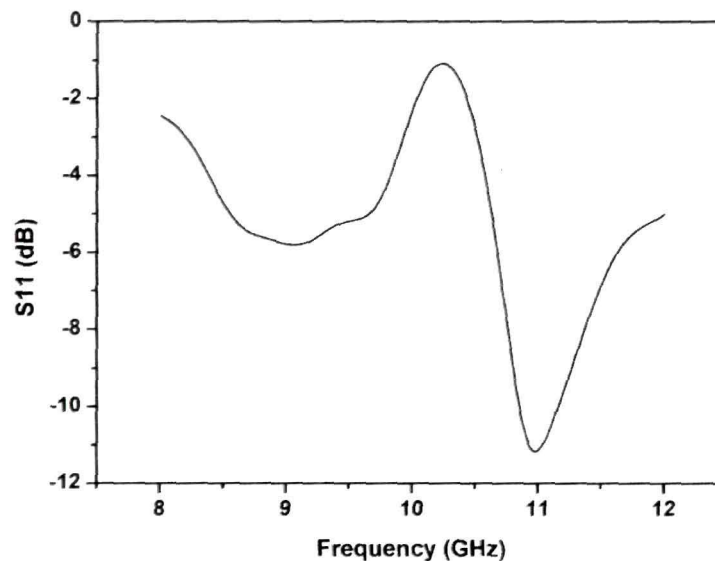
Figure 5.17 Simulated S_{11} results for rectangular patch coupled microstrip antenna

Radiation pattern of amalgamated rectangular and V-slotted semicircular patch antenna in two orthogonal planes at 10 GHz are shown in figure 5.18 - 5.20. Directivity of 11.4 dBi and 11.9 dBi are observed from patterns of figure 5.18 and figure 5.19 respectively. The axial ratio for the whole operating frequency band plotted in figure 5.20 is determined by

Adaptation of Different Patch Geometries to Achieve Broadband Operation of Microstrip Antennas on Customized Substrate in X-band

87

measuring the power received by the antenna in two orthogonal planes of the patch. The axial ratio for the whole operating bandwidth is found to be less than 2.5 dB which is well within the 3 dB accepted standard for circularly polarized antennas [20].
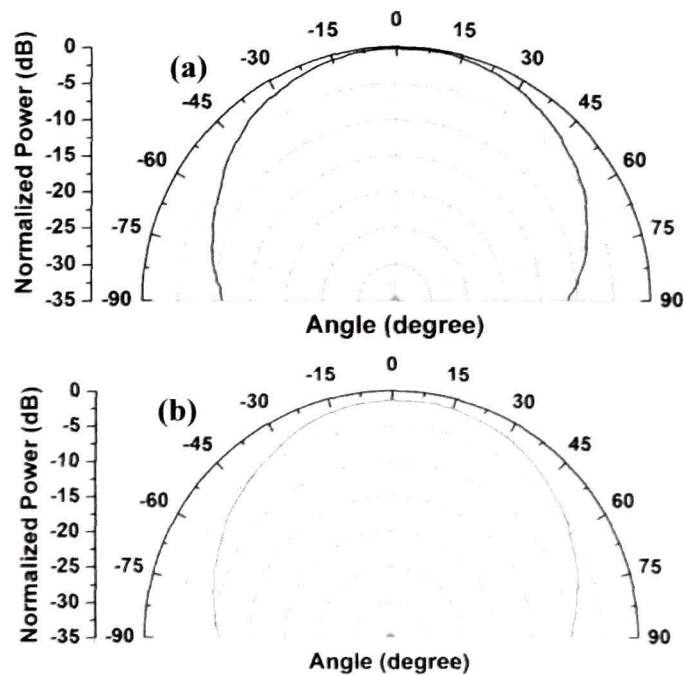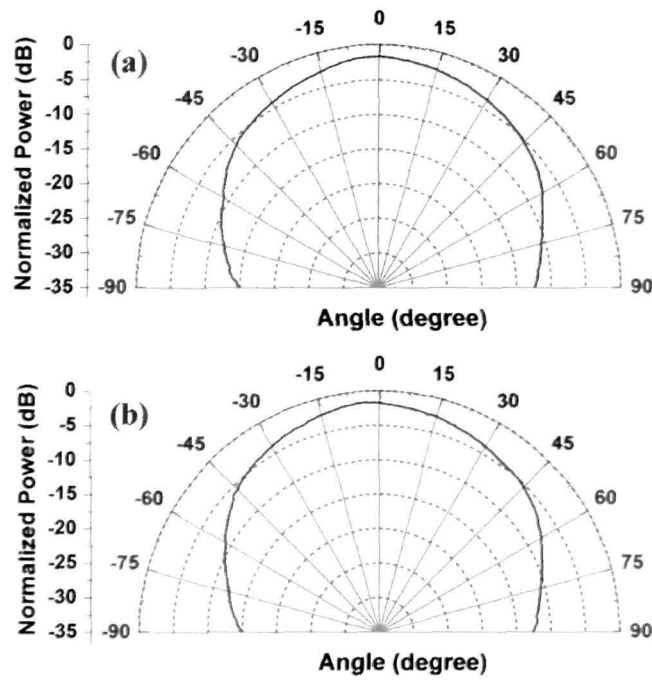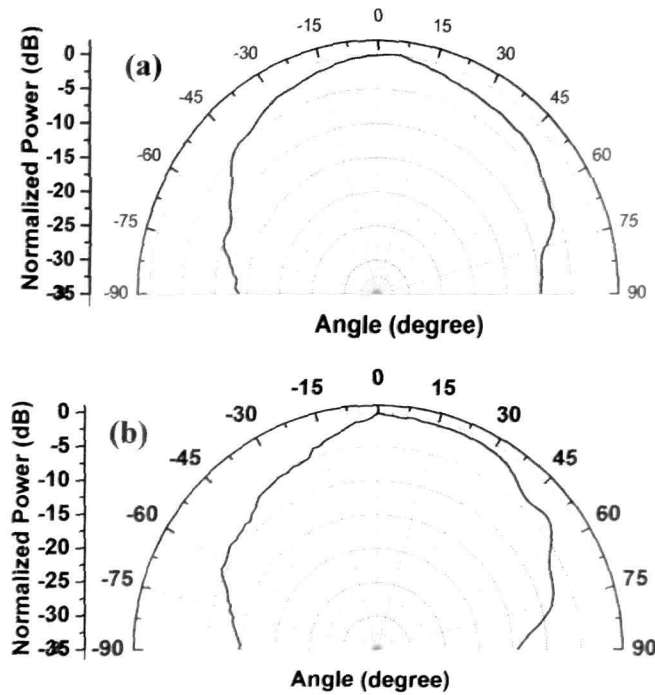

Figure 5.18   Measured radiation pattern in (a) the XZ-plane and (b) YZ-plane for slotted circular patch antenna on graded substrate at 10 GHz in receiving mode and standard transmitting antenna polarization is in the XZ plane (reference figure 5.6 (a))

Adaptation of Different Patch Geometries to Achieve Broadband Operation of Microstrip Antennas on Customized Substrate in X-band

88
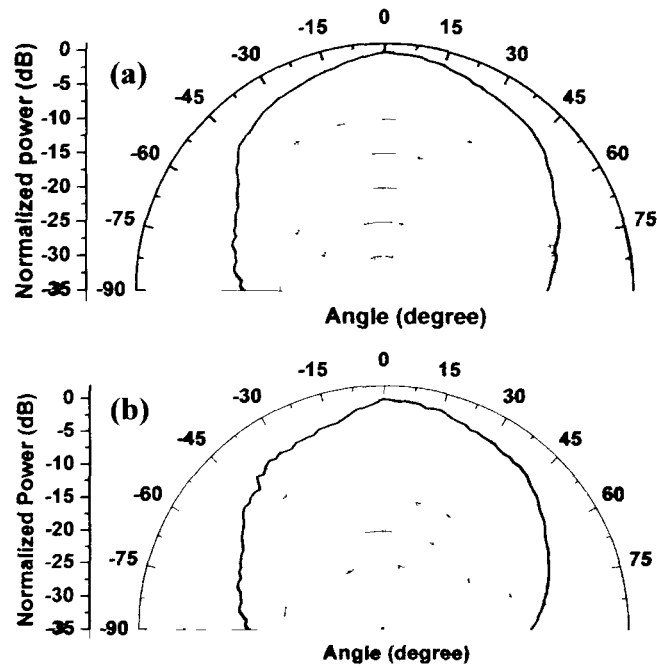
Figure 5.19 Measured radiation pattern in (a) the XZ-plane and (b) YZ-plane for slotted circular patch antenna on graded substrate at 10 GHz in receiving mode and standard transmitting antenna polarization is in the YZ plane (reference figure 5.6 (a))
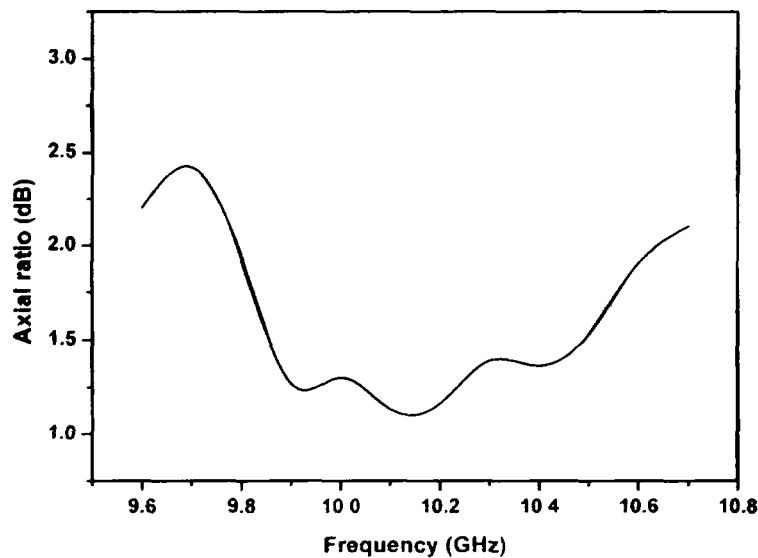
Figure 5.20 Measured axial ratio for slotted semicircular patch coupled rectangular patch antenna on graded substrate

5.5 CONCLUSIONS

Unequal slot arm length incorporated on the circular patch antenna shows both circular polarization and an increase in the operating bandwidth. The resonance frequency shifts from 10.04 GHz for the simple circular patch antenna

Adaptation of Different Patch Geometries to Achieve Broadband Operation of Microstrip Antennas on Customized Substrate in X-band

89

to 9.9 GHz for slotted circular patch antenna. Incorporation of unequal arm length V-slotted semicircular patch antenna capacitively coupled with a centre rectangular patch increases the operating bandwidth from 6.4 % to 9.4 % (table 5.3). The axial ratio for the new design is below 2.5 dB for the whole operating band suggesting that the antenna system can be used as a broadband circularly polarized antenna in X-band. The simulated results show that the amalgamated V-slotted semicircular patch with centre as rectangular patch performs better than the patch with rectangular parasitic element of same dimensions.

Adaptation of Different Patch Geometries to Achieve Broadband Operation of Microstrip Antennas on Customized Substrate in X-band

90

References

[1]   Bahl, I.J. and Bhartia, P., *Microstrip Antennas*, (Artech House, Dedham, MA, 1980).

[2]   Wong, K.-L., *Compact and Broadband Microstrip Antennas*, (John Wiley & Sons, 2002).

[3]   Kumar, G. and Ray, K.P., *Broadband Microstrip Antennas*, (Artech House, Boston, 2003).

[4]   Schaubert, D.H. and Farrar, F.G., Some Conformal Printed Circuit Antenna Designs, *Proc. Workshop Printed Circuit Antenna Tech.*, NM, **5**, 1-21, (1979).

[5]   Kumar, G. and Gupta, K.C., Broadband Microstrip Antennas Using Additional Resonators Gap Coupled to the Radiating Edges, *IEEE Trans. Antennas and Propagat.* **AP-32**, 1375-1379, (1984).

[6]   Kumar, G. and Gupta, K.C., Nonradiating Edges and Four Edges Gap Coupled Multiple Resonator Broadband Microstrip Antennas, *IEEE Trans. Antennas and Propagat.*, **AP-33**, 173-178, (1985).

[7]   Wood, C., Improved Bandwidth of Microstrip Antennas Using Parasitic Elements, *Proc. IEEE*, **127**, 231-234, (1980).

[8]   Entsehladen, E. and Nagel, U., Microstrip Patch Array Antenna, *Electron. Lett.*, **20**, 931-933, (1984).

[9]   Anandan, C.K., Mohanan, P., and Nair, K.G., Broadband Gap Coupled Microstrip Antenna, *IEEE Trans. Antennas and Propagat.*, **AP-38**, 1581-1586, (1990).

[10] Kwaha, B.J., Inyang, O.N. and Amalu, P., The Circular Microstrip Patch Antenna - Design and Implementation, *International Journal of Research and Reviews in Applied Science*, **8**, 86-95, (2011).

[11] Albooyeh, M., Komjani, N. and Shobeyri, M., A Novel Cross-Slot Geometry to Improve Impedance Bandwidth of Microstrip Antennas, *Progress in Electromagnetic Research Letters*, **4**, 63-72, (2008).

[12] Chakraborty, S., Dey, U.K., Panda, S., Gupta, B. and Yasumoto, K., Parasitically Loaded Broad Band Microstrip Antennas for Proposed IEEE

Adaptation of Different Patch Geometries to Achieve Broadband Operation of Microstrip Antennas on
Customized Substrate in X-band

91

802.15.3a (UWB) Communication Systems, *Proceedings of Acia-Pacific Microwave Conference*, (2006).

[13] Dey, S., Anandan, C.K., Mohanan, P. and Nair, K.G., A New Compact Circular Patch Antenna, *Proceedings of Antennas and Propagation Society International Symposium, AP-S. Digest*, **2**, 822-825, (1994).

[14] Deshpande, M.D. and Das, N.K., Rectangular Microstrip antenna for Circular Polarization, *IEEE Trans. Antennas and Propagat.*, **AP-34**, 744, (1986)

[15] Lee, S.K., Sambell, A., Korolkiewicz, E., Ooi, S.F. and Qin, Y., Design of a Circular Polarized Nearly Square Microstrip Patch Antenna with Offset Feed, *Proceedings of High Frequency Postgraduate Student Colloquium*, (2004)

[16] Lu, J.-H. and Yang, K.-P., A Simple Design for Single-feed Circularly Polarized Microstrip Antennas, *Proc. Natl. Sci. Counc. ROC(A)*, **24**, 130-133, (2000).

[17] Nishiyama, E. and Aikawa, M., Circular Polarization Controllable Microstrip Antenna, *IEEE Antennas and Propagation Society International Symposium*, 5195-5198, (2007).

[18] Ray, K.P. and Krishna, D.D., Compact and Dual Band Suspended Semicircular Microstrip Antenna with Half-U slot, *Microwave and Optical Technology Letters*, **48**, 2021-2024, (2006).

[19] Ansari, J.A. and Mishra, A., Half U-Slot Loaded Semicircular Disk Patch Antenna for GSM Mobile Phone and Optical Communications, *Progress in Electromagnetics Letters C*, **18**, 31-45, (2011).

[20] Mak, K.M. and Luk, K.M., A Circularly Polarized Antenna with Wide Axial Ratio Beamwidth, *IEEE Trans. Antennas and Propagat.*, **57**, 3309-3312, (2009)

Adaptation of Different Patch Geometries to Achieve Broadband Operation of Microstrip Antennas on Customized Substrate in X-band

92

CHAPTER VI

EMBEDDED MICROSTRIP ANTENNA STRUCTURE WITH SLOTTED PATCH AND SUPERSTRATE FOR BANDWIDTH ENHANCEMENT

6.1 Introduction

6.2 Embedded Microstrip Antenna Structure

6.2.1 Dimensions of cavity ground structure for embedded rectangular patch antenna

6.2.2 Simulated and measured S_{11} results for embedded microstrip antenna

6.2.3 Radiation pattern studies of the fabricated embedded antenna design

6.3 Embedded Microstrip Antenna Structure with Slotted Patch

6.3.1 S_{11} and radiation pattern studies of embedded slotted patch antenna

6.4 Superstrate Patch on the Embedded Microstrip Antenna with Slotted Patch Structure

6.4.1 Graded composite material as superstrate

6.4.2 Superstrate patch on the embedded slotted patch microstrip antenna structure

6.5 Conclusions

References

6.1 INTRODUCTION

Satellite and other broadcasting communication systems needs small-sized antennas which could be integrated with the body of the system. Such low profile conformal antennas when mounted over airborne vehicles and systems will have better aerodynamic profiles and radar cross-sectional area, with reduced risk of antenna structural damage as compared to the conventional types.

Most commonly, patch antennas are used with a finite ground plane, which usually causes degradation such as increased cross polarization and backward characteristics, thereby leading to decreased antenna gain [1-6]. Also, as the antenna, which is a radiating system, is often integrated with the associated RF circuits and hence is in close proximity, overall system performance may be affected because of EMI due to radiation fields of the antenna. This problem may be addressed by taking the body of the system on which it is mounted as infinite ground plane. This problem can be overcome by using cavity ground structures with the patch antennas [3-8]. In this approach, the space to accommodate the antenna structure is created by a metal cavity located on a metallic body and it enables the antenna to be placed suitably inside the cavity, which serves as a shielding room for the subsystem from the antenna radiation. Cavity backing can be used to suppress surface wave effects, resulting in enhanced impedance bandwidth and directivity [3, 4].

A design has been developed using simple rectangular patch antenna as the radiator, where the ground plane is integrated with the body of the mounting system, and the substrate embedded into the system so that the patch lies in the same plane as the outer surface of the body. As a consequence, the mounting of the antenna will have no influence on the aerodynamics of the host body. Since the radiator is a simple rectangular patch antenna, it suffers from narrow bandwidth, which limits the practical applications. Slots are reported to enhance the operational bandwidth [9, 10].

Adaptation of Different Patch Geometries to Achieve Broadband Operation of Microstrip Antennas on
Customized Substrate in X-band

93

An unequal cross slot and three rectangular slots are incorporated in the rectangular patch structure to enhance the frequency bandwidth of operation.

Superstrate (cover) are often used to protect microstrip antennas from environmental hazards and weather conditions. Proper selection of superstrate layer is reported to enhance the bandwidth of operation [14-18]. A parasitically fed stacked patch is incorporated as superstrate patch and investigated for further enhancement of bandwidth.

6.2 EMBEDDED MICROSTRIP ANTENNA STRUCTURE

A simple rectangular patch antenna at 10 GHz is designed as discussed in Chapter III. A rectangular cavity of depth, (*h+Patch thickness*), equal to the thickness of the graded composite substrate and the patch is designed on the grounded conductor plate. Whole antenna structure is grooved into the cavity. The layout of the embedded microstrip antenna design with rectangular radiating patch is shown in the figure 6.1. The radiating patch is coaxially fed.

Using transmission line model, the minimum dimension of the ground plane can be calculated with the following equations [1-3],

$$L_g = 6h + L \tag{6.1}$$

$$W_g = 6h + W \tag{6.2}$$

where, L is the length of the rectangular patch and W is the width of the patch.

(a)   (b)
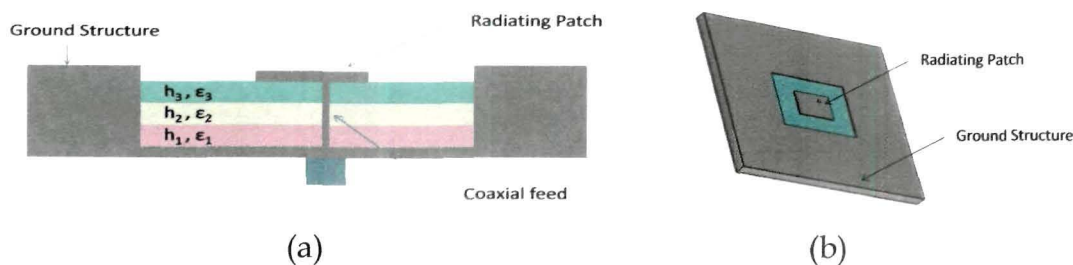
Figure 6.1   (a) Cross sectional view of the cavity grounded design
                     (b) Top view of the cavity grounded design

Adaptation of Different Patch Geometries to Achieve Broadband Operation of Microstrip Antennas on Customized Substrate in X-band

94

6.2.1 Dimensions of cavity ground structure for embedded rectangular patch antenna

The cavity dimension is determined using equation 6.1 and 6.2. The final dimension of the cavity and the patch are optimized using CST Microwave Studio. Accordingly, a rectangular brass cavity of dimension 23.48 mm X 19.29 mm is constructed using wire cut electrical discharge machining (EDM). To practically confirm that this is the optimized dimension, two more cavities are designed and fabricated by changing the dimensions by ± 1 mm. 1 mm is the minimum machining convenience which can be taken. Thus, rectangular cavities of dimensions 22.48 X 18.29 mm and 24.48 mm X 20.29 mm are fabricated and modification in the antenna performance is studied.
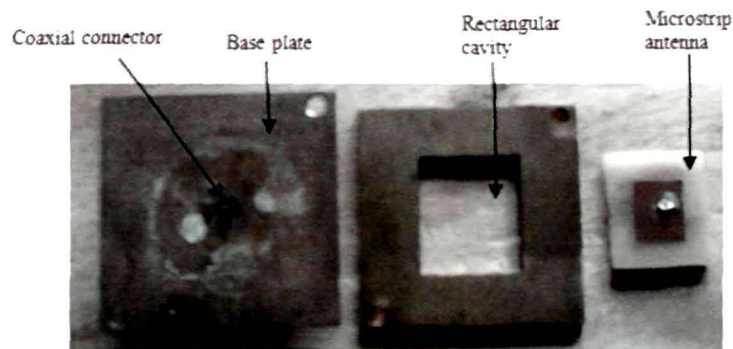
Figure 6.2   Fabricated rectangular cavity ground design

Figure 6.2 shows the different component of the rectangular cavity ground design which is assembled to form a cavity backed structure. The upper plate is 2 mm thick. The graded composite substrate of the same dimension as that of the cavity is fabricated using the chemical process as discussed in chapter III. The substrate with the patch is then embedded within the cavity structure. The coaxial connector feeding the patch is attached to the bottom plate which is 1 mm thick.

Adaptation of Different Patch Geometries to Achieve Broadband Operation of Microstrip Antennas on Customized Substrate in X-band

95

6.2.2 Simulated and measured S_{11} results for embedded microstrip antenna

The S_{11} parameter of the antenna is experimentally determined using Agilent network analyser. Simulated and experimental results of optimized cavity design are shown in Figure 6.3. A bandwidth enhancement is observed as compared to conventional rectangular patch design, which can be attributed to the cavity backing that suppresses guided-wave effects, resulting in enhancement of impedance bandwidth [5].
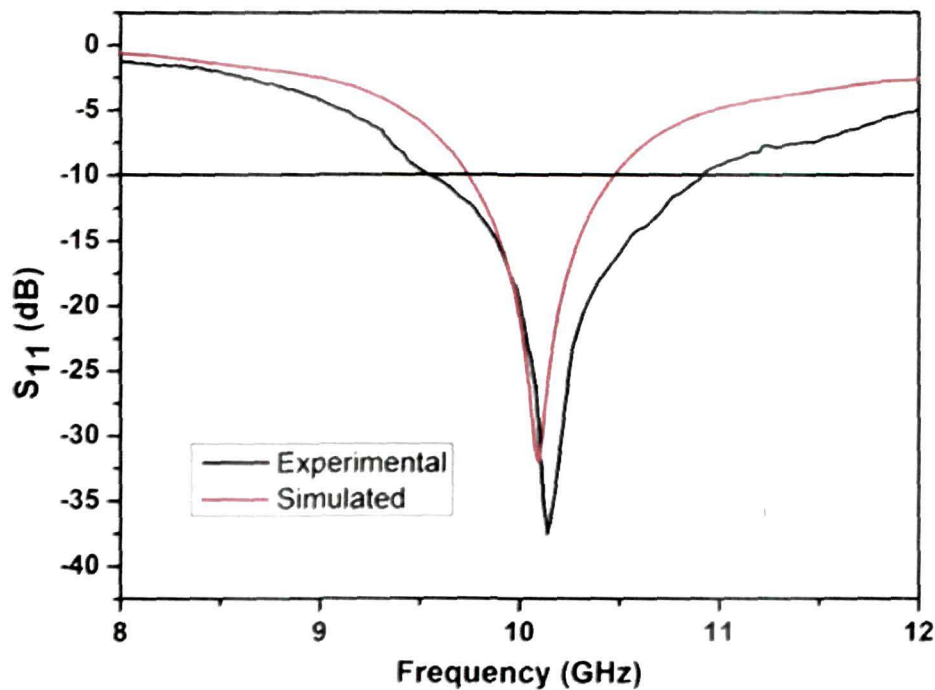
Figure 6.3   Simulated and measured S_{11} results for embedded rectangular patch antenna on graded substrate

Figure 6.4 plots S_{11} parameters for antennas with three different cavity dimensions. The resonant frequency and -10 dB bandwidth results are tabulated in table 6.1. The cavity with dimension 23.48 mm X 19.29 mm, which is also the optimized dimension shows the best operational bandwidth performance.

Adaptation of Different Patch Geometries to Achieve Broadband Operation of Microstrip Antennas on Customized Substrate in X-band

96
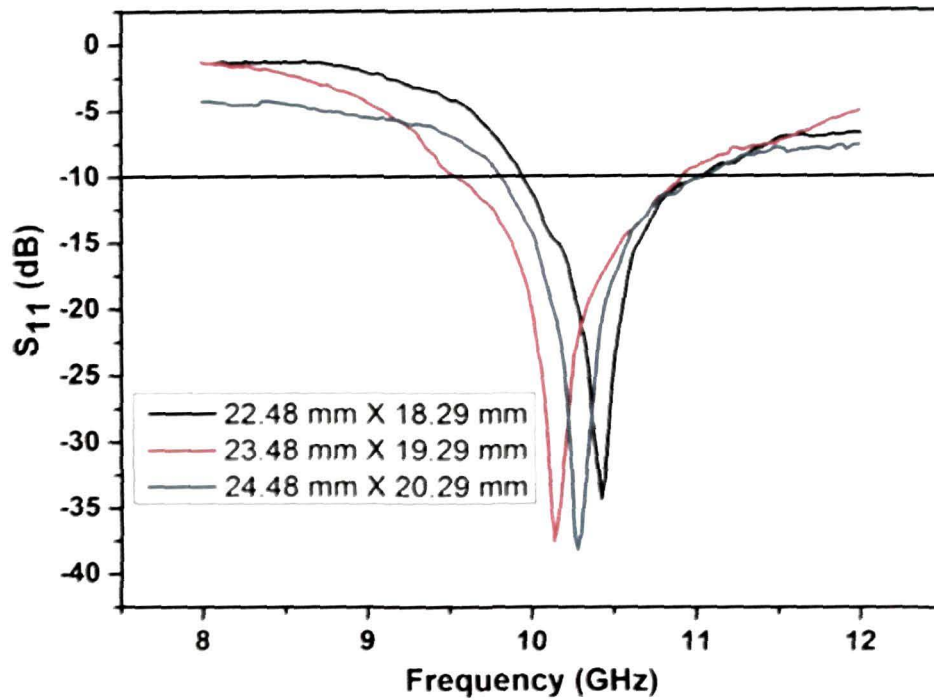
Figure 6.4   Measured S_{11} results for embedded microstrip antenna with different cavity dimension

Table 6.1   Comparison of S_{11} parameters

Groove Dimension	Patch Dimension	Resonating frequency	S_{11} at resonating frequency	-10 dB bandwidth
22.48 mm X 18.29 mm	10.21 mm X 7.12 mm	10.42 GHz	-34.33 dB	10.07 %
23.48 mm X 19.29 mm	10.21 mm X 7.12 mm	10.14 GHz	-37.53 dB	13.01 %
24.48 mm X 20.29 mm	10.21 mm X 7.12 mm	10.28 GHz	-38.17 dB	11.28 %
Simple antenna on Graded Substrate	11.2 mm X 8.1 mm	10.1 GHz	-38.68 dB	6.73 %

6.2.3 Radiation pattern studies of the fabricated embedded antenna design

The radiation pattern for the cavity grounded rectangular patch antenna is consistent over the operating X-band. The E-plane and H-plane radiation pattern for the antenna at 10 GHz are shown in figure 6.5 (a) - (b). The calculated parameters from the radiation pattern studies are included in the table 6.2.

Adaptation of Different Patch Geometries to Achieve Broadband Operation of Microstrip Antennas on Customized Substrate in X-band

97
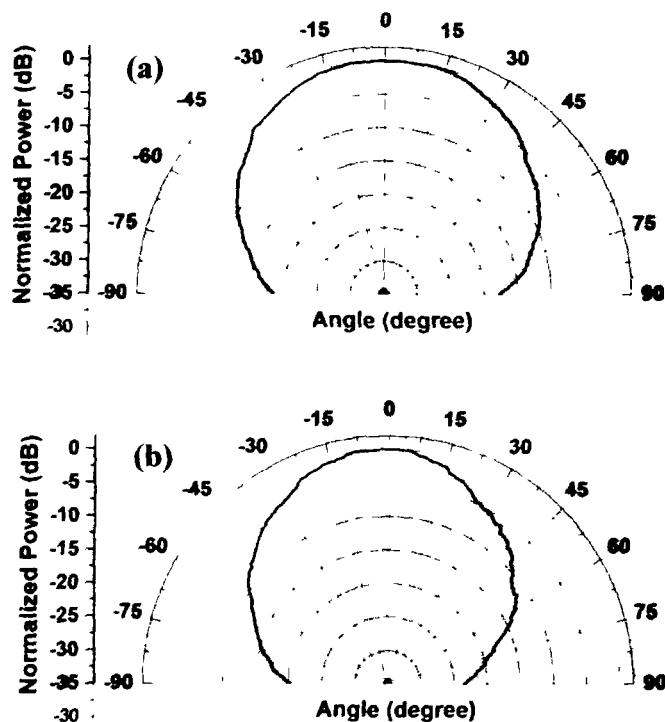
Figure 6.5   Measured (a) E-plane and (b) H-plane radiation pattern for rectangular patch embedded antenna on graded substrate at 10 GHz

Table 6.2   Measured performance comparison of conventional and grooved ground plane antenna

Parameter	Rectangular patch antenna with conventional ground plane	Rectangular patch antenna with grooved ground plane
-10 dB bandwidth	7%	10.5%
S11 at center frequency	-38.7 dB	-37 dB
Directivity	9.91 dBi	11.4 dBi

6.3 EMBEDDED MICROSTRIP ANTENNA STRUCTURE WITH SLOTTED PATCH

A cross slot of unequal arm length is incorporated on the rectangular patch design. Additional, three rectangular slots are incorporated in the radiating edges of the patch to enhance the performance of operation. The design geometry of the patch is shown in figure 6.6. The optimized dimensions of the slots and the patch obtained using simulation are given in

table 6.3. The rectangular patch dimension is kept same as that of simple rectangular patch at 10 GHz. The dimension of the rectangular cavity is taken to be 23.48 mm X 19.29 mm X 2.0 mm.

(a)   (b)
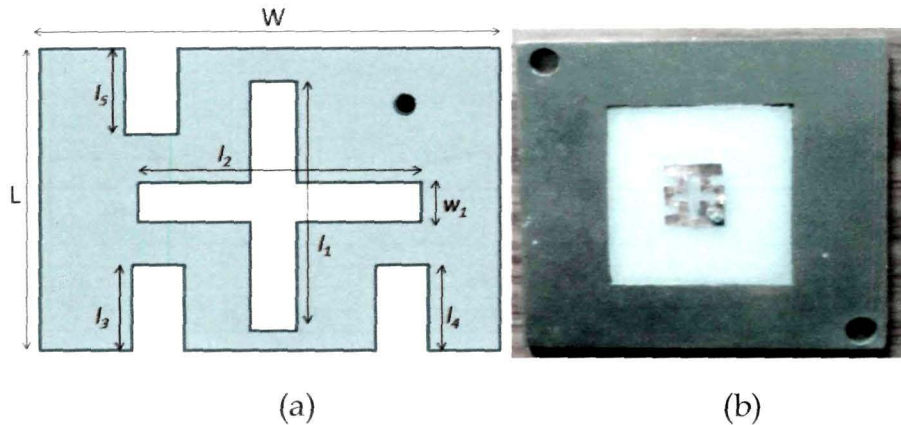
Figure 6.6   (a) Schematic of slotted patch design
                        (b)   Fabricated embedded microstrip antenna design with slotted patch

Table 6.3   Dimension of cavity grounded slotted patch geometry

W (mm)	L (mm)	w_1 (mm)	l_1 (mm)	l_2 (mm)	l_3 (mm)	l_4 (mm)	l_5 (mm)
10.21	7.12	1	6	4.6	1.7	1.8	1.7

Literature [9-13] reports that the lower frequency of operation is mostly controlled by the centre slot of length l_2 and the upper frequency of operation is controlled by the slot of length l_1. The length of the slots on the edges mostly controls the bandwidth of both the bands. The widths of all the slots are kept same as 'w_1'. The position of the feed point is determined using simulation in CST Microwave Studio.

The fabricated slotted patch antenna is shown in figure 6.6 (b). The antenna is fabricated using the hot press lamination technique discussed in the chapter IV.

Adaptation of Different Patch Geometries to Achieve Broadband Operation of Microstrip Antennas on Customized Substrate in X-band

99

6.3.1 S_{11} and radiation pattern studies of embedded slotted patch antenna

The antenna is studied for its performance by measuring the S_{11} parameter and the radiation pattern at the two resonating frequencies.
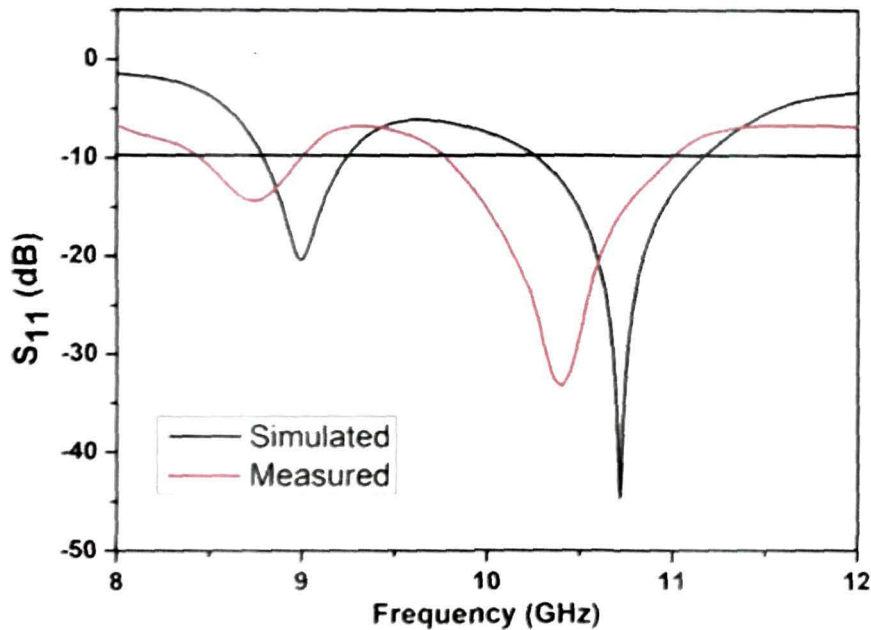
Figure 6.7   Measured S_{11} results for embedded microstrip antenna with slotted patch

The S_{11} measurement result shows that the antenna is resonating with two operating frequency bands in X-band. The presence of slots modifies the surface current distribution of the patch, due to which the resonating frequency of the rectangular patch which is originally designed at 10 GHz also changes [9-13]. The operating frequency bands are dependent on the dimensions of all the slots and the position of the feed point. The lower resonating frequency is 8.74 GHz, and -10 dB bandwidth is observed to be 6.17 % for the lower frequency band and the upper resonating frequency is 10.41 GHz and -10 dB bandwidth for this band is 11.67 %.

The radiation pattern for the cavity grounded slotted rectangular patch antenna is studied in both the band of operation. The E-plane and H-plane radiation pattern for the antenna at 8.6 GHz and 10.3 GHz are shown in figure 6.8 – 6.9. The derived characteristics from the radiation pattern studies are included in the table 6.4.

Adaptation of Different Patch Geometries to Achieve Broadband Operation of Microstrip Antennas on Customized Substrate in X-band

100
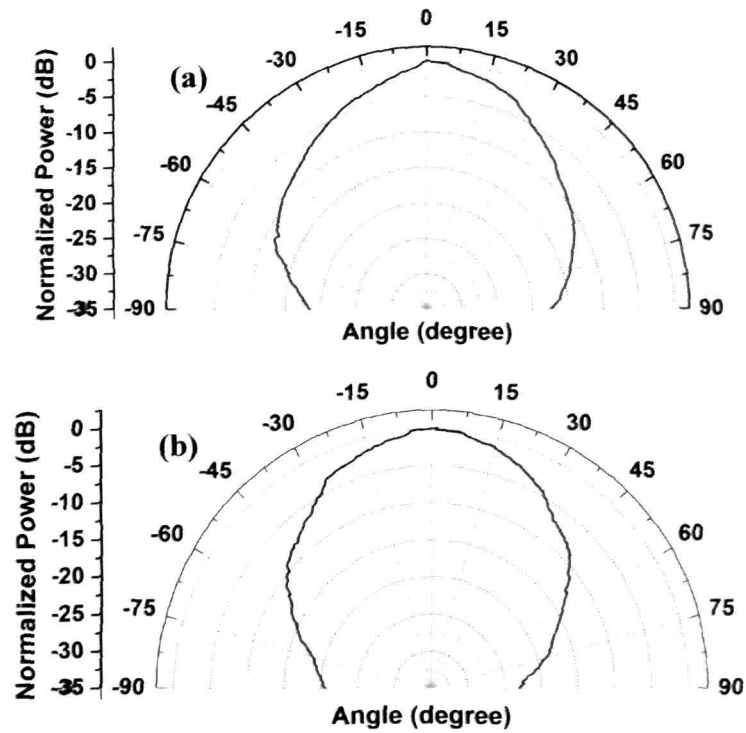
Figure 6.8   Measured (a) E-plane and (b) H-plane radiation pattern for embedded microstrip antenna with slotted patch at 8.74 GHz
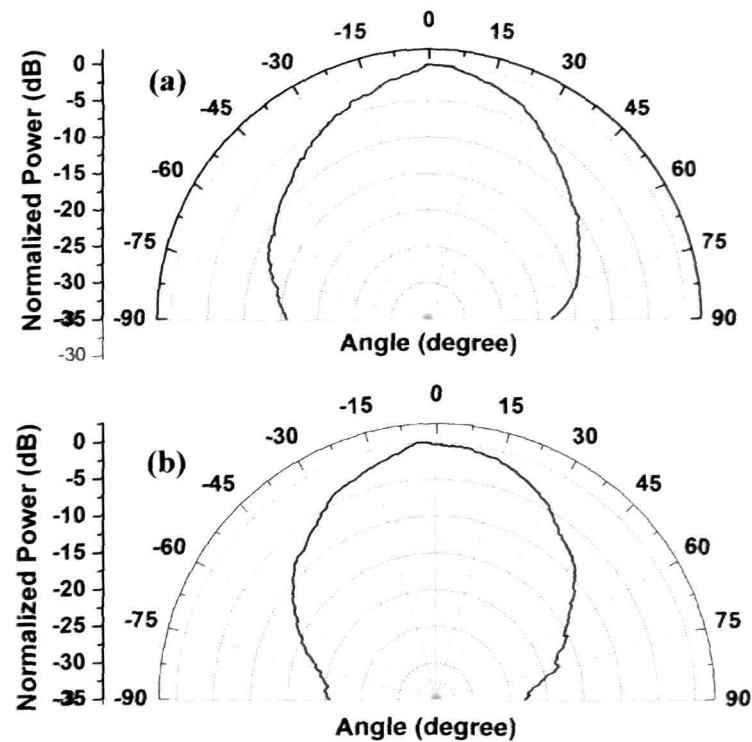
Figure 6.9   Measured (a) E-plane and (b) H-plane radiation pattern for embedded microstrip antenna with slotted patch at 10.41 GHz

Adaptation of Different Patch Geometries to Achieve Broadband Operation of Microstrip Antennas on Customized Substrate in X-band

Table 6.4 Measured performance parameters for embedded patch antenna

Parameter	Embedded microstrip antenna structure	Slotted Patch Embedded microstrip antenna structure	
	(10.1 GHz)	(8.74 GHz)	(10.41 GHz)
-10 dB bandwidth	10.5 %	6.17 %	11.67 %
S11 at center frequency	-37 dB	-14.31 dB	-33.31 dB
Directivity	11.4 dBi	12.03 dBi	12.14 dBi

6.4 SUPERSTRATE PATCH ON THE EMBEDDED MICROSTRIP ANTENNA WITH SLOTTED PATCH STRUCTURE

Superstrate on the antenna are used as covers to protect the antenna from hazardous environmental conditions. The presence of the superstrate shifts the resonant frequency and also enhances the frequency bandwidth. Performance of the slotted patch embedded antenna is investigated using a graded composite superstrate of same dimension and composition as the substrate.

6.4.1 Graded composite material as superstrate

A superstrate of 2 mm thickness is placed over the embedded slotted patch antenna. A shift in resonating frequency towards the lower frequency side is observed for the design. The measured and simulated S_{11} results are shown in figure 6.10.

Adaptation of Different Patch Geometries to Achieve Broadband Operation of Microstrip Antennas on Customized Substrate in X-band

102
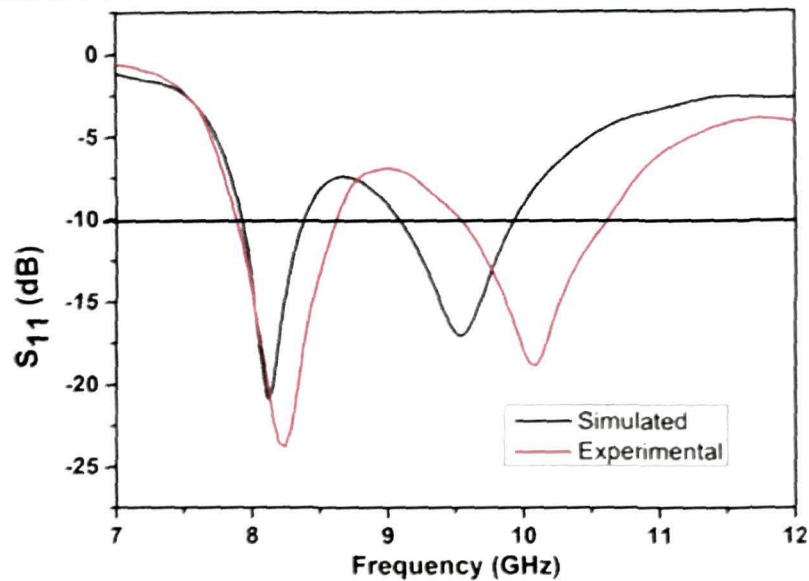
Figure 6.10   Measured and simulated S_{11} results for embedded slotted patch microstrip antenna with superstrate

The lower resonating frequency is shifted from 8.74 GHz to 8.25 GHz, and the upper resonating frequency is shifted from 10.41 GHz to 10.09 GHz, both to the lower side. It is particularly interesting to note that even while the frequency for the lower band has shifted further to the lower side, its -10 dB bandwidth too has increased from 6.17 % to 8.72 % (2.55 % increase) at the cost of reduction in bandwidth for the upper operating band which come down to 10.69 % from 11.67 % (0.98 % decrease). The radiation patterns are found to be practically unchanged from that of the embedded antenna (with slots and without the superstrate) and hence are not included.

6.4.2 Superstrate patch on the embedded slotted patch microstrip antenna structure

A rectangular patch is incorporated as superstrate patch and is parasitically coupled to the slotted patch antenna. Starting from the dimension of the rectangular patch at 10 GHz, the dimension of the superstrate patch is optimized using simulation. The final dimension of the superstrate patch is determined to be 10.4 mm × 8.4 mm. The schematic of the structure is shown in figure 6.11.

Adaptation of Different Patch Geometries to Achieve Broadband Operation of Microstrip Antennas on Customized Substrate in X-band
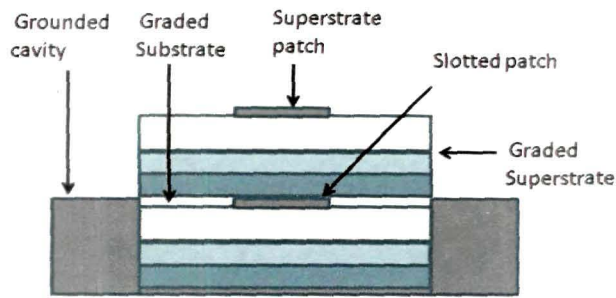
Figure 6.11   Schematic diagram of embedded slotted patch antenna with superstrate patch

A significant increase in bandwidth up to as much as 25.11 % is observed. The frequency spread being from 8.09 GHz to 10.61 GHz. It is worth mentioning that the lower frequency is below the -10 dB cut off for both the simple embedded and with dielectric superstrate structures. At the same time, the upper -10 dB cut off frequency is higher than both these structures.
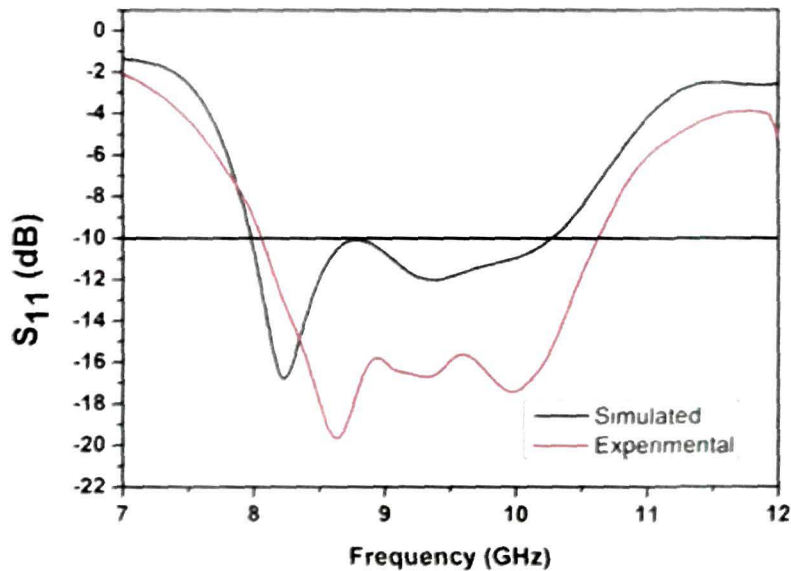
Figure 6.12   Measured and simulated S_{11} results for embedded slotted patch antenna with superstrate patch

Radiation pattern of the embedded slotted patch antenna with superstrate are shown in figure 6.13 – 6.15.

Adaptation of Different Patch Geometries to Achieve Broadband Operation of Microstrip Antennas on Customized Substrate in X-band

104
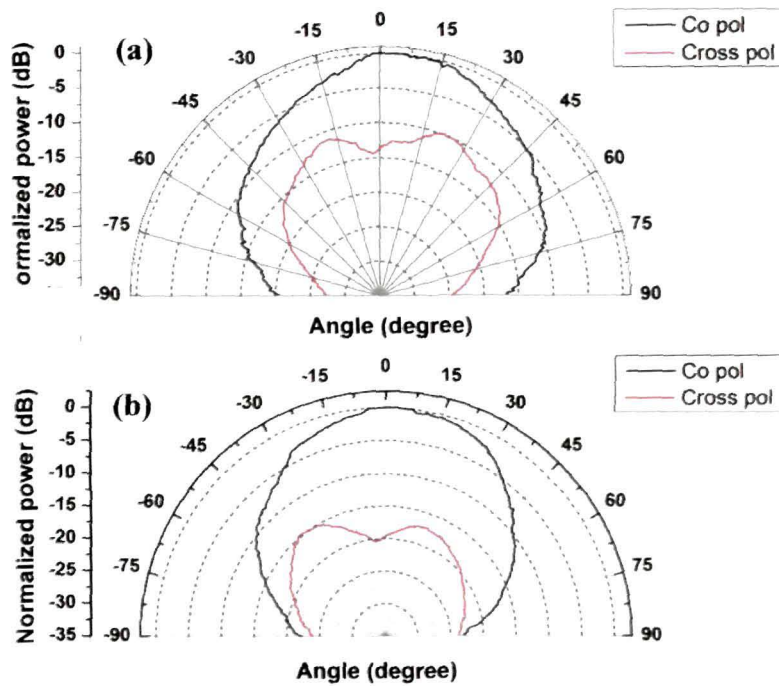
Figure 6.13   Measured (a) E-plane and (b) H-plane radiation pattern for embedded slotted patch antenna with superstrate patch at 8.3 GHz
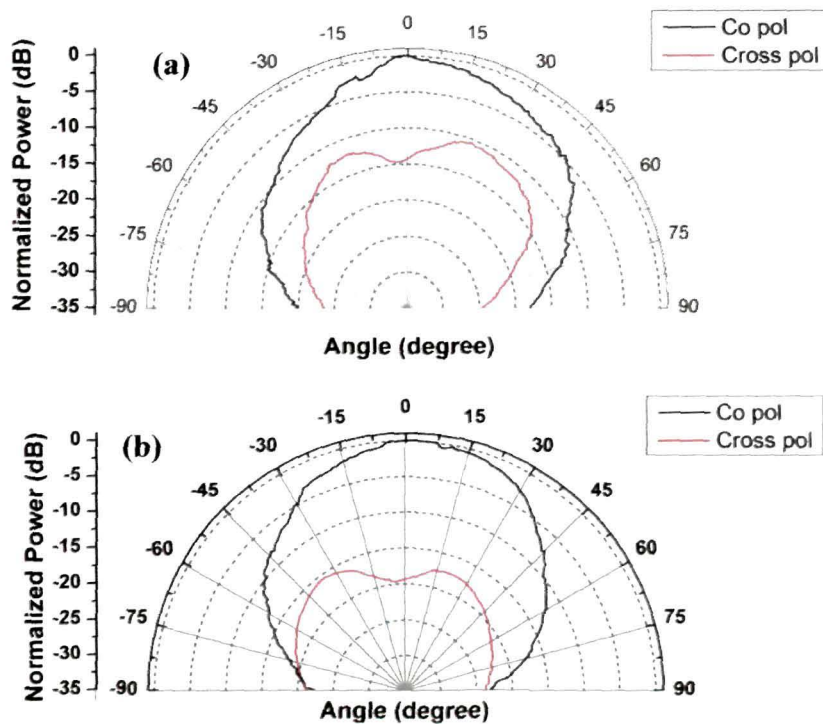
Figure 6.14   Measured (a) E-plane and (b) H-plane radiation pattern for embedded slotted patch antenna with superstrate patch at 9.3 GHz

Adaptation of Different Patch Geometries to Achieve Broadband Operation of Microstrip Antennas on Customized Substrate in X-band
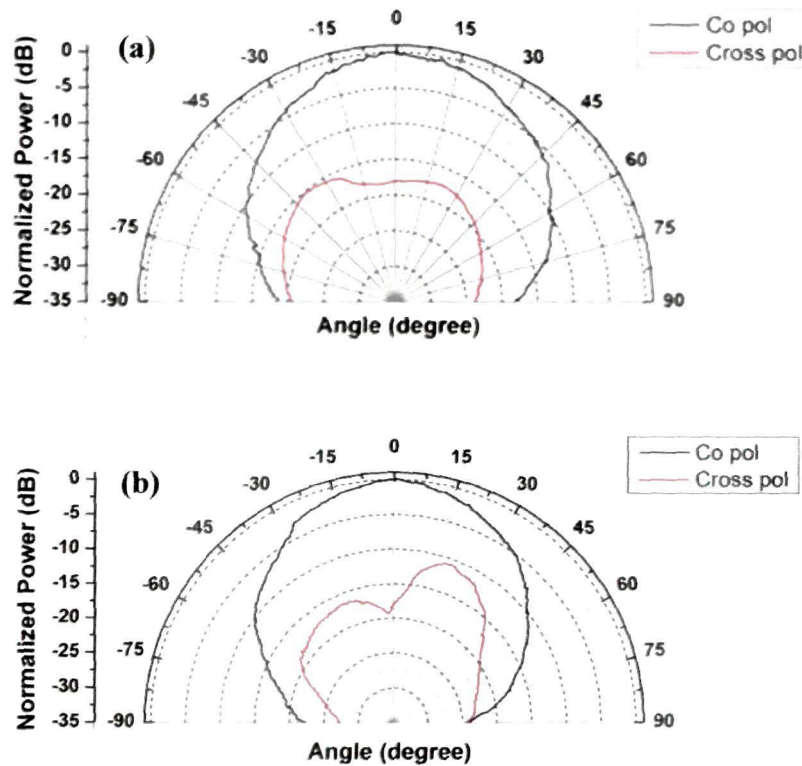
Figure 6.15   Measured (a) E-plane and (b) H-plane radiation pattern for embedded slotted patch antenna with superstrate patch at 10 GHz

Table 6.5   Measured radiation pattern parameters for cavity grounded patch antenna with superstrate patch

Parameter	Embedded slotted patch antenna		Embedded slotted patch antenna with superstrate patch		
	8.74 GHz	10.41 GHz	8.3 GHz	9.3 GHz	10 GHz
Directivity	12.03 dBi	12.14 dBi	11.9 dBi	11.7 dBi	11.83 dBi

The radiation pattern is consistent over the whole operating frequency band (8.09 GHz to 10.61 GHz). The directivity of the antenna is ~11.7 dBi throughout the band

6.5 CONCLUSIONS

The embedded microstrip antenna structure with cavity ground structure show enhancement in operational bandwidth of microstrip antenna on graded composite substrate in X-band. The directivity of the antenna with

Adaptation of Different Patch Geometries to Achieve Broadband Operation of Microstrip Antennas on Customized Substrate in X-band

106

cavity ground structure is more than simple rectangular patch antenna. Incorporation of slots on the radiating patch has changed the surface current distribution of the patch due to which the antenna is capable of radiating in two distinct frequency bands. The resonant frequency and the bandwidth of operation of the antenna are controlled by the length of the slots. Lowering of resonating frequencies for both the operating bands are observed with superstrate over the antenna system with a small increment in operational bandwidth. The operational -10 dB bandwidth is significantly enhanced by using a superstrate patch over the slotted patch geometry. The new antenna structure shows large operational bandwidth of 25.11 % in the X-band. The profile, however, gets marginally raised from the body of mounting system. The final design is an efficient microstrip antenna for wideband applications in X-band.

Adaptation of Different Patch Geometries to Achieve Broadband Operation of Microstrip Antennas on Customized Substrate in X-band

107

References

[1] Wong, K.-L., *Compact and Broadband Microstrip Antennas*, (John Wiley & Sons, 2002).

[2] Zürcher, J. F. and Gardiol, F. E., *Broadband Patch Antennas*, (Artech House, Boston, 1995).

[3] Kumar, G. and Ray, K.P., *Broadband Microstrip Antennas*, (Artech House, Boston, 2003).

[4] Wang, F.J. and Zhang, J.S., Wide Band Cavity-backed Patch Antenna For PCS/IMI2000/2.4 GHz WLAN, *Progress in Electromagnetics Research*, **74**, 39-46, (2007).

[5] Zavosh, F. and Aberle, J.T., Improving the Performance of Microstrip-Patch Antennas, *IEEE Antennas and Propagation Magazine*, **38**, 7-12, (1996).

[6] Li, Q. and Shen, Z., An Inverted Microstrip-Fed Cavity-Backed Slot Antenna for Circular Polarization, *IEEE Antennas and Propagation Letters*, **1**, 190-192, (2002).

[7] Huang, J., The Finite Ground Plane Effect on the Microstrip Antenna Radiation Patterns, *IEEE Trans. On Antennas and Propagat.*, **AP-31**, 649-653, (1983).

[8] Singhal, P.K. and Banerjee, S., A Cavity Backed Rectangular Patch Antenna, *6th International Symposium on Antennas, Propagation and EM Theory*, 112-115, (2003).

[9] Wong, K.-L. and Yang, K.-P., Small dual Frequency Microstrip Antenna with Cross Slot, *Electronics Letters*, **33**, 1916-1917, (1997).

[10] Yang, K.-P., and Wong, K.-L., Inclined-Slot-Coupled Compact Dual-Frequency Microstrip Antenna with Cross Slot, *Electronics Letters*, **34**, 321-322, (1998).

[11] Tong, K.-F., Luk, K.-M., Lee, K.-F. and Lee, R.Q., A Broad Band U-Slot Rectangular Patch Antenna on a Microwave Substrate, *IEEE Trans. On Antennas and Propagat.*, **48**, 954-960, (2000).

Adaptation of Different Patch Geometries to Achieve Broadband Operation of Microstrip Antennas on Customized Substrate in X-band

108

[12] Misran, N., Shakib, M.N., Islam, M.T. and Yatim, B., Design Analysis of a Slotted Microstrip Antenna for Wireless Communication, *World Academy of Science, Engineering and technology*, **49**, 448-450, (2009).

[13] Weigand, S., Huff, G.H., Pan, K.H. and Bernhard, J.T., Analysis and Design of Broad Band Single Layer Rectangular U-slot Microstrip Patch Antennas, *IEEE Trans. Antennas and Propagat.*, **51**, 457-468, (2003).

[14] Choi, W., Pyo, C., Cho, Y. H., Choi, J. and Chae, J., High gain and broadband microstrip patch antenna using a superstrate layer, *Proc. IEEE Antennas Propagat. Soc. Int. Symp.*, **2**, 292-295, (2003).

[15] Alexopoulos, N. G. and Jackson, D. R., Fundamental superstrate (cover) effects on printed circuit antennas, *IEEE Trans. Antennas Propagat.*, **32**, 807-816, (1984).

[16] Luk, K. M., Tam, W. Y. and Yip, C. L., Analysis of circular microstrip antennas with superstrate, *IEE Proc.*, **136**, 261-262, (1989).

[17] Bernard, L., Loison, R., Gillard, R. and Lucidarme, T., High directivity multiple superstrate antennas with improved bandwidth, *IEEE Antennas Propagat. Soc. Int. Symp.*, **2**, 522-525, (2002).

[18] Gürel, Ç.S. and Yazgan, E., Bandwidth widening in an annular ring microstrip antenna with superstrate, *Proc. IEEE Antennas Propagat. Soc. Int. Symp.*, 692-695, (1995).

Adaptation of Different Patch Geometries to Achieve Broadband Operation of Microstrip Antennas on Customized Substrate in X-band

109

CHAPTER VII

DEVELOPMENT OF 3D FDTD APPROACH FOR MICROSTRIP ANTENNA ON GRADED SUBSTRATE

7.1 Introduction

7.2 Problem Formulation

7.2.1 Expression of E and H curl equations in partial differential form

7.2.2 Expression of E and H partial differential equations in finite differential form in spatial and temporal coordinates

7.3 Implementation of FDTD Code

7.3.1 Stability criteria in FDTD

7.3.2 Absorbing boundary conditions

7.3.3 Source considerations

7.3.4 Frequency dependent parameters

7.4 Implementation in Computer Program

7.4.1 Stability criteria

7.4.2 Source consideration

7.4.3 PML terminating condition

7.4.4 Post processing of the results

7.5 Full-Wave Fdtd Analysis of Rectangular Microstrip Antenna on Single Layer and Graded Composite Substrate

7.5.1 E_z field distribution within microstrip antenna substrate

7.5.2 S_{11} parameter analysis

7.6 Conclusions

References

7.1 INTRODUCTION

Solutions to Maxwell's equations play a fundamental role in solving electromagnetic problems. Finite Difference Time Domain (FDTD) technique is an efficient tool that can be used to analyse electromagnetic problems such as radiations, microwave devices and scattering by solving the Maxwell's equations on any scale with almost all kinds of environments [1-6]. The technique can be effectively applied to analyse the electric field distribution inside the antenna structure as well as in the surrounding area of interest [1].

Kane S. Yee in 1966 [1] was first to develop the algorithm for FDTD method to determine initial boundary value problems involving Maxwell's equations in isotropic media. The FDTD method discretizes the time dependent Maxwell's equation for vector components using central difference approximations for space and partial derivatives for time. The em wave solution in FDTD is fully worked out in space grid and time-stepping algorithm within the computation domain, where, at any point in space the updated value of the E-field in time is dependent on the stored value of the E-field and the numerical curl of the local distribution of the H-field in space. Similarly, the updated value of the H-field in time is dependent on the stored value of the H-field and the numerical curl of the local distribution of the E-field in space (leap frog arrangement) [1-4].

The 3D FDTD formulation developed here is for rectangular microstrip antenna on graded composite substrates fed at 50 Ω impedance matching point within the patch. A Gaussian discrete pulse is used to excite the radiating patch at the feed point. The substrate is dielectric and the permittivity is taken isotropic.

Initially, the FDTD method analyzes rectangular microstrip patch antenna on single layer composite systems and then extends for graded system. The implementation of numerical features like the computational domain, stability criteria, boundary conditions, subsequent gridding and time stepping for updating electric and magnetic fields is discussed. An in-house program is developed to analyze the field distribution of the antenna.

Adaptation of different patch geometries to achieve broad band operation of microstrip antenna on customized composite substrate in X-band

110

7.2 PROBLEM FORMULATION

The FDTD method provides a direct time domain solutions of Maxwell's equations in differential form by discretizing both the physical region and time interval using a uniform grid, known as Yee cells (figure 7.1(a)). An electromagnetic wave interaction structure is mapped into the three dimensional space lattice by assigning appropriate values of permittivity to each electric field component, and permeability to each magnetic field component as shown in figure 7.1(b).

(a)   (b)
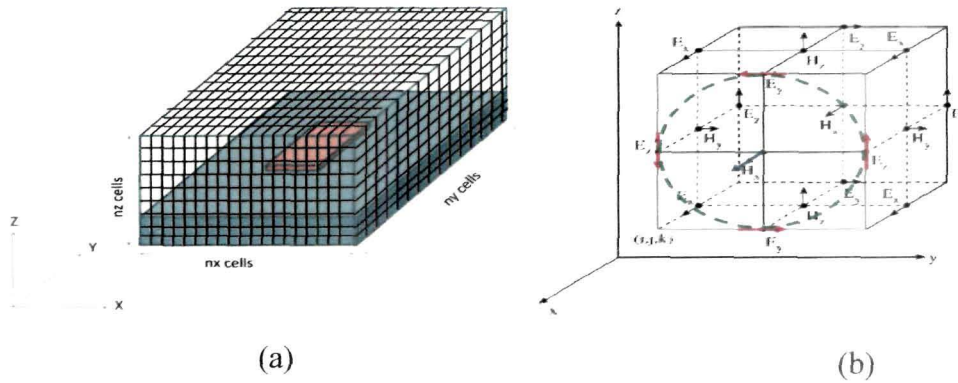
Figure 7.1   (a) Three dimensional griding in FDTD (b) Basic Yee cell in three dimensions

The general form of Maxwell's equation for the dielectric media are given as [22],

$$\frac{\partial \underline{D}}{\partial t} = \nabla \times \underline{H} \tag{7.1 a}$$

$$\underline{D}(\omega) = \varepsilon_0 \varepsilon_r \underline{E}(\omega) \tag{7.1 b}$$

$$-\overline{\mu} \frac{\partial \underline{H}}{\partial t} = \nabla \times \underline{E} \tag{7.1 c}$$

Where, $\underline{E}$ is the electric field, $\underline{H}$ is the magnetic field, $\underline{B}$ is the magnetic flux density, ε_r relative electrical permittivity of substrate and ε_0 is the free space electrical permittivity. μ is the magnetic permeability and is expressed as $\mu = \mu_0 \mu_r$ where μ_0 is the free space magnetic permeability and μ_r is the relative magnetic permeability. The geometry considered is a planar homogeneous dielectric composite system taken in cartesian co-ordinate system. The origin of co-ordinate system is $(i, j, k) = (0, 0, 0)$. EM wave is fed at the 50 Ω impedance point calculated using TLM technique.

Adaptation of different patch geometries to achieve broad band operation of microstrip antenna on customized composite substrate in X-band

111

The 3D FDTD scheme for microstrip antenna on dielectric substrates can be realized in two modules:

a) Maxwell's curl equations are expressed in partial differential form

b) These scalar equations are expressed in finite differential form in spatial and temporal coordinates

The electric field and magnetic field gets updated, both at every space grid coordinates and time stepping.

7.2.1 Expression of E and H curl equations in partial differential form

The Maxwell's curl equations 7.1 (a) and (c) are quite similar. As μ_0 and ε_0 differ by several orders of magnitude, $\underline{E}$ and $\underline{H}$ also differ by several orders of magnitude. This is circumvented by normalizing the Maxwell's curl equations considering the following change of the variables as

$$E = \sqrt{\frac{\varepsilon_0}{\mu_0}} \underline{E} \qquad (7.2)$$

$$H = \sqrt{\frac{\varepsilon_0}{\mu_0}} \underline{H} \qquad (7.3)$$

All the $\underline{E}$ and $\underline{H}$ components of isotropic dielectric systems from the Maxwell's equations 7.1 (a) and 7.1 (c) can be expressed in scalar form as,

$$\frac{\partial D_x}{\partial t} = \frac{1}{\sqrt{\varepsilon_0 \mu_0}} \left(\frac{\partial H_z}{\partial y} - \frac{\partial H_y}{\partial z} \right) \qquad (7.4\ a)$$

$$\frac{\partial D_y}{\partial t} = \frac{1}{\sqrt{\varepsilon_0 \mu_0}} \left(\frac{\partial H_x}{\partial z} - \frac{\partial H_z}{\partial x} \right) \qquad (7.4\ b)$$

$$\frac{\partial D_z}{\partial t} = \frac{1}{\sqrt{\varepsilon_0 \mu_0}} \left(\frac{\partial H_y}{\partial x} - \frac{\partial H_x}{\partial y} \right) \qquad (7.4\ c)$$

$$\frac{\partial H_x}{\partial t} = \frac{-1}{\sqrt{\varepsilon_0 \mu_0}} \left(\frac{\partial E_z}{\partial y} - \frac{\partial E_y}{\partial z} \right) \qquad (7.5\ a)$$

$$\frac{\partial H_y}{\partial t} = \frac{-1}{\sqrt{\varepsilon_0 \mu_0}} \left(\frac{\partial E_x}{\partial z} - \frac{\partial E_z}{\partial x} \right) \qquad (7.5\ b)$$

Adaptation of different patch geometries to achieve broad band operation of microstrip antenna on customized composite substrate in X-band

112

$$\frac{\partial H_z}{\partial t} = \frac{-1}{\sqrt{\varepsilon_0 \mu_0}} \left(\frac{\partial E_y}{\partial x} - \frac{\partial E_x}{\partial y} \right)$$ (7.5 c)

7.2.2 Expression of E and H partial differential equations in finite differential form in spatial and temporal coordinates
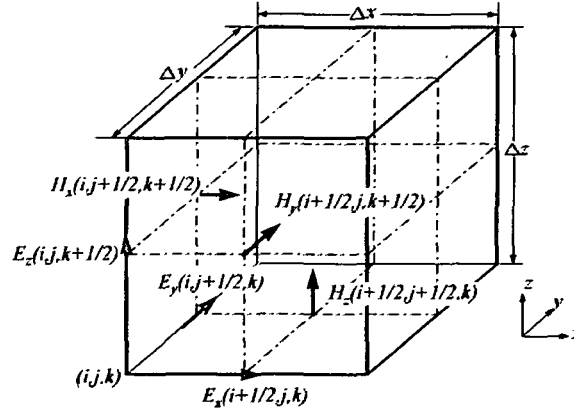
Figure 7.2 Yee's mesh

Finite difference approximation solution of the Maxwell's partial differential equations 7.4 (a-c) and 7.5 (a-c) are found by discretizing the problem space over a finite three dimensional computational domain in spatial and temporal coordinates in accordance to the Yee's mesh as shown in figure 7.2.

$$D_x^{n+\frac{1}{2}}\left(i+\frac{1}{2}, j, k\right) = D_x^{n-\frac{1}{2}}\left(i+\frac{1}{2}, j, k\right) + \frac{\Delta t}{\Delta y \cdot \sqrt{\varepsilon_0 \mu_0}}\left[H_z^n\left(i+\frac{1}{2}, j+\frac{1}{2}, k\right)\right.$$

$$\left. - H_z^n\left(i+\frac{1}{2}, j-\frac{1}{2}, k\right)\right] - \frac{\Delta t}{\Delta z \cdot \sqrt{\varepsilon_0 \mu_0}}\left[H_y^n\left(i+\frac{1}{2}, j, k+\frac{1}{2}\right) - H_y^n\left(i+\frac{1}{2}, j, k-\frac{1}{2}\right)\right]$$ (7.6 a)

$$D_y^{n+\frac{1}{2}}\left(i, j+\frac{1}{2}, k\right) = D_y^{n-\frac{1}{2}}\left(i, j+\frac{1}{2}, k\right) + \frac{\Delta t}{\Delta z \cdot \sqrt{\varepsilon_0 \mu_0}}\left[H_x^n\left(i, j+\frac{1}{2}, k+\frac{1}{2}\right) - H_x^n\left(i, j+\frac{1}{2}, k-\frac{1}{2}\right)\right]$$

$$- \frac{\Delta t}{\Delta x \cdot \sqrt{\varepsilon_0 \mu_0}}\left[H_z^n\left(i+\frac{1}{2}, j+\frac{1}{2}, k\right) - H_z^n\left(i-\frac{1}{2}, j+\frac{1}{2}, k\right)\right]$$ (7.6 b)

$$D_z^{n+\frac{1}{2}}\left(i, j, k+\frac{1}{2}\right) = D_z^{n-\frac{1}{2}}\left(i, j, k+\frac{1}{2}\right) + \frac{\Delta t}{\Delta x \cdot \sqrt{\varepsilon_0 \mu_0}}\left[H_y^n\left(i+\frac{1}{2}, j, k+\frac{1}{2}\right)\right.$$

$$\left. - H_y^n\left(i-\frac{1}{2}, j, k+\frac{1}{2}\right)\right] - \frac{\Delta t}{\Delta y \cdot \sqrt{\varepsilon_0 \mu_0}}\left[H_x^n\left(i, j+\frac{1}{2}, k+\frac{1}{2}\right) - H_x^n\left(i, j-\frac{1}{2}, k+\frac{1}{2}\right)\right]$$ (7.6 c)

Adaptation of different patch geometries to achieve broad band operation of microstrip antenna on customized composite substrate in X-band

113

The modified finite difference equations for the scalar equations 7.5 a through 7.5 c are,

$$H_x^{n+\frac{1}{2}}\left(i, j+\frac{1}{2}, k+\frac{1}{2}\right) = H_x^{n-\frac{1}{2}}\left(i, j+\frac{1}{2}, k+\frac{1}{2}\right) - \frac{\Delta t}{\Delta y \cdot \sqrt{\varepsilon_0 \mu_0}}\left[E_z^n\left(i, j+1, k+\frac{1}{2}\right)\right.$$

$$\left. - E_z^n\left(i, j, k+\frac{1}{2}\right)\right] + \frac{\Delta t}{\Delta z \cdot \sqrt{\varepsilon_0 \mu_0}}\left[E_y^n\left(i, j+\frac{1}{2}, k+1\right) - E_y^n\left(i, j+\frac{1}{2}, k\right)\right]$$

(7.7 a)

$$H_y^{n+\frac{1}{2}}\left(i+\frac{1}{2}, j, k+\frac{1}{2}\right) = H_y^{n-\frac{1}{2}}\left(i+\frac{1}{2}, j, k+\frac{1}{2}\right) - \frac{\Delta t}{\Delta z \cdot \sqrt{\varepsilon_0 \mu_0}}\left[E_x^n\left(i+\frac{1}{2}, j, k+1\right)\right.$$

$$\left. - E_x^n\left(i+\frac{1}{2}, j, k\right)\right] + \frac{\Delta t}{\Delta x \cdot \sqrt{\varepsilon_0 \mu_0}}\left[E_z^n\left(i+1, j, k+\frac{1}{2}\right) - E_z^n\left(i, j, k+\frac{1}{2}\right)\right]$$

(7.7 b)

$$H_z^{n+\frac{1}{2}}\left(i+\frac{1}{2}, j+\frac{1}{2}, k\right) = H_z^{n-\frac{1}{2}}\left(i+\frac{1}{2}, j+\frac{1}{2}, k\right) - \frac{\Delta t}{\Delta x \cdot \sqrt{\varepsilon_0 \mu_0}}\left[E_y^n\left(i+1, j+\frac{1}{2}, k\right)\right.$$

$$\left. - E_y^n\left(i, j+\frac{1}{2}, k\right)\right] + \frac{\Delta t}{\Delta y \cdot \sqrt{\varepsilon_0 \mu_0}}\left[E_x^n\left(i+\frac{1}{2}, j+1, k\right) - E_x^n\left(i+\frac{1}{2}, j, k\right)\right]$$

(7.7 c)

7.3 IMPLEMENTATION OF FDTD CODE

At first the computational domain is to be defined over which the FDTD will be implemented. Figure 7.3 shows the computational domain. The gridding of the 3D structure (figure 7.1 (a)) is carried out considering the stability conditions. The geometry of the concern structure is expressed in terms of material properties and the PML boundary conditions are initialized to define the actual computational domain. A Gaussian pulse is applied as the input stimulus at the feed point and at discreet time steps, the E and the H field components are updated in leap frog manner. The spatial field distribution can be visualized from the simulated E and H components in

Adaptation of different patch geometries to achieve broad band operation of microstrip antenna on customized composite substrate in X-band

114

three dimensions. To extract the scattering parameters, Fourier transformation

of the transient response is taken.
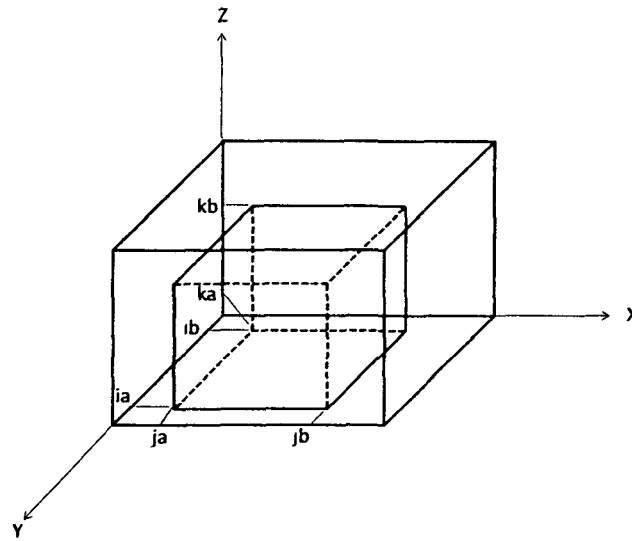
Figure 7.3 Three dimensional problem cell

Important numerical features of the 3D FDTD scheme implementation

are described in the following sub-sections:

7.3.1 Stability criteria in FDTD

In order to ensure that the central-difference algorithm is numerically

stable, there exists a maximum value for the time step and also space

discretization which can be used. An electromagnetic wave propagating in

free space cannot go faster than the speed of light. To propagate a distance of

one cell of dimension Δx, required a minimum time of $\Delta t = \Delta x / c_{max}$. Kunz

and Luebbers [2] recommend that to ensure stability, there should be at least

four cells per minimum wavelength. For good stability, some particularly

sensitive problems [1-12], up to twenty cells per wavelength is required at the

frequency of interest in order to get the required accuracy. Depending on the

cell size, the size of the time step, Δt, can be determined from the Courant's

stability criterion. For the three dimensional case, the Courant's stability

criterion is defined as [1-6]

Adaptation of different patch geometries to achieve broad band operation of microstrip antenna on customized
composite substrate in X-band

115

$$\Delta t \leq \frac{1}{c_{max}\sqrt{\dfrac{1}{\Delta x^2} + \dfrac{1}{\Delta y^2} + \dfrac{1}{\Delta z^2}}}$$ (7.8)

where, c_{max} is the maximum velocity of light within the computational volume. Typically, c_{max} is taken as the velocity of light in free space unless the entire volume is filled with dielectric. Δx, Δy and Δz are the Cartesian space increments which must be within an order or magnitude of each other. In n dimensional simulation, the maximum time step can be defined in simplified form as

$$\Delta t = \frac{\Delta x}{\sqrt{n} \cdot c_{max}}$$ (7.9)

7.3.2 Absorbing boundary conditions

The finite computational capacity of the computers puts a restriction in implementation of infinite FDTD mesh in all the three dimensions. Thus, effective absorbing boundary conditions (ABC) are to be used to truncate an infinite or unbound simulation region. A two dimensional boundary condition proposed by Berenger in 1994, called the perfectly matched layer (PML), enables the efficient absorption of outgoing radiation [17-21]. The work of Katz *et al* has demonstrated that the PML ABC is easily extensible to three dimensions [19]. Considering the issues such as problem definition, efficient memory utilization and execution speed, implementation of PML ABC has been demonstrated by Saario in his Ph. D. thesis [15].

The basic scheme of the PML is that if a wave is propagating in medium A and it impinges upon medium B, the amount of reflection is dictated by the intrinsic impedances of the two media, η_A and η_B (figure 7.4)

$$\Gamma = \frac{\eta_A - \eta_B}{\eta_A + \eta_B}$$ (7.10)

Where,

Adaptation of different patch geometries to achieve broad band operation of microstrip antenna on customized composite substrate in X-band

116

$$\eta = \sqrt{\frac{\mu}{\varepsilon}}$$ (7.11)

and are determined by the permittivity ε and permeability μ of the two media.
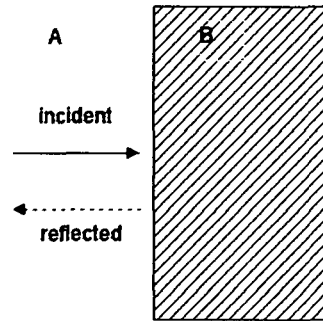
Figure 7.4 The reflection at the interface of two media

The propagating pulse in the absorbing medium covering the computational domain should die out before it reaches the external boundary. For this "fictitious" dielectric constant and permeability of the absorbing media is considered to be lossy and is added to the implementation codes. Thus, the flux density formulations of the Maxwell's curl equations with "fictitious" ε and μ are,

$$\varepsilon_F^* \frac{\partial \underline{E}}{\partial t} = \nabla \times \underline{H}$$ (7.12)

$$\underline{D}(\omega) = \varepsilon^*(\omega)\underline{E}(\omega)$$ (7.13)

$$\mu_F^* \frac{\partial \underline{H}}{\partial t} = -\nabla \times \underline{E}$$ (7.14)

There are two conditions to formulate a PML [20, 21]:

1. The impedance going from the background medium to the PML must be constant,

$$\eta_0 = \eta_m = \sqrt{\frac{\mu_{Fx}^*}{\varepsilon_{Fx}^*}} = 1$$ (7.15)

The impedance is one because of our normalized units (free space).

Adaptation of different patch geometries to achieve broad band operation of microstrip antenna on customized composite substrate in X-band

117

2. In the direction perpendicular to the boundary (the x direction, for instance), the relative dielectric constant and relative permeability must be the inverse of those in the other directions, i.e.,

$$\varepsilon^{*}_{rx} = \frac{1}{\varepsilon^{*}_{ry}}$$ (7.16 a)

$$\mu^{*}_{rx} = \frac{1}{\mu^{*}_{ry}}$$ (7.16 b)

The 3D PML ABC [23] is included in developing the algorithm for the absorbing boundary treatment and the detail formulation is given as Appendix-A.

7.3.3 Source considerations

The excitation can be of any shape, but, normally a Gaussian pulse is considered. This type of pulse has a frequency spectrum that is also Gaussian and thus provides frequency domain information from dc up to a desired cut-off frequency by adjusting the width of the pulse [22, 23]. In order to simulate a voltage source excitation, the pulse is fed as the vertical electric field, E_z, in a rectangular region underneath the patch. The form of the input signal in a continuous form is

$$E_z = f(t) = e^{\frac{-(T-T_0)^2}{T_1}}$$ (7.17)

where, T is the current time-step, T_0 the pulse delay time-step and T_1 the width of the pulse in time-steps. The width of the Gaussian pulse sets the required cut-off frequency. The pulse width is normally chosen to have at least 20 points per wavelength at the highest frequency significantly represented in the pulse. The numerical dispersion and truncation error is minimized. Initially, in the simulation, all the electric and magnetic fields are set to zero. The Gaussian pulse applied at the source has only a field component which is perpendicular to the ground plane (i.e, E_z). Thus, E_y and E_x, at the source, are always zero. A change in the electric field at the source w ith respect to time causes a change in the magnetic field in the x-direction.

Adaptation of different patch geometries to achieve broad band operation of microstrip antenna on customized composite substrate in X-band

118

7.3.4 Frequency dependent parameters

The final transient E field values, obtained after the FDTD simulation, are used to get wide band frequency response. The Fourier transform of the E field $E(t)$ at a frequency f_1 is done by the equation [3]

$$E(f_1) = \int_0^{t_T} E(t) \cdot e^{-j2\pi \cdot f_1 t} dt \qquad (7.18)$$

The lower limit of the integral in equation (7.18) is 0, because the FDTD program assumes all casual functions. The upper limit is t_T, the time at which the FDTD iteration is halted. Equation (7.18) can be rewritten in a finite difference form as

$$E(f_1) = \sum_{n=0}^{T} E(n \cdot \Delta t) \cdot e^{-j2\pi \cdot f_1 (n \cdot \Delta t)} \qquad (7.19)$$

Where T is the number of iterations and Δt is the time step and hence $t_T = T \cdot \Delta t$. Equation (7.19) is now divided into its real and imaginary parts as

$$E(f_1) = \sum_{n=0}^{T} E(n \cdot \Delta t) \cdot \cos(2\pi f_1 \cdot \Delta t \cdot n) - j \sum_{n=0}^{T} E(n \cdot \Delta t) \cdot \sin(2\pi f_1 \cdot \Delta t \cdot n) \qquad (7.20\text{ a})$$

$$\Rightarrow E(f_1) = \text{Re}(E) - \text{Im}(E) \qquad (7.20\text{ b})$$

7.4 IMPLEMENTATION IN COMPUTER PROGRAM

The existing finite difference approximation equations for simple rectangular microstrip antenna are modified for single layer and graded composite dielectric substrate materials. Performance of microstrip antenna is analysed by S_{11} parameter. In the formulation the antenna S_{11} parameter and internal field distribution are focused rather than the radiation pattern. The microstrip antenna is modelled with a small surrounding area. As S_{11} parameter depends on the geometry of the antenna, so it is crucial to model

Adaptation of different patch geometries to achieve broad band operation of microstrip antenna on customized composite substrate in X-band

119

the antenna with minimum possible dimensional error. Thus, different cell dimensions in different directions are used [3, 24, 25].

Table 7.1 Cell size in different directions for microstrip antennas on single layer and graded substrate

Substrate	dimension of the patch (w x l) (mm)	Δx (mm)	Δy (mm)	Δz (mm)	Δt (picosec.)
2 % VF of titania in LDPE	11.4×8.3	0.259	0.285	0.25	0.41
Graded Substrate	11.2×8.1	0.253	0.28	0.25	0.41

In case of graded substrates five material layers are to be considered; free space, three composite material layers and the metal as shown in figure 7.5.
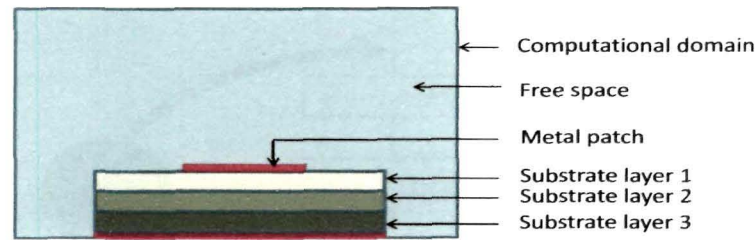
Figure 7.5 FDTD computational domain showing different material zones

The materials are defined in the FDTD code with their relative permittivity. From equation 7.1 (a), the electric field in the media is given by expressions,

$$E_x[i, j.k] = gax[i, j, k] * D_x[i, j, k] \qquad (7.21\ a)$$

$$E_y[i, j.k] = gay[i, j, k] * D_y[i, j, k] \qquad (7.21\ b)$$

$$E_z[i, j.k] = gaz[i, j, k] * D_z[i, j, k] \qquad (7.21\ c)$$

Where,

$$gax[i, j, k] = 1/\varepsilon_r \qquad (7.22\ a)$$

Adaptation of different patch geometries to achieve broad band operation of microstrip antenna on customized composite substrate in X-band

120

$$gay[i,j,k] = 1/\varepsilon_r \qquad\qquad (7.22\,b)$$

$$gaz[i,j,k] = 1/\varepsilon_r \qquad\qquad (7.22\,c)$$

where, ε_r is the relative permittivity of the media. The metal can be modelled by considering *gax, gay* and *gaz* to be zero at those points constituting the patch and the ground plane.

The complete flowchart for FDTD algorithm is shown in figure 7.6, highlighting the electric field and magnetic field updating modules. A program in MATLAB is developed to implement this algorithm for study of microstrip antenna and E and H updating code modules are listed in Appendix B. Other considerations in the algorithm for implementation in the code are summarised in the following sub-sections.
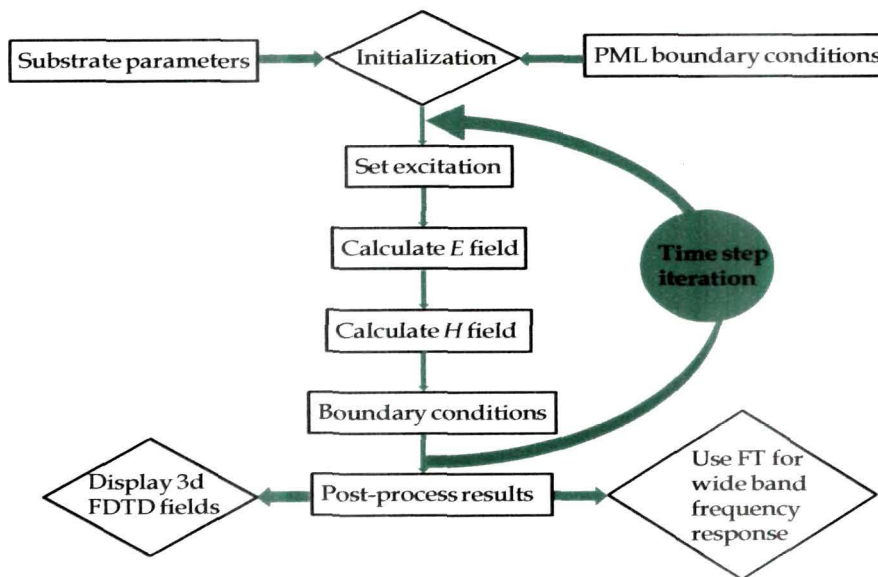
Figure 7.6   Main modules of 3D FDTD simulation algorithm

7.4.1 Stability criteria

The microstrip patch geometry, fabricated on different composite substrates has different patch dimensions. The height of the substrate is fixed for all the designs. The Yee's mesh is generated for the geometry by dividing

Adaptation of different patch geometries to achieve broad band operation of microstrip antenna on customized composite substrate in X-band

121

the geometry into grid of different dimensions in different directions in the computational domain. The computational volume is only partially filled with the composite dielectric material, hence the maximum velocity, c_{max}, is taken as the velocity of light in free space. In choosing the time step, the smallest grid dimension (Δx, Δy or Δz) is used in the Courant stability criterion, given by equation 7.8. Table 7.1 gives the time steps for different element sizes modelled.

7.4.2 Source consideration

The width of the Gaussian pulse for the specified cut-off frequency is determined from the equation 7.17. The pulse delay, T_0, is set at 50 time steps. The width of the pulse, T_1, is set as 20 time-step in order to achieve larger bandwidth. This pulse width of 20 time step and $\Delta t = 0.031$ picoseconds, gives a 15 GHz bandwidth. The Gaussian pulse has optimum pulse-width and desired cut-off frequency and is used as excitation from port 1.

7.4.3 PML terminating condition
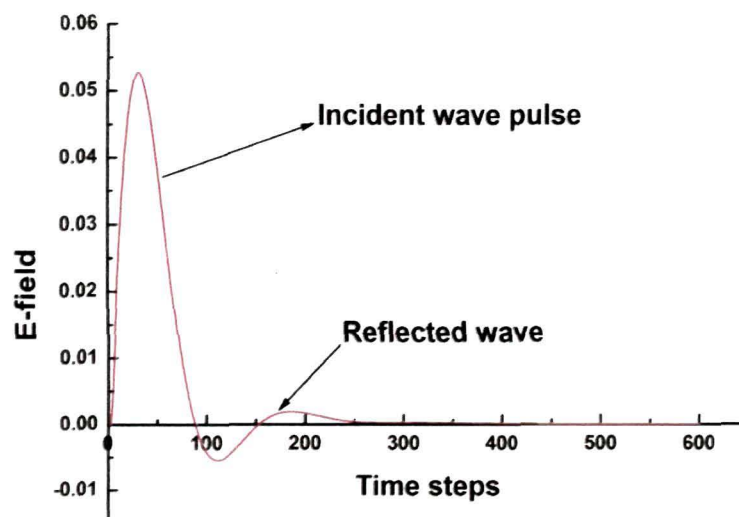
Figure 7.7   Gaussian pulses applied at the input feed point

Adaptation of different patch geometries to achieve broad band operation of microstrip antenna on customized composite substrate in X-band

122

The PML ABC is employed in the current program. Figure 7.7 illustrates the effectiveness of a 15 point PML with the source offset of one cell from the centre in the x, y and z directions. The outgoing pulse gets partially reflected when the pulse gets within fifteen points of the edge, which is inside the PML, where the distortion starts to occur.

7.4.4 Post processing of the results

After completion of the simulation process, the full wave distribution of the *E* and *H* wave is viewed in all the planes of interest.

To calculate the S_{11} we need the information at a single point (for microstrip antenna it is at the feed point). After the simulation is over, the frequency response is calculated over the entire range of frequencies using Fourier transform. S_{11} parameter is calculated by gathering the voltage information at the point of interest. When the voltage is known, the values of E_z field at the ground plane and the point of interest can be found. For first 350 time steps, the field values at the point are considered as input and the rest is considered as the reflected signal. The S_{11} in decibels is then expressed as,

$$S_{11}(f)_{dB} = 10.\log\frac{E_{out}(f)}{E_{in}(f)}$$ (7.23)

7.5 FULL-WAVE FDTD ANALYSIS OF RECTANGULAR MICROSTRIP ANTENNA ON SINGLE LAYER AND GRADED COMPOSITE SUBSTRATE

The FDTD full wave analysis is applied to microstrip antenna designed on LDPE/titania single layer and graded dielectric substrates. For implementation of FDTD simulation design parameters given in table 7.1 are used. The FDTD simulation implementation is realizes as following:

The FDTD simulation generates data which helps in visualizing the time progression of vector fields throughout the three-dimensional solution space. It gives a physical insight of complex field interactions at different

Adaptation of different patch geometries to achieve broad band operation of microstrip antenna on customized composite substrate in X-band

123

stages of field propagation. In the present analysis, snap shot of E and H field distribution in 3D space is taken at different time step.

The radiation response of the microstrip antenna is analyzed by finding the scattering parameters by taking Fourier transformation of the transient E field component.

The 3D algorithm applied for the microstrip antenna on substrate is given by the flow chart shown in figure 7.8.
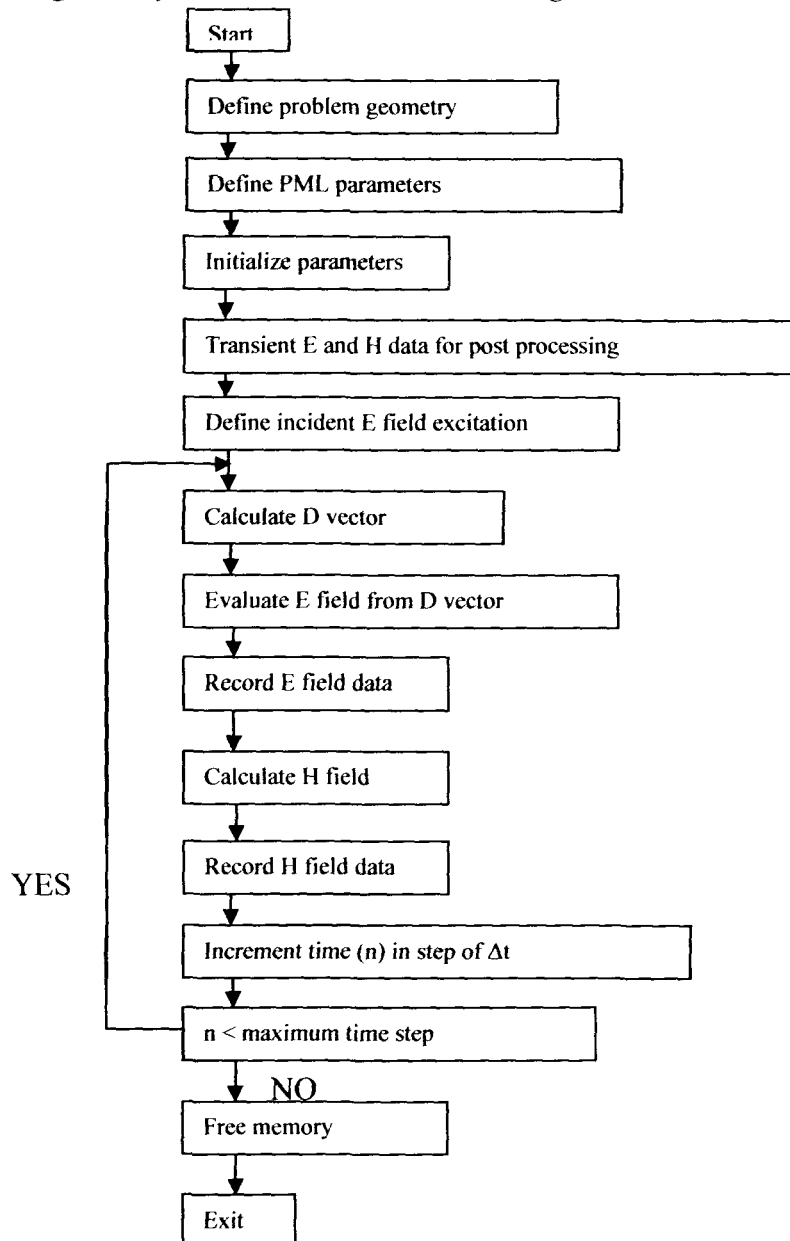
Figure 7.8   FDTD algorithm flow chart for microstrip antenna analysis

Adaptation of different patch geometries to achieve broad band operation of microstrip antenna on customized composite substrate in X-band

124

7.5.1 E_z field distribution within microstrip antenna substrate

Figures 7.9 to 7.17 gives the mode of propagation of E_z component of electric field in the plane perpendicular to the patch and parallel to the non radiating edges through the antenna geometry at different time steps.

Figure 7.9 The FDTD simulated electric field components within the substrate of microstrip antenna at 200 time steps (a) Single layer substrate (b) Graded substrate

Adaptation of different patch geometries to achieve broad band operation of microstrip antenna on customized composite substrate in X-band

125

Figure 7.10   The FDTD simulated electric field components within the substrate of microstrip antenna at 250 time steps (a) Single layer substrate (b) Graded substrate

Figure 7.11   The FDTD simulated electric field components within the substrate of microstrip antenna at 300 time steps (a) Single layer substrate (b) Graded substrate

Adaptation of different patch geometries to achieve broad band operation of microstrip antenna on customized composite substrate in X-band
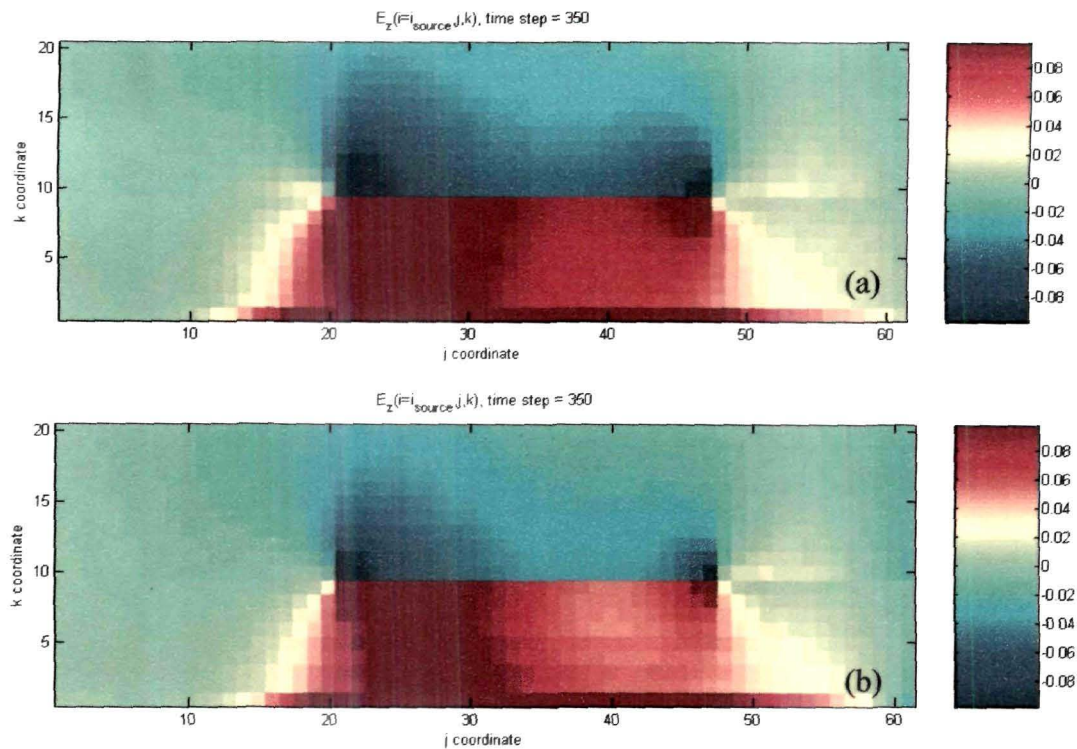
Figure 7.12   The FDTD simulated electric field components within the substrate of microstrip antenna at 350 time steps (a) Single layer substrate (b) Graded substrate
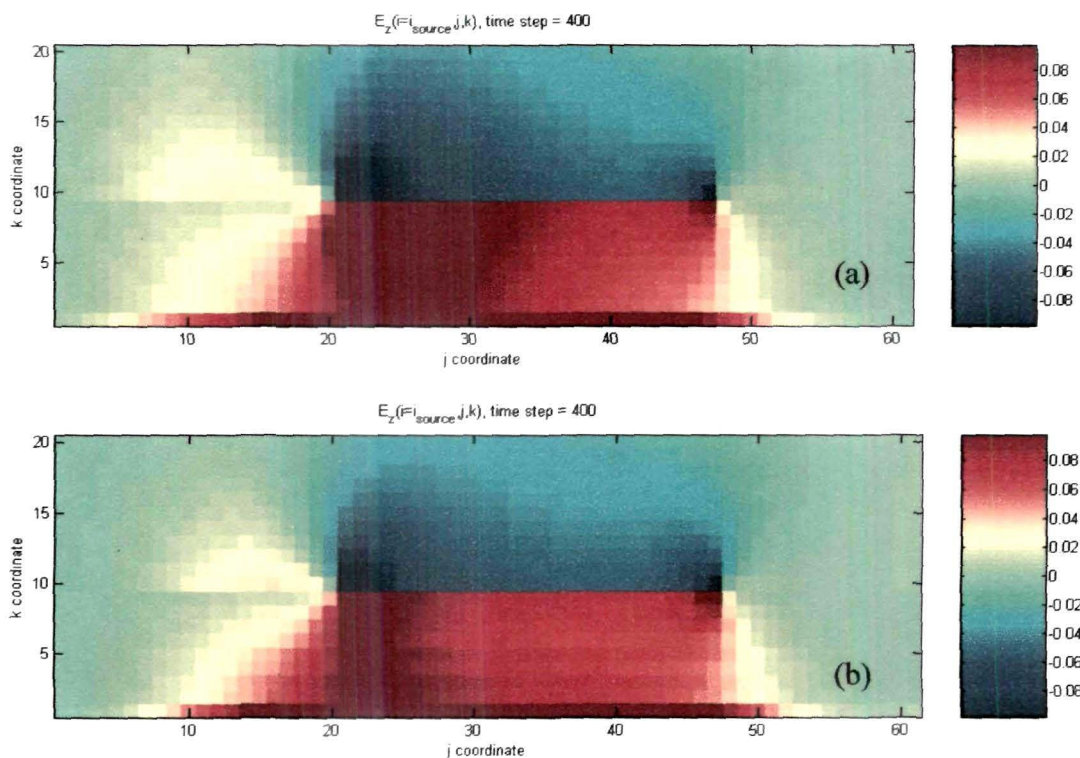
Figure 7.13   The FDTD simulated electric field components within the substrate of microstrip antenna at 400 time steps (a) Single layer substrate (b) Graded substrate

Adaptation of different patch geometries to achieve broad band operation of microstrip antenna on customized composite substrate in X-band
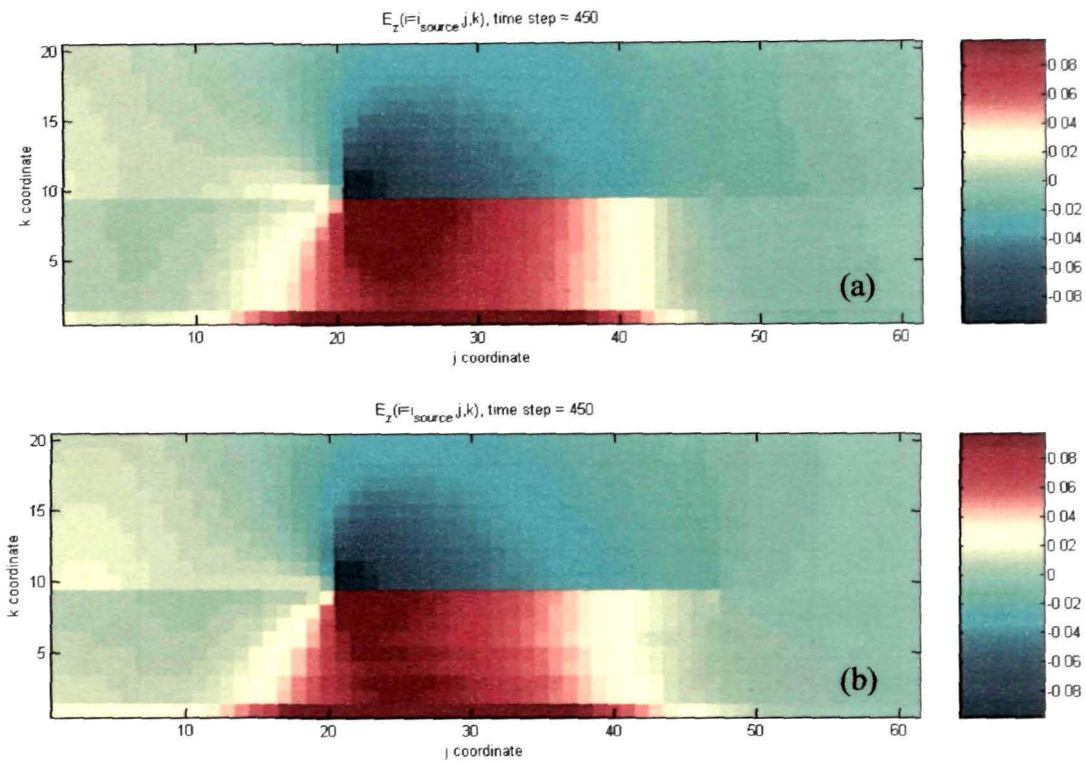
Figure 7.14   The FDTD simulated electric field components within the substrate of microstrip antenna at 450 time steps (a) Single layer substrate (b) Graded substrate
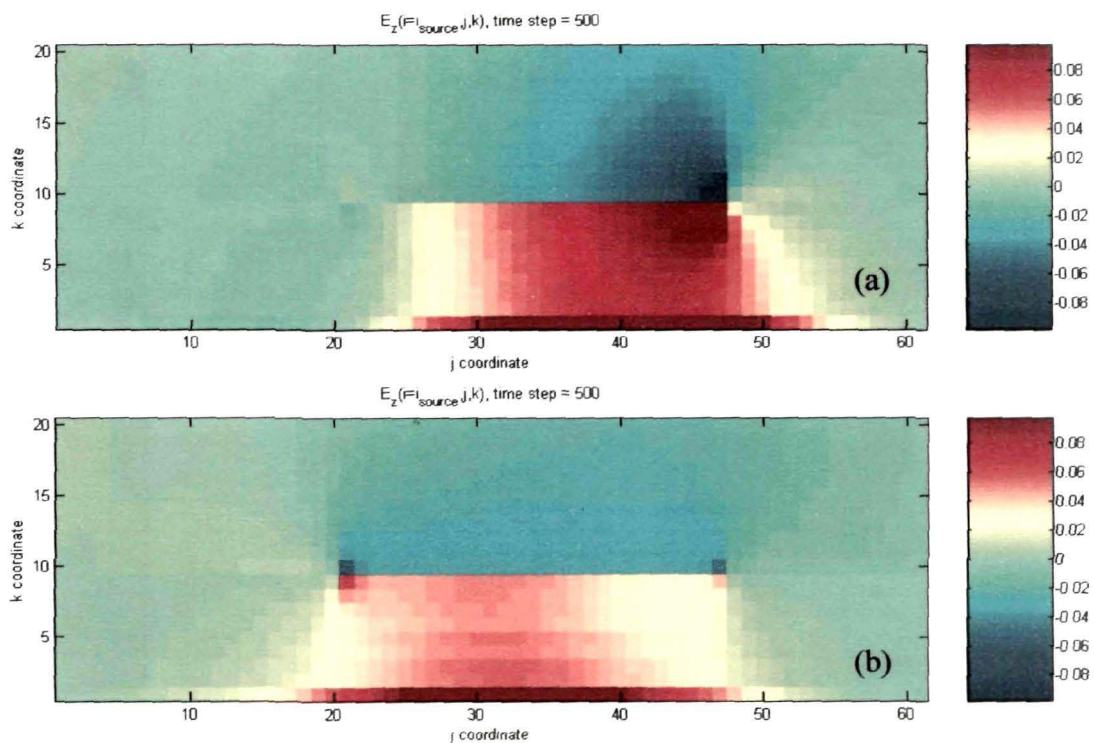
Figure 7.15   The FDTD simulated electric field components within the substrate of microstrip antenna at 500 time steps (a) Single layer substrate (b) Graded substrate

Adaptation of different patch geometries to achieve broad band operation of microstrip antenna on customized composite substrate in X-band
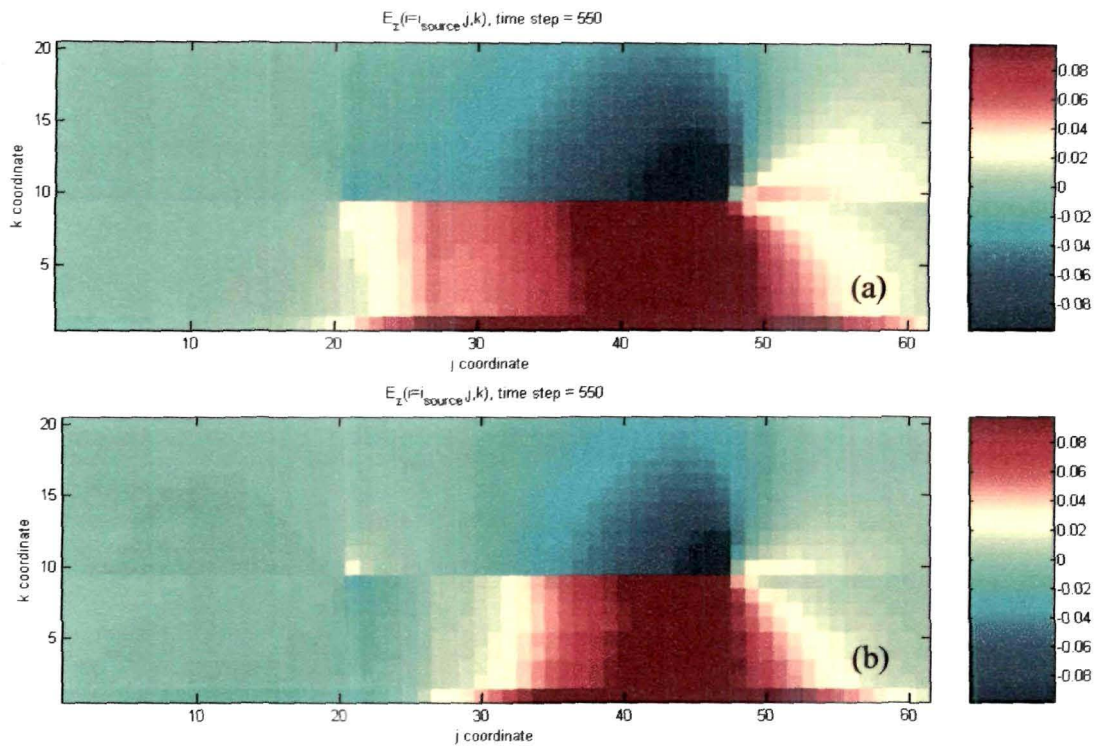
Figure 7.16 The FDTD simulated electric field components within the substrate of microstrip antenna at 550 time steps (a) Single layer substrate (b) Graded substrate
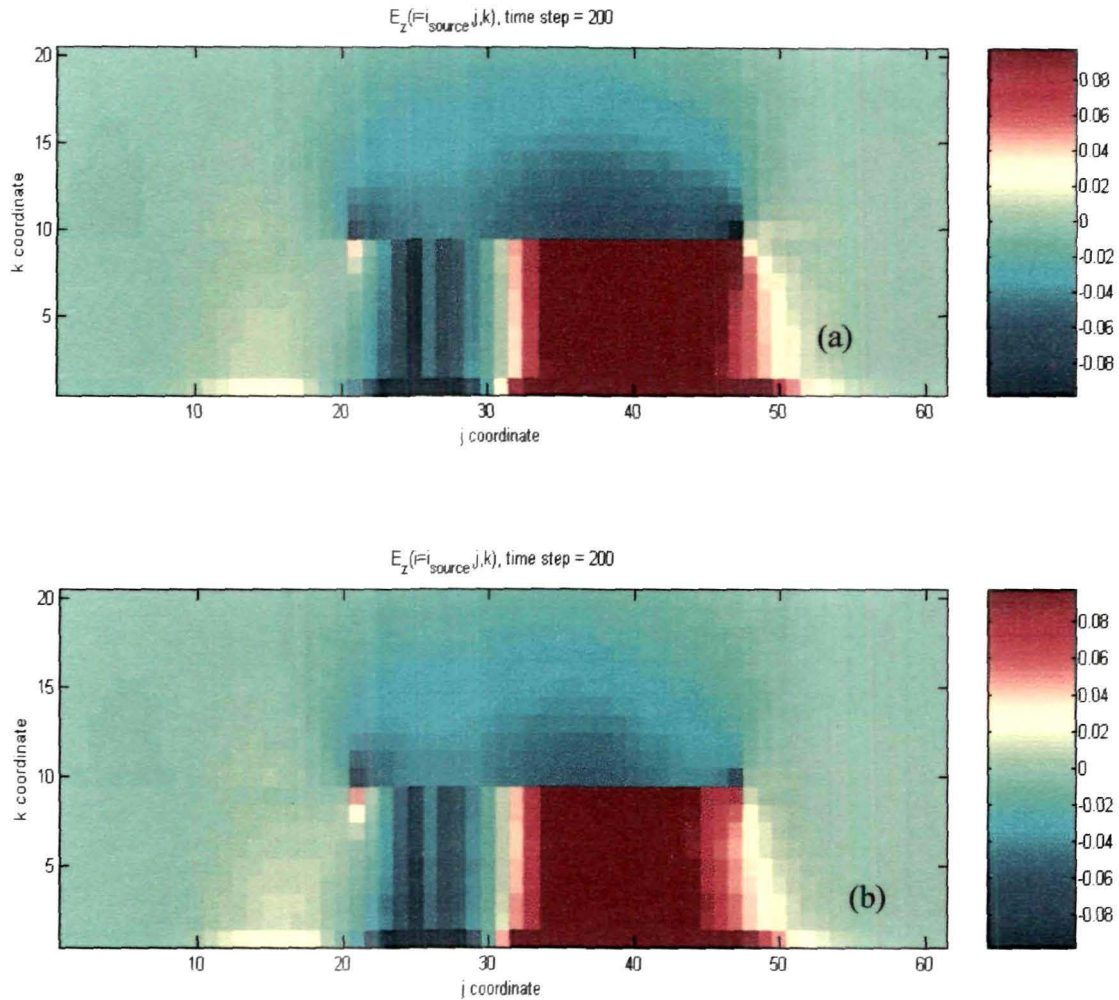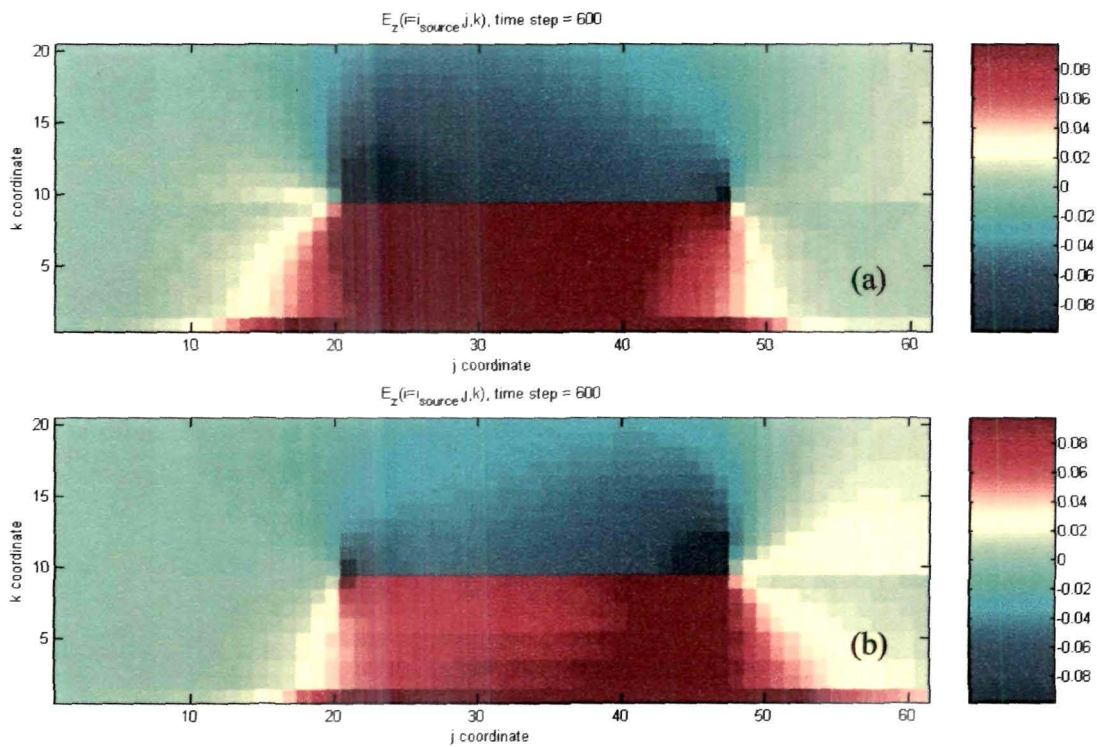

Figure 7.17 The FDTD simulated electric field components within the substrate of microstrip antenna at 600 time steps (a) Single layer substrate (b) Graded substrate
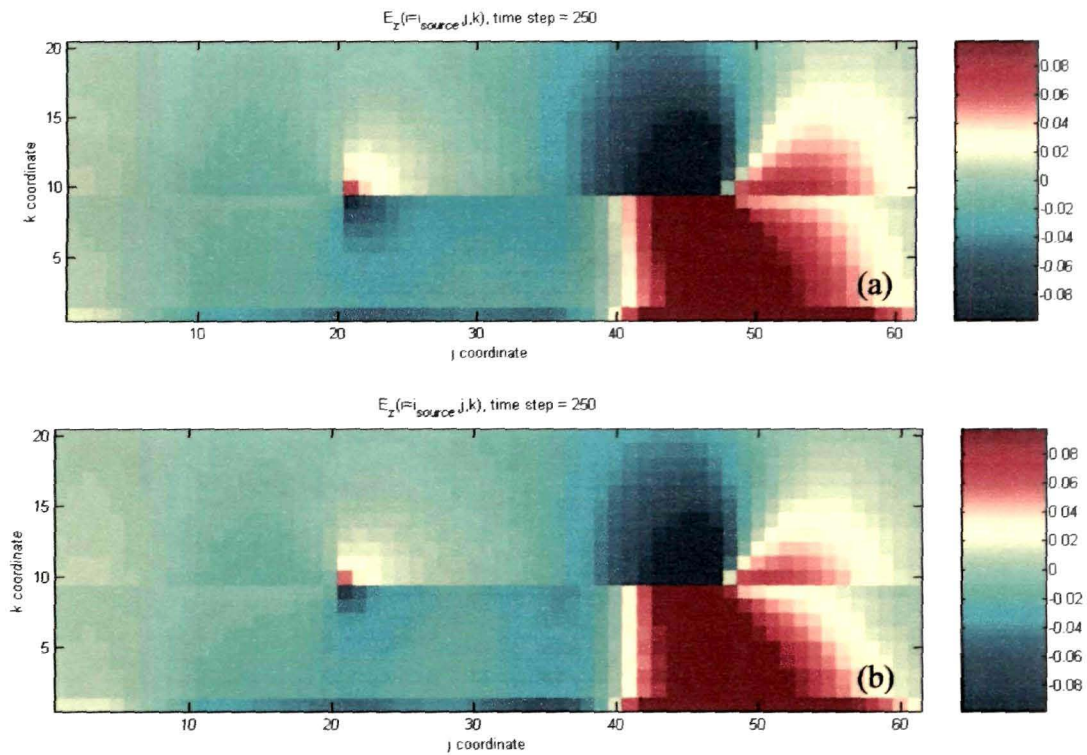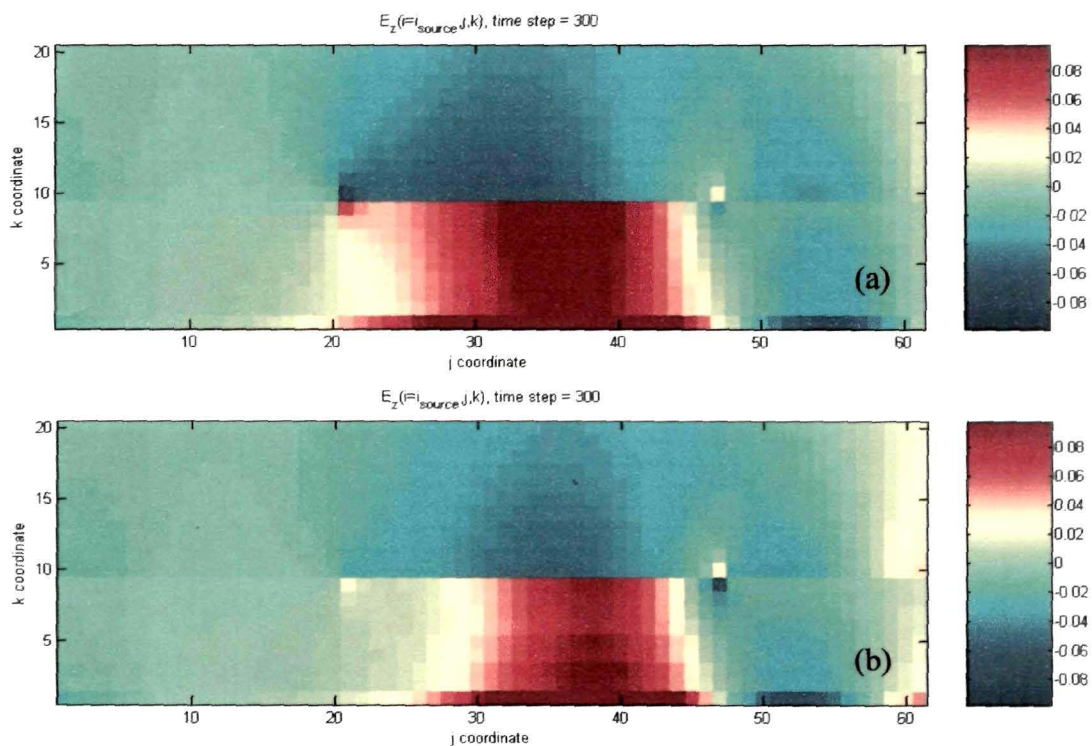
Adaptation of different patch geometries to achieve broad band operation of microstrip antenna on customized composite substrate in X-band

129

7.5.2 S₁₁ parameter analysis

S_{11} parameters of the antennas are calculated in the FDTD program using the equation 7.23. The S_{11} obtained for both the single layer substrate microstrip antenna and the graded substrate antenna are compared with the measured and simulated (using CST Microwave Studio) results and shown in figure 7.18-7.19.
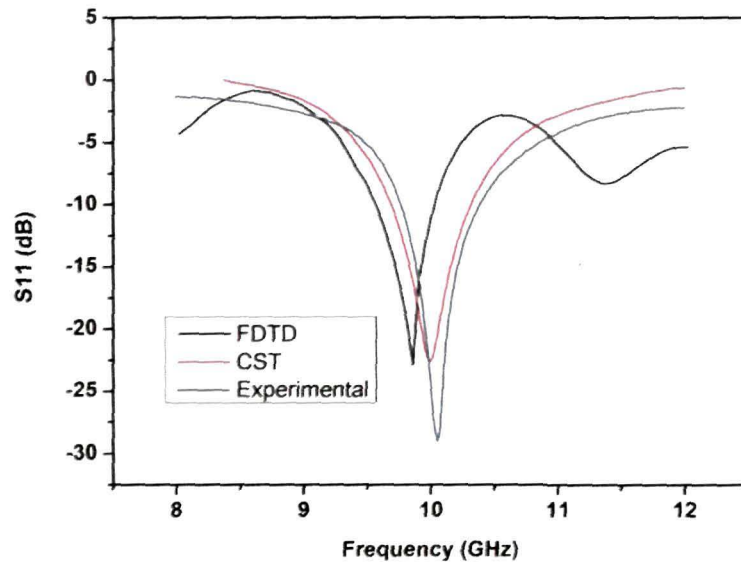
Figure 7.18 S_{11} parameter of rectangular patch antenna on 2 % VF of titania in LDPE composite substrate
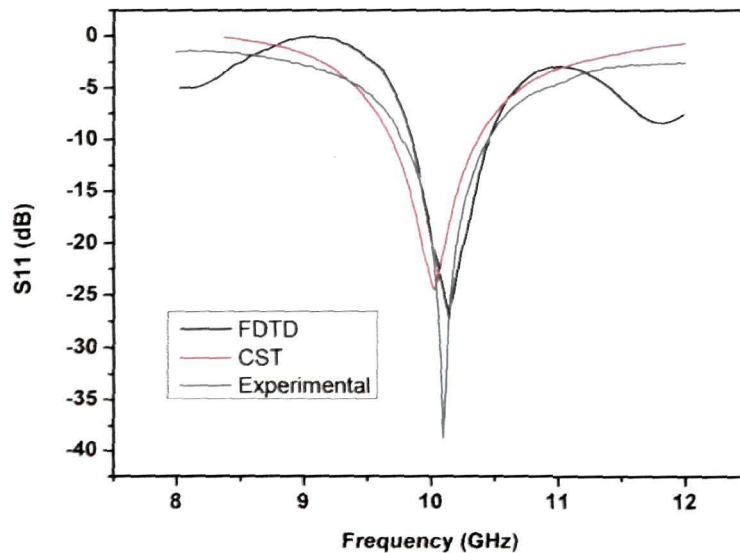
Figure 7.19 S_{11} parameter of rectangular patch antenna on graded composite substrate

Adaptation of different patch geometries to achieve broad band operation of microstrip antenna on customized composite substrate in X-band

130

The S_{11} results shows that the -10 dB bandwidth and the S_{11} at the resonating frequency are increasing in microstrip antenna on graded substrate in comparison to the single layer substrate.

7.6 CONCLUSION

The FDTD technique is implemented for analysis of microstrip antenna structure on graded substrate, having isotropic permittivity over the layer. This technique is successfully analyses the full-wave electric field distribution and return loss of microstrip antenna, fabricated on LDPE/titania dielectric composite substrate. The electric field pattern shows that due to change in permittivity at different sections of the graded substrate, the field distribution changes in comparison to the single layer counter part. This could be due to suppression of surface waves within the graded substrate leading to enhancement of the radiation phenomena and S_{11} parameter.

Adaptation of different patch geometries to achieve broad band operation of microstrip antenna on customized composite substrate in X-band

131

References

[1]   Taflove, A., *Computation Electrodynamics: The Finite-Difference Time-Domain Method.* (Boston, MA: Artech House, 1995).

[2]   Kunz K. S. and Luebbers, R. J., *The Finite Difference Time Domain Method for Electromagnetics,* (Boca Raton, FL, CRC Press, 1993).

[3]   Sullivan, D. M., *Electromagnetic Simulation Using the FDTD Method.* (N.Y.: IEEE Press, 2000).

[4]   Taflove, A. and Hagness, S. C., *Computation Electrodynamics: The Finite-Difference Time-Domain Method, 2ⁿᵈ Edition.* (Boston, MA: Artech House, 2000).

[5]   Yee, K. S., Numerical solution of initial boundary value problems involving Maxwell's equations in isotropic media, *IEEE Trans. Antennas Propagat.* **14**, 302-307(May 1966).

[6]   Taflove, A., Application of the finite-difference time-domain method to sinusoidal steady state electromagnetic penetration problems, *IEEE Transactions on Electromagnetic Compatibility,* **22(3)**, 191–202 (1980).

[7]   Taflove A. and Umashankar, K. R., Review of FD-TD numerical modeling of electromagnetic wave scattering and radar cross section, *Proc. IEEE,* **77**, 682-699(May 1989).

[8]   Gwarek, W. K., Analysis of arbitrarily shaped two-dimensional microwave circuits by finite-difference time-domain method, *IEEE Trans. Microwave Theory Tech.* **36**, 738- 744 (Apr. 1988).

[9]   Zhang X. and Mei, K. K., Time-domain finite difference approach to the calculation of the frequency-dependent characteristics of microstrip discontinuities, *IEEE Trans. Microwave Theory Tech.* **36**, 1775-1787(Dec. 1988).

[10]   Kashiwa T. and Fukai, I., A treatment by the FD-TD method of the dispersive characteristics associated with electronic polarization, *Microwave and Oprical Technol. Lett.* **3**, 203-205 (June 1990).

Adaptation of different patch geometries to achieve broad band operation of microstrip antenna on customized composite substrate in X-band

132

[11] Luebbers, R., Hunsherger, F. P., Kunz, K. S., Standler, R. B. and Schneider, M., A frequency-dependent finite-difference time-domain formulation for dispersive materials, *IEEE Trans. Electromngnetic Compat.* **32**, 222-227(Aug. 1990).

[12] Lee, C. F., Shin, R. T. and J. A. Kong, *Progress in Electromagnetic Research*, **4**, 373-442 (1991).

[13] Choi D. H. and Hoefer, W. J. R., The Finite-Difference Time-Domain method and its application to eigenvalue problems, *IEEE Trans. Microwave Theory Tech.* **34**, 1464 – 1470 (Dec. 1986).

[14] Dou, L. and Sebak, A. R., 3D FDTD method for arbitrary anisotropic materials, *Microwave and Optical Technology Letters*, **48(10)**, 2083-2090 (October 2006).

[15] Saario, S. A., FDTD modelling for wireless communications: antennas and materials, *Ph. D. Thesis*, (Griffith University, September 2002).

[16] Mur, G., Absorbing boundary conditions for the finite-difference approximation of the time domain electromagnetic field equations, *IEEE Trans. Electromagn. Compat.* **23**, 377-382 (1981).

[17] Berenger, J. P., A perfectly matched layer for the absorbtion of electromagnetic waves, *J. Comput. Phys.* **114**, 185-200 (1994).

[18] Berenger, J. P., Perfectly matched layer for the FDTD solution of wave-structure interaction problems, *IEEE Trans. Antennas Propagat.* **44**, 110-117 (1996).

[19] Katz, D. S., Thiele, E. T. and Taflove, A., Validation and extension to three dimensions of the berenger PML absorbing boundary condition for FD-TD meshes, *IEEE Microwave Guided Wave Lett.* **4**, 268-270 (1994).

[20] Sullivan, D. M., A simplified PML for use with the FDTD method, *IEEE Microwave and Guided Wave Letters*, **6**, 97-99 (1996).

Adaptation of different patch geometries to achieve broad band operation of microstrip antenna on customized composite substrate in X-band

133

[21] Sacks, Z. S., Kingsland, D. M., Lee, R. and Lee, J. F., A perfectly matched anisotropic absorber for use as an absorbing boundary condition, *IEEE Trans. Anten. and Prop.* **43**, 1460-1463 (Dec. 1995).

[22] Sheen, D., Ali, S., Abouzahra, M. and Kong, J., Application of three-dimensional finite- difference method to the analysis of planar microstrip circuits, *IEEE MTT*, **38**, 849–857 (Jul. 1990).

[23] Buchanan, W. J., Analysis of electromagnetic wave propagation using the 3D Finite-Difference Time-Domain method with parallel processing, *Ph. D. Thesis, Napier University*, (March 1996).

[24] Kragalott, M., Kluskens, M.S. and Pala, W.P., Time-domain Fields Exterior to a Two Dimensional FDTD Space, *IEEE Trans. On Antennas and Propagation*, **AP-45**, 1655-1663, (1997).

[25] Zhao, A.P., Juntunen, J. and Rasisanen, A.V., An Efficient FDTD Algorithm for the analysis of Microstrip Patch Antennas Printed on a General Anisotropic Dielectric Substrate, *IEEE Trans. Microwave Theory Tech.*, **MTT-47**, 1142-1146, (1999).

Adaptation of different patch geometries to achieve broad band operation of microstrip antenna on customized composite substrate in X-band

134

CHAPTER VIII

ACHIEVEMENTS, LIMITATIONS AND FUTURE DIRECTIONS

The present work is carried out with an objective to develop light weight, compact, patch antennas for broadband applications in X-band to be used in handheld devices and airborne vehicles. Instead of conventional commercially available substrates, which do not allow flexibility of tailoring the properties, particulate polymer composite material with LDPE as matrix and alumina/titania as the inclusions is developed as substrate. Morphological studies of the composites show that the alumina and titania particles do not lose their crystalline properties within the matrix and they are homogenously distributed within the polymer matrix ensuring uniform microwave properties throughout the composite. The developed composites are tested for water absorbance, density, thermal dissipation and expansion and are found to be suitable for use in humid conditions and upto a temperature of 80 °C without performance degradation. The complex permittivity value measured using cavity perturbation technique and Nicolsson-Ross technique confirms suitability as microstrip antenna substrate, in the X-band. The results show that the real part of complex permittivity increase with increase in filler concentration in the composite. The imaginary part of complex permittivity is of the order of 10^{-3}.

The developed composite system is tested as substrates for microstrip antennas. The rectangular patch designs fabricated using transmission line model and CST Microwave Studio simulation for optimization of dimensions, on the composite substrates of 2 mm thickness at 10 GHz shows S_{11} of $-$ 25 dB for 2 %VF LDPE/alumina composite and -30dB for 2% VF LDPE/titania composite respectively. The antennas on both the composites have -10 dB operating bandwidth of about 5.5 %, which is comparable to the rectangular patch antennas designed on other conventional substrates of same thickness. The radiation pattern studies reveal that the antenna on LDPE/alumina substrate has a directivity of 5.91 dBi and the antenna on LDPE/titania substrate has a value of 6.29 dBi.

Adaptation of Different Patch Geometries to Achieve Broadband Operation of Microstrip Antennas on Customized Substrate in X-band

135

Further enhancement in bandwidth is obtained by grading the substrate. LDPE/titania composite is used to develop a three layer graded substrate with the top layer being 2 % VF of titania in LDPE of 1 mm thickness, middle layer is of 3 % VF of titania in LDPE composite of 0.5 mm thickness and the bottom layer is 0.5 mm thick which is formed of 4 % VF of titania in LDPE. The -10 dB operational bandwidth of rectangular patch designed at 10 GHz on the graded structure is 6.73 %, which is more than the operational bandwidth of rectangular patch antennas fabricated on single layer substrates of 2 mm thickness. The directivity of the antenna on graded substrate (9.91 dBi) is also more than the antenna on single layer substrate.

A transverse line terminated E-shaped patch is designed to enhance the bandwidth of operation of microstrip antenna on graded substrate. The special patch design is a combination of simple E-shaped design and a T-shaped stub patch design. The dimension of each arm of E- and terminating stub is optimized using simulation. A -10dB bandwidth enhancement of 15% over 9.1 % for simple E-patch is observed. The radiation pattern studies show that the pattern is in general unaltered throughout the operational bandwidth.

A compact broadband circularly polarized antenna integrating two V-slotted semicircular patches capacitively coupled with a simple rectangular patch is designed at 10 GHz. Simulation of the fabricated design, shows a -10 dB bandwidth of 9.4 % with directivity of 11.29dBi. The axial ratio is less than 2.5 dB throughout the operating bandwidth.

A ground plane modification is carried out to develop embedded antenna systems for such mounting on airborne systems. A substrate is grooved into a rectangular cavity ground structure for shielding of integrated RF circuits from electromagnetic interference. The rectangular patch antenna designed on the modified ground structure at 10 GHz shows a broad band performance with operational bandwidth of 13% as compared to 6.7 % for the

Adaptation of Different Patch Geometries to Achieve Broadband Operation of Microstrip Antennas on Customized Substrate in X-band

136

simple rectangular patch design on the same substrate. The design is shown more directivity as the sideways radiations are suppressed due to presence of the conducting walls on the sides of the substrate. A cross slot on the middle of the patch and three rectangular slots along the width of the patch are employed to further enhance the bandwidth of operation to around 18 % in two bands. The directivity of the design is ~12 dBi. Application of one superstrate patch on the slotted embedded patch structure enhances the operational bandwidth up to 25.11 % with radiation pattern remaining unaltered over the bands.

The FDTD technique is implemented for analysis of microstrip antenna structure on graded substrate, having isotropic permittivity over the layer. This technique successfully analyses the full-wave electric field distribution and return loss of microstrip antenna fabricated on LDPE/titania dielectric composite substrate. The electric field pattern shows that due to change in permittivity at different regionsof the graded substrate, the field distribution changes in comparison to the single layer counterpart. This could be due to suppression of surface waves within the graded substrate leading to enhancement of the radiation mechanism and S_{11} parameter.

The present work provides ample indication of the potential of using particulate composite as substrate for microstrip antenna. Further studies on composites as future substrate materials for fabricating flexible, compact and cost effective antennas. The designed modification in the patch, substrate and ground plane enhances the operational -10 dB bandwidth of the antenna. However a small shift in resonant frequency ~ ± 0.1GHz is observed in some cases. A system for post fabrication fine tuning like a shorting plate/pin or loading can be developed. This may also help in enhancement of operational bandwidth. The superstrate patch design in embedded structure is, however, marginally uplifted from the body of mounting system which may increase

Adaptation of Different Patch Geometries to Achieve Broadband Operation of Microstrip Antennas on
Customized Substrate in X-band

137

the aero dynamical friction. The superstrate material property will be further modified and the design optimized to develop the system in the same plane.

The 3D FDTD technique developed will be extended to other broad band structures studied in this work.

Adaptation of Different Patch Geometries to Achieve Broadband Operation of Microstrip Antennas on Customized Substrate in X-band

138

APPENDIX - A

THREE-DIMENSIONAL PERFECTLY MATCHED LAYER (PML) EQUATIONS

The Maxwell's equations for TM mode

$$\frac{\partial D_z}{\partial t} = \frac{1}{\sqrt{\varepsilon_0 \mu_0}} \left(\frac{\partial H_y}{\partial x} - \frac{\partial H_x}{\partial y} \right) \qquad \text{(A.1.a)}$$

$$D_z(\omega) = \varepsilon_r^*(\omega).E_z(\omega) \qquad \text{(A.1.b)}$$

$$\frac{\partial H_x}{\partial t} = -\frac{1}{\sqrt{\varepsilon_0 \mu_0}} \frac{\partial E_z}{\partial y} \qquad \text{(A.1.c)}$$

$$\frac{\partial H_y}{\partial t} = \frac{1}{\sqrt{\varepsilon_0 \mu_0}} \frac{\partial E_z}{\partial x} \qquad \text{(A.1.d)}$$

If a wave is propagating in medium A and it impinges upon medium B, the amount of reflection can be calculated by the intrinsic impedances of the two media as,

$$\Gamma = \frac{\eta_A - \eta_B}{\eta_A + \eta_B} \qquad \text{(A.2)}$$

Where,

$$\eta = \sqrt{\frac{\mu}{\varepsilon}} \qquad \text{(A.3)}$$

Now the two dimensional Maxwell's curl equations ((1.a) to (1.d), in Fourier domain are,

$$j\omega D_z = c_0 \left(\frac{\partial H_y}{\partial x} - \frac{\partial H_x}{\partial y} \right) \qquad \text{(A.4.a)}$$

$$D_z(\omega) = \varepsilon_r^*(\omega).E_z(\omega) \qquad \text{(A.4.b)}$$

$$j\omega H_x = -c_0 \frac{\partial E_z}{\partial y} \qquad \text{(A.4.c)}$$

$$j\omega H_y = c_0 \frac{\partial E_z}{\partial x} \qquad \text{(A.4.d)}$$

The permittivity ε and permeability μ is replaced by fictitious dielectric constant and permeability. Thus,

$$j\omega D_z . \varepsilon^*_{Fz}(x).\varepsilon^*_{Fz}(y) = c_0 \left(\frac{\partial H_y}{\partial x} - \frac{\partial H_x}{\partial y} \right)$$

(A.5.a)

$$D_z(\omega) = \varepsilon^*_r(\omega).E_z(\omega)$$

(A.5.b)

$$j\omega H_x . \mu^*_{Fx}(x).\mu^*_{Fx}(y) = -c_0 \frac{\partial E_z}{\partial y}$$

(A.5.c)

$$j\omega H_y . \mu^*_{Fy}(x).\mu^*_{Fy}(y) = c_0 \frac{\partial E_z}{\partial x}$$

(A.5.d)

The two conditions to form PML:

A. The impedance going from the background medium to the PML must be constant,

$$\eta_0 = \eta_m = \sqrt{\frac{\mu^*_{Fx}}{\varepsilon^*_{Fx}}} = 1$$

(A.6)

B. In the direction perpendicular to the boundary the ε^*_{Fx} and μ^*_{Fx} must be inverse of those in the other directions, i.e.

$$\varepsilon^*_{Fx} = \frac{1}{\varepsilon^*_{Fy}}$$

(A.7.a)

$$\mu^*_{Fx} = \frac{1}{\mu^*_{Fy}}$$

(A.7.b)

Now,

$$\varepsilon^*_{Fm} = \varepsilon_{Fm} + \frac{\sigma_{Dm}}{j\omega\varepsilon_0} \qquad for \qquad m = x \; or \; y$$

(*A.8.a*)

$$\mu^*_{Fm} = \mu_{Fm} + \frac{\sigma_{Hm}}{j\omega\mu_0} \qquad for \qquad m = x \; or \; y$$

(*A.8.b*)

The following selection of parameters satisfies equations (A.7.a) and (A.7.b)

$$\varepsilon_{Fm} = \mu_{Fm} = 1$$

(A.9.a)

$$\frac{\sigma_{Dm}}{\varepsilon_0} = \frac{\sigma_{Hm}}{\mu_0} = \frac{\sigma_D}{\varepsilon_0}$$

(A.9.b)

So, equation (A.6) becomes,

$$\eta_0 = \eta_m = \sqrt{\frac{\mu^*_{Fx}}{\varepsilon^*_{Fx}}} = \sqrt{\frac{1 + \sigma(x)/j\omega\varepsilon_0}{1 + \sigma(x)/j\omega\varepsilon_0}} = 1$$

Implementing a PML only in the X direction, equations ((A.5.a)-(A.5.d))

$$j\omega D_z . \varepsilon^*_{Fz}(x) = c_0 \left(\frac{\partial H_y}{\partial x} - \frac{\partial H_x}{\partial y} \right)$$

$$j\omega H_x . \mu^*_{Fx}(x) = -c_0 \frac{\partial E_z}{\partial y}$$

$$j\omega H_y . \mu^*_{Fy}(x) = c_0 \frac{\partial E_z}{\partial x}$$

And use the values of equations (A.9.a) and (A.9.b),

$$j\omega \left(1 + \frac{\sigma_D(x)}{j\omega\varepsilon_0} \right) D_z = c_0 \left(\frac{\partial H_y}{\partial x} - \frac{\partial H_x}{\partial y} \right) \tag{A.10.a}$$

$$j\omega \left(1 + \frac{\sigma_D(x)}{j\omega\varepsilon_0} \right)^{-1} H_x = -c_0 \frac{\partial E_z}{\partial y} \tag{A.10.b}$$

$$j\omega \left(1 + \frac{\sigma_D(x)}{j\omega\varepsilon_0} \right) H_y = c_0 \frac{\partial E_z}{\partial x} \tag{A.10.c}$$

Again to put into the FDTD formulation, following modifications are performed,

$$j\omega \left(1 + \frac{\sigma_D(x)}{j\omega\varepsilon_0} \right) D_z = j\omega D_z + \frac{\sigma_D(x)}{\varepsilon_0} D_z$$

$$\frac{\partial D_z}{\partial t} + \frac{\sigma_D(i)}{\varepsilon_0} D_z \cong \frac{D_z^{n+1/2}(i,j) - D_z^{n-1/2}(i,j)}{\Delta t} + \frac{\sigma_D(i)}{\varepsilon_0} \frac{D_z^{n+1/2}(i,j) + D_z^{n-1/2}(i,j)}{2}$$

$$= D_z^{n+1/2}(i,j) \frac{1}{\Delta t} \left[1 + \frac{\sigma_D(i).\Delta t}{2.\varepsilon_0} \right] - D_z^{n-1/2}(i,j) \frac{1}{\Delta t} \left[1 - \frac{\sigma_D(i).\Delta t}{2.\varepsilon_0} \right]$$

$$D_z^{n+1/2}(i,j) = gi3(i).D_z^{n-1/2}(i,j) +$$
$$gi2(i).0.5.\left[H_y^n(i+1/2,j) - H_y^n(i-1/2,j) - H_x^n(i,j+1/2) + H_x^n(i,j-1/2) \right]$$

$$\tag{A.11}$$

Using the Courant stability,

$$\frac{\Delta t}{\Delta x} c_0 = \frac{\Delta x/(2.c_0)}{\Delta x} c_0 = \frac{1}{2}$$

The parameters are defined as,

$$gi2(i) = \frac{1}{1 + \sigma_D(i).\Delta t /(2.\varepsilon_0)} \tag{A.12.a}$$

$$gi3(i) = \frac{1 - \sigma_D(i).\Delta t/(2.\varepsilon_0)}{1 + \sigma_D(i).\Delta t/(2.\varepsilon_0)}$$

(A.12.b)

An identical treatment to equation no (A.10.c) gives,

$$H_y^{n+1}(i+1/2,j) = fi3(i+1/2).H_y^n(i+1/2,j) + fi2(i+1/2).0.5\left[E_z^{n+1/2}(i+1,j) - E_z^{n+1/2}(i,j)\right]$$

(A.13)

where,

$$fi2(i+1/2) = \frac{1}{1 + \sigma_D(i+1/2).\Delta t/(2.\varepsilon_0)}$$

(A.14.a)

$$fi3(i+1/2) = \frac{1 - \sigma_D(i+1/2).\Delta t/(2.\varepsilon_0)}{1 + \sigma_D(i+1/2).\Delta t/(2.\varepsilon_0)}$$

(A.14.b)

Equation (A.10.b) require a somewhat different treatment as,

$$j\omega H_x = -c_0\left[\frac{\partial E_z}{\partial y} + \frac{\sigma_D(x)}{\varepsilon_0}\frac{1}{j\omega}\frac{\partial E_z}{\partial y}\right]$$

$$\frac{\partial E_z}{\partial y} \cong \frac{E_z^{n+1/2}(i,j+1) - E_z^{n+1/2}(i,j)}{\Delta x} = -\frac{curl\_e}{\Delta x}$$

$$\frac{H_x^{n+1}(i,j+1/2) - H_x^n(i,j+1/2)}{\Delta t} = -c_0\left[\frac{curl\_e}{\Delta x} - \frac{\sigma_D(x)}{\varepsilon_0}\Delta t\sum_{n=0}^{i}\frac{curl\_e}{\Delta x}\right]$$

$$H_x^{n+1}(i,j+1/2) = H_x^n(i,j+1/2) + \frac{c_0.\Delta t}{\Delta x}curl\_e + \frac{c_0.\Delta t}{\Delta x}\frac{\sigma_D(x).\Delta t}{\varepsilon_0}I_{Hx}^{n+1/2}(i,j+1/2)$$

$$= H_x^n(i,j+1/2) + \frac{c_0.\Delta t}{\Delta x}curl\_e + \frac{\sigma_D(x).\Delta t}{2\varepsilon_0}I_{Hx}^{n+1/2}(i,j+1/2)$$

Equation (A.10.b) is implemented as the following series,

$$curl\_e = \left[E_z^{n+1/2}(i,j) - E_z^{n+1/2}(i,j+1)\right]$$

(A.15.a)

$$I_{Hx}^{n+1/2}(i,j+1/2) = I_{Hx}^{n-1/2}(i,j+1/2) + curl\_e$$

(A.15.b)

$$H_x^{n+1}(i,j+1/2) = H_x^n(i,j+1/2) + 0.5.curl\_e + fi1(i).I_{Hx}^{n+1/2}(i,j+1/2)$$

(A.15.c)

With,

$$fi1(i) = \frac{\sigma(i).\Delta t}{2\varepsilon_0}$$

(A.16)

Instead of varying conductivities, we calculate an auxiliary parameter,

$$xn = \frac{\sigma.\Delta t}{2.\varepsilon_0}$$

Then,

$$xn(i) = .333 * \left(\frac{i}{length\_pml} \right)^3 \qquad\qquad i = 1,2,\ldots,length\_pml$$

(A.17)

$$fi1(i) = xn(i)$$

(A.18.a)

$$gi2(i) = \left(\frac{1}{1 + xn(i)} \right)$$

(A.18.b)

$$gi3(i) = \left(\frac{1 - xn(i)}{1 + xn(i)} \right)$$

(A.18.c)

Similarly considering y- direction,

$$j\omega \left(1 + \frac{\sigma_D(x)}{j\omega\varepsilon_0}\right)\left(1 + \frac{\sigma_D(y)}{j\omega\varepsilon_0}\right) D_z = c_0 \left(\frac{\partial H_y}{\partial x} - \frac{\partial H_x}{\partial y} \right)$$

(A.19.a)

$$j\omega \left(1 + \frac{\sigma_D(x)}{j\omega\varepsilon_0}\right)^{-1}\left(1 + \frac{\sigma_D(y)}{j\omega\varepsilon_0}\right) H_x = c_0 \left(-\frac{\partial E_z}{\partial y} \right)$$

(A.19.a)

$$j\omega \left(1 + \frac{\sigma_D(x)}{j\omega\varepsilon_0}\right)\left(1 + \frac{\sigma_D(y)}{j\omega\varepsilon_0}\right)^{-1} H_y = c_0 \left(\frac{\partial E_z}{\partial x} \right)$$

(A.19.c)

Equation (A.11) is replaced by the following,

$$D_z^{n+1/2}(i,j) = gi3(i).gj3(j).D_z^{n-1/2}(i,j)$$
$$+ gi2(i).gj2(j).(0.5)\left[H_y^n(i+1/2,j) - H_y^n(i-1/2,j) - H_x^n(i,j+1/2) + H_x^n(i,j-1/2)\right]$$

H_y will be implemented as,

$$curl\_e = \left[E_z^{n+1/2}(i+1,j) - E_z^{n+1/2}(i,j)\right]$$

(A.20.a)

$$I_{Hy}^{n+1/2}(i+1/2,j) = I_{Hy}^{n-1/2}(i+1/2,j) + curl\_e$$

(A.20.b)

$$H_y^{n+1}(i+1/2,j) = fi3(i+1/2).H_y^n(i+1/2,j)$$
$$- fi2(i+1/2).(0.5).curl\_e + fj1(j).I_{Hy}^{n+1/2}(i+1/2,j)$$

(A.20.c)

Finally, H_x in the X direction becomes,

$$curl\_e = \left[E_z^{n+1/2}(i,j) - E_z^{n+1/2}(i,j+1)\right]$$

(A.21.a)

$$I_{Hx}^{n+1/2}(i,j+1/2) = I_{Hx}^{n-1/2}(i,j+1/2) + curl\_e$$

(A.21.b)

$$H_x^{n+1}(i,j+1/2) = \textit{fj}3(j+1/2).H_x^{n}(i,j+1/2)$$
$$+ \textit{fj}2(j+1/2).(0.5).\textit{curl\_e} + \textit{fi}1(i).J_{Hx}^{n+1/2}(i,j+1/2)$$

(A.21.c)

In three dimensional problem,

$$j\omega\left(1+\frac{\sigma_x(x)}{j\omega\varepsilon_0}\right)\left(1+\frac{\sigma_y(y)}{j\omega\varepsilon_0}\right)\left(1+\frac{\sigma_z(z)}{j\omega\varepsilon_0}\right)^{-1}D_z = \left(\frac{\partial H_y}{\partial x}-\frac{\partial H_x}{\partial y}\right)$$

(A.22)

Rewriting equation (A.22),

$$j\omega\left(1+\frac{\sigma_x(x)}{j\omega\varepsilon_0}\right)\left(1+\frac{\sigma_y(y)}{j\omega\varepsilon_0}\right)D_z = c_0\left(1+\frac{\sigma_z(z)}{j\omega\varepsilon_0}\right)\left(\frac{\partial H_y}{\partial x}-\frac{\partial H_x}{\partial y}\right)$$

$$= c_0.\textit{curl\_h} + c_0.\frac{\sigma_z(z)}{\varepsilon_0}\frac{1}{j\omega}\textit{curl\_h}$$

(A.23)

where,

$$I_{Dz} = \frac{1}{j\omega}\textit{curl\_h}$$

Equation (A.23) becomes,

$$j\omega\left(1+\frac{\sigma_x(x)}{j\omega\varepsilon_0}\right)\left(1+\frac{\sigma_y(y)}{j\omega\varepsilon_0}\right)D_z = c_0\left(\textit{curl\_h}+\frac{\sigma_z(z)}{\varepsilon_0}I_{Dz}\right)$$

(A.24)

Equation (A.24) is implemented into FDTD as,

$$\textit{curl\_h} = \begin{bmatrix} H_y^n(i+1/2,j,k+1/2)-H_y^n(i-1/2,j,k+1/2) \\ -H_x^n(i,j+1/2,k+1/2)+H_x^n(i,j-1/2,k+1/2) \end{bmatrix}$$

(A.25.a)

$$I_{Dz}^n(i,j,k+1/2) = I_{Dz}^{n-1}(i,j,k+1/2) + \textit{curl\_h}$$

(A.25.b)

$$D_z^{n+1/2}(i,j,k+1/2) = gi3(i).gj3(j).D_z^{n-1/2}(i,j,k+1/2)$$
$$+ gi2(i).gj2(j).0.5.\left(\textit{curl\_h} + gk1(k).I_{Dz}^n(i,j,k+1/2)\right)$$

(A.25.c)

Appendix B

3D FDTD CODE MODULES FOR Dz, Ez AND Hz UPDATE FOR MICROSTRIP ANTENNA ON COMPOSITE DIELECTRIC SUBSTRATE

The variables used in the code are defined in chapter V. After initialization of variables and specifying the calculation domain, the D, E and H fields are updated using FDTD update equations. Here the codes for updating D_z, E_z and H_z fields are illustrated in the following sections,

B1. Code for updating D_z field

```
for i=2:IE
    for j=2:JE
        for k=ka+1:kb
            curl_h=(ra_x*(hy(i,j,k)-hy(i-1,j,k))-ra_y*(hx(i,j,k)-hx(i,j-1,k)));
            dz(i,j,k)=gi3(i)*gj3(j)*dz(i,j,k)+gi2(i)*gj2(j)*.5*(curl_h);
        end
    end
end


for i=2:IE
    for j=2:JE
        for k=kb+1:KE
            kzh=k-kb;
            curl_h=ra_x*(hy(i,j,k)-hy(i-1,j,k))-ra_y*(hx(i,j,k)-hx(i,j-1,k));

            idzh(i,j,kzh)=idzh(i,j,kzh)+curl_h;

            dz(i,j,k)=gi3(i)*gj3(j)*dz(i,j,k)+gi2(i)*gj2(j)*.5*(curl_h+gk1(k)*idzh(i,j,kzh));
        end
    end
end
```

B2. E_z field calculation from D_z values

```
for i=1:IE
    for j=1:JE
        for k=1:KE
            ez(i,j,k)=gaz(i,j,k)*dz(i,j,k);
        end
    end
end
```

B3. Code for updating H$_z$ fields .

```
for i=1:IE-1
      for j=1:JE-1
        for k=1:kb
          curl_e=(ra_y*(ex(i,j+1,k)-ex(i,j,k))-ra_x*(ey(i+1,j,k)-ey(i,j,k)));
          hz(i,j,k)=fi3(i)*fj3(j)*hz(i,j,k)+fi2(i)*fj2(j)*.5*(curl_e);
        end
      end
end


    for i=1:IE-1
      for j=1:JE-1
        for k=kb+1:KE
          kzh=k-kb;

          curl_e=(ra_y*(ex(i,j+1,k)-ex(i,j,k))-ra_x*(ey(i+1,j,k)-ey(i,j,k)));
          ihzh(i,j,kzh)=ihzh(i,j,kzh)+curl_e;
          hz(i,j,k)=fi3(i)*fj3(j)*hz(i,j,k)+fi2(i)*fj2(j)*.5
                    *(curl_e+fk1(k)*ihzh(i,j,kzh));
        end
      end
    end
```

APPENDIX - C

3D FDTD CODE IN MATLAB

```
clc;
clear all;
close all;
data=[];
IE=72;
JE=120;
KE=25;
ia=15;
ja=15;
ka=5;

ic=IE/2;
ib=IE-ia;
jb=JE-ja;
kb=KE-5;
ktop=ka+10;
ipatch_st=ia+5;
ipatch_end=ipatch_st+31;
jpatch_end=jb-5;
jpatch_st=jpatch_end-39;
j_ref=jpatch_st+5;
k_ref=ktop-1;
jc=JE/2;

kc=KE/2;
ddz=0.265e-3;
dt=ddz/6e8;
ra_y=.6625;
ra_x=.6812;
epsz=8.8e-12;
muz=4*pi*1e-7;
X=1:IE;
Y=1:JE;

refl=0;

ex(1:IE,1:JE,1:KE)=0;
ey(1:IE,1:JE,1:KE)=0;
```

```
ez(1:IE,1:JE,1:KE)=0;
dx(1:IE,1:JE,1:KE)=0;
dy(1:IE,1:JE,1:KE)=0;
dz(1:IE,1:JE,1:KE)=0;
hx(1:IE,1:JE,1:KE)=0;
hy(1:IE,1:JE,1:KE)=0;
hz(1:IE,1:JE,1:KE)=0;
gax(1:IE,1:JE,1:KE)=1;
gay(1:IE,1:JE,1:KE)=1;
gaz(1:IE,1:JE,1:KE)=1;
idxl(1:IE,1:JE,1:KE)=0;
idxh(1:IE,1:JE,1:KE)=0;
idyl(1:IE,1:JE,1:KE)=0;
idyh(1:IE,1:JE,1:KE)=0;
idzl(1:IE,1:JE,1:KE)=0;
idzh(1:IE,1:JE,1:KE)=0;
ihxl(1:IE,1:JE,1:KE)=0;
ihxh(1:IE,1:JE,1:KE)=0;
ihyl(1:IE,1:JE,1:KE)=0;
ihyh(1:IE,1:JE,1:KE)=0;
ihzl(1:IE,1:JE,1:KE)=0;
ihzh(1:IE,1:JE,1:KE)=0;


gj3(1:JE)=1;
gj2(1:JE)=1;
gj1(1:JE)=0;
fj1(1:JE)=0;
fj2(1:JE)=1;
fj3(1:JE)=1;
ez_inc(1:JE)=0;
hx_inc(1:JE)=0;


gi1(1:IE)=0;
gi2(1:IE)=1;
gi3(1:IE)=1;
fi1(1:IE)=0;
fi2(1:IE)=1;
fi3(1:IE)=1;


gk1(1:KE)=0;
gk2(1:KE)=1;
```

```
gk3(1:KE)=1;
fk1(1:KE)=0;
fk2(1:KE)=1;
fk3(1:KE)=1;

RL=[];


%pml in i direction%%%%%%%%%%%%%%%%%%%%%%%%%

n_pml=15;
npml=n_pml;

i=1:n_pml;
 xxn=(npml-i+1)./npml;
 xn=0.33.*(xxn.^3);

 fi1(1:ia)=xn;
 i1(ib+1:IE)=fliplr(xn);
 gi2(1:ia)=1./(1 +xn);
 gi2(ib+1:IE)=fliplr(1./(1+xn));
 gi3(1:ia)=(1-xn)./(1+xn);
 gi3(ib+1:IE)=fliplr((1-xn)./(1+xn));
 xxn=(npml-i+0.5)./npml;
 xn=0.33*(xxn.^3);
 gi1(1:ia)=xn;
 gi1(ib+1:IE)=fliplr(xn);
 fi2(1:ia)=1./(1+xn);
 fi2(ib+1:IE)=fliplr(1./(1+xn));
 fi3(1:ia)=(1-xn)./(1+xn);
 fi3(ib+1:IE)=fliplr((1-xn)./(1+xn));

%% pml in j direction%%%%%%%%%%%%%%%%%%%%%%%%

n_pmlj=15;
npmlj=n_pmlj;
j=1:n_pmlj;
 xxn=(npmlj-j+1)./npmlj;
 xn=0.33.*(xxn.^3);

 fj1(1:ja)=xn;
 fj1(jb+1:JE)=fliplr(xn);
 gj2(1:ja)=1./(1 +xn);
 gj2(jb+1:JE)=fliplr(1./(1+xn));
 gj3(1:ja)=(1-xn)./(1+xn);
```

```
gj3(jb+1:JE)=fliplr((1-xn)./(1+xn));
xxn=(npmlj-j+0.5)./npmlj;
xn=0.33.*(xxn.^3);
gj1(1:ja)=xn;
gj1(jb+1:JE)=fliplr(xn);
fj2(1:ja)=1./(1+xn);
fj2(jb+1:JE)=fliplr(1./(1+xn));
fj3(1:ja)=(1-xn)./(1+xn);
fj3(jb+1:JE)=fliplr((1-xn)./(1+xn));


n_pmlk=5;
npmlk=n_pmlk;

%pml boundary condition in k direction %%%%%%%%%%%%%%%%%

k=1:n_pmlk;
  xxn=(npmlk-k+1)./npmlk;
  xn=0.33.*(xxn.^3);
  fk1(kb+1:KE)=fliplr(xn);
  gk2(kb+1:KE)=fliplr(1./(1 +xn));
  gk3(kb+1:KE)=fliplr((1-xn)./(1+xn));
  xxn=(npmlk-k+0.5)./npmlk;
  xn=0.33.*(xxn.^3);
  gk1(kb+1:KE)=fliplr(xn);
  fk2(kb+1:KE)=fliplr(1./(1+xn));
  fk3(kb+1:KE)=fliplr((1-xn)./(1+xn));


eps_sub1=2.27;
eps_sub2=2.29;
eps_sub3=2.31;

gax(1:IE,1:JE,ka+2:ka+3)=1./eps_sub3;
gay(1:IE,1:JE,ka+2:ka+3)=1./eps_sub3;
gaz(1:IE,1:JE,ka+2:ka+3)=1./eps_sub3;

gax(1:IE,1:JE,ka+4:ka+5)=1./eps_sub2;
gay(1:IE,1:JE,ka+4:ka+5)=1./eps_sub2;
gaz(1:IE,1:JE,ka+4:ka+5)=1./eps_sub2;

gax(1:IE,1:JE,ka+6:ka+9)=1./eps_sub1;
gay(1:IE,1:JE,ka+6:ka+9)=1./eps_sub1;
gaz(1:IE,1:JE,ka+6:ka+9)=1./eps_sub1;
```

```
a=(0.5/eps_sub3)+(0.5/eps_sub2)+(1/eps_sub1);
eps_sub=2/a;


%ground plane%%%%%%%%%%%%%%%%%%%%%%%%%%%%%%%%%%%

gax(1:IE,1:JE,ka+1)=0;
gay(1:IE,1:JE,ka+1)=0;


istart=ia+6;
iend=istart+6;
i_ref=istart+(iend-istart)./2;
half_wv=(iend-istart)./2;


shape(istart:iend,1:ktop-1)=1;

%%%%%%%%%%%add rectangular patch at ktop%%%%%%%%%%%%%

gax(ipatch_st:ipatch_end,jpatch_st:jpatch_end,ktop)=0;
gay(ipatch_st:ipatch_end,jpatch_st:jpatch_end,ktop)=0;

%%%%%%%%%%%%%%%specify the source%%%%%%%%%%%%%%%

t0=150;
spread=25;
T=0;
nsteps=1;
r=0;
while nsteps>0
  nsteps =input('no. of steps');

  for n=1:nsteps
    T=T+1;
    disp(T);

%%%%start of the main loop%%%%

%input buffer %%%%%%%%%%%%%%%%%%%%%%%%%%%%%%


ez_inc(2:JE)=gj3(2:JE).*ez_inc(2:JE)+gj2(2:JE).*(.5.*ra_y./eps_sub).*(hx_inc(1:JE
-1)-hx_inc(2:JE));
```

```
        pulse=exp(-.5*((t0-T)/spread).^2);
        ez_inc(j_ref)=pulse;


%%%%%calculate the dx field%%%%%%
    for i=2:ia-1
        for j=2:JE
            for k=2:KE
                curl_h=ra_y*(hz(i,j,k)-hz(i,j-1,k))-hy(i,j,k)+hy(i,j,k-1);
                idxl(i,j,k)=idxl(i,j,k)+curl_h;

dx(i,j,k)=gj3(j)*gk3(k)*dx(i,j,k)+gj2(j)*gk2(k)*.5*(curl_h+gi1(i)*idxl(i,j,k));
            end
        end
    end


    for i=ia:ib
        for j=2:JE
            for k=2:KE
                curl_h=(ra_y*(hz(i,j,k)-hz(i,j-1,k))-hy(i,j,k)+hy(i,j,k-1));
                dx(i,j,k)=gj3(j)*gk3(k)*dx(i,j,k)+gj2(j)*gk2(k)*.5*(curl_h);
            end
        end
    end


    for i=ib+1:IE
        ixh=i-ib;
        for j=2:JE
            for k=2:KE
                curl_h=(ra_y*(hz(i,j,k)-hz(i,j-1,k))-hy(i,j,k)+hy(i,j,k-1));
                idxh(ixh,j,k)=idxh(ixh,j,k)+curl_h;

dx(i,j,k)=gj3(j)*gk3(k)*dx(i,j,k)+gj2(j)*gk2(k)*.5*(curl_h+gi1(i)*idxh(ixh,j,k));
            end
        end
    end


    %calculating dy%%%%%%%%%%%%%%%%%%%%%%%


    for i=2:IE
        for j=2:ja
            for k=2:KE
                curl_h=(hx(i,j,k)-hx(i,j,k-1))-ra_x*(hz(i,j,k)-hz(i-1,j,k));
                idyl(i,j,k)=idyl(i,j,k)+curl_h;

dy(i,j,k)=gi3(i)*gk3(k)*dy(i,j,k)+gi2(i)*gk2(k)*.5*(curl_h+gj1(j)*idyl(i,j,k));
```

```
            end
         end
      end

   for i=2:IE
      for j=ja:jb
         for k=2:KE
            curl_h=(hx(i,j,k)-hx(i,j,k-1))-ra_x*(hz(i,j,k)-hz(i-1,j,k));
            dy(i,j,k)=gi3(i)*gk3(k)*dy(i,j,k)+gi2(i)*gk2(k)*.5*curl_h;
         end
      end
   end

      %PML%%%%%%%%%%%%%%%%%%%%%%%%%
   for i=2:IE
      for j=jb+1:JE
         jyh=j-jb;
         for k=2:KE
            curl_h=hx(i,j,k)-hx(i,j,k-1)-ra_x*(hz(i,j,k)-hz(i-1,j,k));
            idyh(i,jyh,k)=idyh(i,jyh,k)+curl_h;

dy(i,j,k)=gi3(i)*gk3(k)*dy(i,j,k)+gi2(i)*gk2(k)*.5*(curl_h+gj1(j)*idyh(i,jyh,k));
         end
      end
   end


   for i=2:IE
      for j=2:JE
         for k=ka+1:kb
            curl_h=(ra_x*(hy(i,j,k)-hy(i-1,j,k))-ra_y*(hx(i,j,k)-hx(i,j-1,k)));
            dz(i,j,k)=gi3(i)*gj3(j)*dz(i,j,k)+gi2(i)*gj2(j)*.5*(curl_h);
         end
      end
   end

   for i=2:IE
      for j=2:JE
         for k=kb+1:KE
            kzh=k-kb;
            curl_h=ra_x*(hy(i,j,k)-hy(i-1,j,k))-ra_y*(hx(i,j,k)-hx(i,j-1,k));
            idzh(i,j,kzh)=idzh(i,j,kzh)+curl_h;

dz(i,j,k)=gi3(i)*gj3(j)*dz(i,j,k)+gi2(i)*gj2(j)*.5*(curl_h+gk1(k)*idzh(i,j,kzh));
         end
```

```
      end
end

%incident dz%%%%%%%%%%%%%%%%%%%%%%

for i=istart:iend
   for k=1:ktop-1
      dz(i,j_ref+1,k)=dz(i,j_ref+1,k)+(.5/eps_sub)*shape(i,k)*hx_inc(j_ref);
   end
end

%calculating e from d%%%%%%%%%%%%%%%

for i=1:IE
   for j=1:JE
      for k=1:KE
         ex(i,j,k)=gax(i,j,k)*dx(i,j,k);
         ey(i,j,k)=gay(i,j,k)*dy(i,j,k);
         ez(i,j,k)=gaz(i,j,k)*dz(i,j,k);
      end
   end
end

%calculating incident field%%%%%%%%%%%%%%%%%%%%%%%%%%
for j=1:JE-1
   hx_inc(j)=fj3(j)*hx_inc(j)+.5*fj2(j)*(ez_inc(j)-ez_inc(j+1));
end

%calculate the hx field%%%%%%%%%%%%%%%%%%%%%%%%

for i=1:ia-1
for j=1:JE-1
   for k=1:KE-1
      curl_e=(ey(i,j,k+1)-ey(i,j,k)-ra_y*(ez(i,j+1,k)-ez(i,j,k)));
      ihxl(i,j,k)=ihxl(i,j,k)+curl_e;
      hx(i,j,k)=fj3(j)*fk3(k)*hx(i,j,k)+fj2(j)*fk2(k)*.5*(curl_e +fi1(i)*ihxl(i,j,k));
   end
end
end

for i=ia:ib
for j=1:JE-1
   for k=1:KE-1
      curl_e=(ey(i,j,k+1)-ey(i,j,k)-ra_y*(ez(i,j+1,k)-ez(i,j,k)));
      hx(i,j,k)=fj3(j)*fk3(k)*hx(i,j,k)+fj2(j)*fk2(k)*.5*(curl_e);
```

```
      end
    end
  end

  for i=ib+1:IE-1
    ixh=i-ib;
  for j=1:JE-1
    for k=1:KE-1
      curl_e=(ey(i,j,k+1)-ey(i,j,k)-ra_y*(ez(i,j+1,k)-ez(i,j,k)));
      ihxh(ixh,j,k)=ihxh(ixh,j,k)+curl_e;

hx(i,j,k)=fj3(j)*fk3(k)*hx(i,j,k)+fj2(j)*fk2(k)*.5*(curl_e+fi1(i)*ihxh(ixh,j,k));
    end
  end
end

%incident hx%%%%%%%%%%%%%%%%%%%%%%%%%%%%%%%%%%

for i=istart:iend
  for k=1:ktop-1
    hx(i,j_ref-1,k)=hx(i,j_ref-1,k)+(.5/eps_sub)*shape(i,k)*ez_inc(j_ref);
  end
end

%calculating hy field%%%%%%%%%%%%%%%%%%%%%%%%

for i=1:IE-1
for j=1:ja-1
  for k=1:KE-1
    curl_e=(ra_x*(ez(i+1,j,k)-ez(i,j,k))-ex(i,j,k+1)+ex(i,j,k));
    ihyl(i,j,k)=ihyl(i,j,k)+curl_e;
    hy(i,j,k)=fi3(i)*fk3(k)*hy(i,j,k)+fi2(i)*fk2(k)*.5*(curl_e+fj1(j)*ihyl(i,j,k));
  end
 end
end

for i=1:IE-1
for j=ja:jb
  for k=1:KE-1
    curl_e=ra_x*(ez(i+1,j,k)-ez(i,j,k))-ex(i,j,k+1)+ex(i,j,k);
    hy(i,j,k)=fi3(i)*fk3(k)*hy(i,j,k)+fi2(i)*fk2(k)*.5*(curl_e);
  end
 end
end
```

```
for i=1:IE-1
    for j=jb+1:JE-1
        jyh=j-jb;
        for k=1:KE-1
            curl_e=ra_x*(ez(i+1,j,k)-ez(i,j,k))-ex(i,j,k+1)+ex(i,j,k);
            ihyh(i,jyh,k)=ihyh(i,jyh,k)+curl_e;
            hy(i,j,k)=fi3(i)*fk3(k)*hy(i,j,k)+fi2(i)*fk2(k)*.5*(curl_e +
fj1(j)*ihyh(i,jyh,k));
        end
    end
end

for i=1:IE-1
    for j=1:JE-1
        for k=1:kb
            curl_e=(ra_y*(ex(i,j+1,k)-ex(i,j,k))-ra_x*(ey(i+1,j,k)-ey(i,j,k)));
            hz(i,j,k)=fi3(i)*fj3(j)*hz(i,j,k)+fi2(i)*fj2(j)*.5*(curl_e);
        end
    end
end

for i=1:IE-1
    for j=1:JE-1
        for k=kb+1:KE
            kzh=k-kb;

            curl_e=(ra_y*(ex(i,j+1,k)-ex(i,j,k))-ra_x*(ey(i+1,j,k)-ey(i,j,k)));
            ihzh(i,j,kzh)=ihzh(i,j,kzh)+curl_e;

            hz(i,j,k)=fi3(i)*fj3(j)*hz(i,j,k)+fi2(i)*fj2(j)*.5*(curl_e+fk1(k)*ihzh(i,j,
            kzh));
        end
    end
end
ezv1(T)=ez(i_ref,j_ref,k_ref);
if T<=350
    inp =ezv1;
end
```

Publications

In referred journals:

1. Sarmah, D., Deka, J.R., Bhattacharyya, S. and Bhattacharyya, N.S., Study of LDPE/TiO2 and PS/TiO2 Composites as Potential Substrates for Microstrip Patch Antennas, *Journal of electronic materials*, 39 2359-2365, (2010).

2. Sarmah, D., Bhattacharyya, S. and Bhattacharyya, N.S., Graded Composite (Ldpe/Tio2) As Substrate For Microstrip Patch Antenna, *IEEE Transactions in Dielectric and Electrical Insulations, 20 (5), 1845-1850, (2013).*

In peer reviewed international/ national conference proceedings:

3. Debashis Sarmah, Satyajib Bhattacharyya, Nidhi S. Bhattacharyya and Jyoti P. Gogoi, "Study of LDPE/Al2O3 composite material as substrate for microstrip antenna" *Proceedings of ICCESD 2013.*

Oral paper presentation in national/ international conferences:

4. Gogoi, A., Sarmah, D. and Bhattacharyya, N.S., Improved microwave and thermal properties of LDPE/TiO2 composite polymer system as the Titania reinforcers approaches the percolation limit, *POLY 2007,* Guwahati, Assam.

Communicated

5. Sarmah, D., Bhattacharyya, S. and Bhattacharyya N. S., Broadband Transverse Line Terminated E-Arm Patch Antenna on Graded Composite Substrate, Electronics letters (communicated).

6. Sarmah, D., Bhattacharyya, S. and Bhattacharyya N. S., Circularly polarized Amalgamated Rectangular and V-slotted Semicircular Patch Antenna on Graded Substrate, (Ready to be communicated)

7. Sarmah, D., Bhattacharyya, S. and Bhattacharyya N. S., Embedded Microstrip Antenna with Slotted Patch for Broadband Applications, (To be communicated)